https://dspace.org/

Slag Adherence Variation of Oxy Fuel Cutting Gases

Kawawa, Muammar Mwalimu Rashidi

2025
University of the Witwatersrand, Johannesburg
https://hdl.handle.net/10539/47500
Kawawa, Muammar Mwalimu Rashidi. (2025). Slag Adherence Variation of Oxy Fuel Cutting Gases [Master's dissertation , University of the Witwatersrand, Johannesburg]. WIReDSpace. https://hdl.handle.net/10539/47500

Downloaded from a DSpace repository. https://dspace.org/



UNIVERSITY OF THE
WITWATERSRAND,
JOHANNESBURG

Slag Adherence Variation of Oxy Fuel Cutting Gases

Muammar Mwalimu Rashidi Kawawa

A research report submitted to the Faculty of Engineering and the Built Environment, University of the Witwatersrand, Johannesburg, in partial fulfilment of the requirements for the degree of Master of Science in Engineering.

Johannesburg, 2024

Declaration

I declare that this research report is my own unaided work. It is being submitted for the Degree of Master of Science at the University of the Witwatersrand, Johannesburg. It has not been submitted before for any degree or examination to any other University.

.....
(Signature of Candidate)

..... day of ....., ...
(day) (month) (year)

Abstract

Oxy-fuel cutting otherwise known as flame or oxygen cutting is a method used to separate steel sections during metal fabrication wherein the process slag produced may adhere to the bottom of the cut face. Adherent slag is a detrimental factor on the cut quality and subsequent post processing activities. In this study, the slag adherence during oxy-propane and oxy-acetylene cutting of 8 mm and 16 mm mild steel plates was investigated. The cutting tests were performed according to nominal Harris chart parameters, which were set at predetermined ranges to simulate workshop conditions. This was preceded by experimental testing which included visual observation, surface roughness, hardness, microscopic and elemental analysis. Utilising the Harris chart prescribed cutting parameters generally yields a good quality cut with no adherent slag. The slag is prone to adherence on the thinner plate cut with oxy-acetylene and the thicker plate cut with oxy-propane due to a higher content of free iron in the slags.

In memory of my late parents whom I lost during this research journey

Joseph & Phindile Kawawa

Acknowledgements

I would like to express my heartfelt gratitude to my late supervisor, Prof Josias Van Der Merwe, whose guidance and unwavering support profoundly influenced my research journey. I am also deeply thankful to my current supervisor, Dr Alani Nyembe, for his invaluable insights and encouragement throughout this process. A special thanks to my employer Air Liquide, for providing the mentorship by Mr Serge Suzan who is a Senior International Expert regarding flame industrial processes and allowing me the flexibility necessary to pursue my studies. Finally, I extend my deepest appreciation to my family for their constant love and support, which have been my foundation during this challenging yet rewarding endeavour.

Table of Contents

Declaration **2**

Abstract **3**

Acknowledgements **5**

List of Figures **8**

List of Tables **10**

Abbreviations **11**

Terms and Definitions **12**

Chapter 1 - Introduction **14**

1.1. Background 14

1.2. Problem Statement 15

1.3. Research Questions 16

1.4. Research Objectives 17

Chapter 2 - Literature review **18**

2.1. Overview 18

2.2. Background 21

2.3. Oxy-Fuel Flame Characteristics 21

2.4. Industrial Oxy-Fuel Flame Processes 25

2.5. Industrial Gas Cutting Methods 26

2.6. Oxy-Fuel Cutting Process Gases 37

2.7. Oxy-Fuel Cutting Process Equipment 41

2.8. Oxy-Fuel Cutting Process Parameters 41

2.9. Mild Steel Metallography 43

2.10. Oxy-Fuel Cut Quality 45

2.10.1. Post-Cutting Characterisation 45

2.10.2. Effect Of Cutting Speed On The Post-Cutting Surface Quality 49

2.11. Oxy-Fuel Cutting Slag 52

Chapter 3 - Experimental Procedure **54**

3.1. Raw Materials and Equipment 54

3.2. Cutting Pre-Trials 56

3.2.1. Cutting Nozzles 57

3.2.2. Cutting Pressure....57
3.2.3. Nozzle Standoff and Flame....58
3.2.4. Cutting Speed....59
3.3. Cutting Trial Samples....61
3.4. Characterisation of steel samples....65
3.4.1. Base Material Composition....65
3.4.2. Cutting Process Visual Examination....65
3.4.3. Macro Examination....66
3.4.4. Surface Roughness Testing....66
3.4.5. Test Piece Sample Preparation....66
3.4.6. Hardness Testing....67
3.4.7. SEM and EDS Evaluation....67
3.4.8. Optical Microscope....68
Chapter 4 - Results....69
4.1. Cutting Process Visual Examination....69
4.2. Macro Examination....73
4.3. Surface Roughness....76
4.4. Transverse Hardness....77
4.5. SEM and EDS Analysis....78
4.6. Optical Microscopy Images....93
Chapter 5 - Discussion....101
5.1. Cutting Performance....101
5.2. Factors Affecting Slag Adherence....109
5.3. Comparison with Previous Studies....112
5.4. Slag Adherence Mechanisms and Explanations....118
5.5. Practical Implications....119
5.6. Limitations....120
Chapter 6 - Conclusion and Recommendations....122
6.1. Conclusion....122
6.2. Recommendations....123
References....124

Appendices.....127

Appendix A - Cutting Machine.....128

Appendix B - Cutting Tips.....129

Appendix C - Cut Quality Chart.....130

Appendix D - Roughness Test Results.....131

Appendix E - Hardness Test Results.....139

Appendix F - Base Metal Test Certificates.....142

List of Figures

Figure 1. Heat from preheating flame and iron combustion
Figure 2. Representation of the OFC process
Figure 3. Oxy-acetylene flame
Figure 4. Cut faces of 15mm thick mild steel
Figure 5. HAZ of 15mm thick mild steel
Figure 6. Laser cutting surface characteristics
Figure 7. Laser fusion cutting
Figure 8. Laser vaporisation cutting
Figure 9. Roughness value versus cut sheet thickness
Figure 10. Surface roughness vs Cutting speed of low carbon steel sheets
Figure 11. Optimal cutting speed versus cut sheet thickness
Figure 12. Cut zone of stainless steel laser cutting
Figure 13. Oxygen cutting striations
Figure 14. Oxygen assisted laser cutting
Figure 15. Dross attachment vs cutting speed for stainless steel LBC
Figure 16. Dross attachment vs gas pressure for stainless steel
Figure 17. Effect of impurity of cutting oxygen on cutting speed
Figure 18. Effect of metal temperature on cutting speed for 28.5mm mild steel thick plate
Figure 19. Two piece oxy-acetylene cutting nozzle
Figure 20. Three stages of the OFC process
Figure 21. Microstructure of mild steel equiaxed ferrite and pearlite
Figure 22. Microstructure of mild steel with elongated ferrite grains
Figure 23. Three types of cuts
Figure 24. Dragline
Figure 25. Concavity
Figure 26. Surface roughness
Figure 27. Top edge melting
Figure 28. Gouging
Figure 29. The HAZ martensite region
Figure 30. The HAZ mixed phase region

Figure 31. The HAZ tempered base metal region
Figure 32. Specimens cut with oxy-acetylene
Figure 33. Surface roughness vs cutting speed of oxy acetylene and oxy propane
Figure 34. Cut drag displacement vs Cutting speed of oxy acetylene and oxy propane
Figure 35. Surface hardness vs Distance from the surface of oxy acetylene and oxy propane cut samples
Figure 36. Heat tint on 25 mm thick plate cut faces
Figure 37. Variation of hardness with cutting speed for 20 mm mild steel plate
Figure 38. Variation of roughness with cutting speed for 20 mm mild steel plate
Figure 39. Harris Plus Portable Cutting System
Figure 40. Experimental cutting pressures
Figure 41. Experimental nozzle standoff and flames
Figure 42. Sample preparation example - 8 mm thick plate for the 6 mm and 15mm nozzle standoff
Figure 43. Sample preparation - Bandsaw
Figure 44. Sample preparation - Wire cutter and mounting
Figure 45. Slag oxygen to iron atomic ratio
Figure 46. Variation of roughness with cutting speed for 8 mm mild steel plate at 6mm nozzle standoff (a) and 15mm nozzle standoff (b)
Figure 47. Variation of roughness with cutting speed for 16 mm mild steel plate at 6mm nozzle standoff (a) and 15mm nozzle standoff (b)
Figure 48. Variation of hardness with cutting speed for 8 mm mild steel plate at 6mm nozzle standoff (a) and 15mm nozzle standoff (b)
Figure 49. Variation of hardness with cutting speed for 16 mm mild steel plate at 6mm nozzle standoff (a) and 15mm nozzle standoff (b)

List of Tables

Table 1. Industrial flame processes

Table 2. Fuel gas characteristics

Table 3. List of equipment

Table 4. Cutting speed estimation

Table 5. Potentiometer calibration

Table 6. Nominal cutting speed deviation

Table 7. Oxy-acetylene sample cutting parameters

Table 8. Oxy-propane sample cutting parameters

Table 9. Base material test report

Table 10. Visual examination of the cut face

Table 11. Macro examination of the cut face

Table 12: Surface roughness (Ra) and (Rz5) - Acetylene

Table 13. Surface roughness (Ra) and (Rz5) - Propane

Table 14. Vickers hardness

Table 15. SEM analysis

Table 16. EDS slag analysis

Table 17. EDS slag composition

Table 18. Base metal microstructures

Abbreviations

BS - British Standard

acetylene - acetylene

EDS - Energy dispersive spectroscopy

EN - European Standards

FG - Fuel gas

HAZ - Heat affected zone

HV - Vickers hardness

HVOF - High Velocity Oxygen Fuel

ISO - International Organisation for Standardization

LBC - Laser beam cutting

LHV - Lower Heating Value

LPG - Liquefied petroleum gas

MPa - Megapascal

OEM - Original equipment manufacturer

OFC - Oxy-fuel cutting

Ra - Average roughness

Rz - Average maximum profile height

SABS - South African Bureau of Standards

SANS - South African National Standards

SEM - Scanning electron microscopy

Vc - Cutting Speed

Terms and Definitions

Alternate fuel gases - Fuel gases that are not produced by processing petroleum, these include propane, methane and liquefied petroleum gas (LPG)

Atomic ratio: The weight percentage composition divided by the atomic weight

Assist gas - Gas that is used to flush out the molten material during laser cutting including oxygen, nitrogen, compressed air or a mixture

Backfire - Occurs during cutting when the flame goes back into the cutting tip thereafter the flame extinguishes

Base metal - Engineering material that is being processed by a fabrication method/s e.g. welding or cutting

Blow torch - The tube / pipe like device that is used to deliver the mixture of ignited fuel gas with oxygen and cutting oxygen through the cutting nozzle

Burr - A residue of material that is left during cutting which may be subsequently removed by post processing e.g. grinding or scraping

Combustion ratio - The volumetric flow rate ratio of the oxygen to fuel gas

Concavity - The extent of distortion to flatness (90° for a straight cut) of the cut face and is determined by measuring the distance between two parallel straight points on the cut face

Crash event - When the flame is extinguished as a result of the cutting nozzle touching the cut surface during cutting

Cutting oxygen jet - The stream of cutting oxygen delivered through the centre of the cutting nozzle that is activated subsequent to preheat upon reaching the kindling temperature

Cutting nozzle - Also referred to a cutting tip is the piece that fits onto the cutting torch (blow torch) and delivers both the preheat flame mixture of fuel gas and oxygen as well as the cutting jet

Cutting Speed - This is the speed at which the cutting tip end moves across the surface of the sample or piece being cut

Dragline - The lines / striations visible on the surface of a cut face caused by exit of the cutting oxygen stream out of the kerf

Dross - The solidified oxidised molten metal deposit that adheres to the cut face subsequent to cutting

Flashback - Occurs during cutting when the flame goes back into the cutting torch's mixing chamber

Gouges - Irregular sized grooves or scourings of removed material appearing on the cut face

Impurity - An undesirable substance or component in the process gas that makes it less pure

Iron oxide molecular ratio - The ratio of the atomic ratio of oxygen to iron

Kerf - The channel or gap that is formed as a result of cutting wherein the reactions take place and the material is removed

Kindling / ignition temperature - This is the temperature at which a material auto ignites in an oxidising atmosphere

Lower Heating Value - This is the amount of heat released by combusting a kilogram of fuel gas in one hour at 25℃ and having the combustion products at 150℃

Machine cutting - Occurs when the travel speed and the nozzle standoff are controlled automatically

Manual Cutting - Occurs when the travel speed and nozzle standoff are controlled manually by an operator

Metal oxide - The compound formed when a metal reacts with oxygen

Nozzle standoff - The distance between the end of the nozzle and the surface of the workpiece being processed

Slag - The nonmetallic material consisting of oxides and impurities

Travel speed - See cutting speed

Chapter 1 - Introduction

1.1. Background

Flame cutting, also known as Oxy-fuel Gas Cutting (OFC), was invented at the beginning of the last century (American Welding Society, 2001). It consists of a jet of oxygen, also called cutting oxygen, which burns the metal and expels the slag produced during combustion. The motion of this cutting oxygen jet produces a kerf, which is the width of a cut or the width of a material removed by a cutting process. An oxy-fuel flame, known as a preheat flame, provides the energy required to reach and maintain the combustion temperature of the metal at the top of the kerf.

Several oxy-fuel flame processes utilise various fuel gases and oxygen to provide the energy required to work and process material. These processes can be grouped into five main categories namely joining, cutting, shaping, surface treatment, and heating (Suzan, 2014). The selection of the fuel gases depends on various factors including the volume of fuel required for the task, the cost of the fuel and the availability of the fuel in that particular market.

OFC cannot be used for non ferrous engineering materials such as aluminium and, nickel based alloys as well as ferrous stainless steel because the OFC process requires materials that can oxidise easily and the metal oxide melting temperature must be lower than that of the metal itself. Oxy-fuel is widely used in the steel industry sectors, including automotive manufacturing, metal fabrication and marine construction for manual and mechanised processes. These processes include joining, cutting, shaping, surface treatment, and heating (Suzan, 2014). Cutting is by far the most widely used process across all the sectors and will be the focus of this study whereby the variation in slag adherence utilising different nozzle fuel gas combinations will be investigated.

OFC relies on the combustion of the metal in presence of oxygen. It is sustained by an oxy-fuel flame which maintains the upper cut front at the combustion temperature of the metal. One of the critical factors influencing the efficiency and quality of the OFC process is the adherence of the slag, a by-product of the cutting process composed of metallic oxides.Slag adherence is detrimental to the efficiency and quality of the cutting process,

requiring the slag to be removed thereby increasing production costs. The adherence of slag to the cut face can vary significantly depending on several factors, including the oxide-to-free iron ratio, preheat, plate thickness, choice of fuel gas, cutting equipment, and cutting parameters (Slotman & Edward, 1951). Furthermore excessive slag adherence can lead to increased post cutting processing time and cost as well as potential safety risks.

Understanding and controlling slag adherence is therefore of paramount importance to optimise the efficiency, productivity and safety of the OFC operations. This research project aims to investigate the variation in slag adherence associated with different OFC nozzles and fuel gases namely acetylene and propane under varying cutting parameters. By comprehensively analysing the factors influencing slag adherence, we seek to provide valuable insights that can help optimise the OFC process and improve the overall quality of the cut face.

1.2. Problem Statement

During oxy-fuel gas cutting, slag formation is part of the process and should therefore be managed to enable optimal cutting performance and desirable product quality. An ideal cut quality is one that has a linear smooth-cut face surface with no gouges, no draglines, non-meltdown of the top surface, and non-adherent slag (Slotman & Edward, 1951). The adherence of the slag affects the quality of the cut face thus the slag must be removed which increases post processing costs.

In general, productivity is a priority and regardless of the fuel gas used, slag removal should be a seamless process and the slag should not be adherent. This is evident in machine cutting as opposed to manual cutting, as the former has a constant cutting speed (Slotman & Edward, 1951). The higher percentage ratio of iron oxides to unoxidized iron results in easier slag removal. The unoxidized iron rate in the slag is expected to be lower in the case of thickness above 10-12 mm therefore slag removal should be easier (Slotman & Edward, 1951).

Slag removal for thicknesses above 10-12 mm is easier as a result of the heat generated by the combustion of iron H_{mc} (oxide formation and slag jet) providing most of the cutting energy for thicker gauge material as opposed to thicknesses below 10 - 12 mm. Figure 1

below shows that the preheating flame heat (H_{phf}) propels the cutting for thicknesses below 10 - 12 mm as it is the main source of energy required to cut (Glizmanenko & Yeveseyev, 1961).

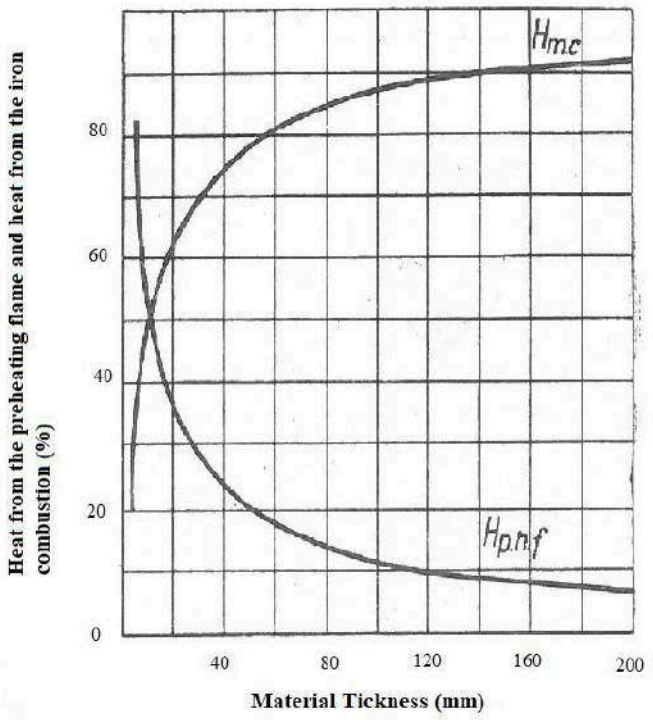


Figure 1. Heat from preheating flame and iron combustion (Glizmanenko & Yeveseyev, 1961)

1.3. Research Questions

OFC is a relatively old process and the available research on the slag adherence is limited. Laser and Plasma cutting are the alternative production thermal cutting processes and are in mainstream fabrication replacing OFC as the preferred methods of thermal cutting. Laser cutting is more recent than OFC and there is more research around this technology and consumers have an appetite for the most powerful machines, whilst the OFC research is limited (Davis, 2024). Adherent “dross” is a common occurrence during laser cutting of mild steels with oxygen (Garcia et al., 2015). During laser cutting, the dross is formed by liquid metal expelled from the kerf which attaches itself to the sidewall of the plate below the cut face and is oxidised by atmospheric oxygen (Cariston, 2002).

This research will aim to address the following questions:

- How does the selection of a fuel gas for an OFC operation affect the cut quality?
- What is the volume fraction of slag to unoxidized iron of an 8 mm and 16 mm plate at different cutting parameters?
- What are the optimal cutting parameters and fuel gas for an 8 mm and 16 mm plate?
- How does the ease of slag removal vary with fuel gas and cutting parameters?

1.4. Research Objectives

This research principally aims to evaluate the slag adherence variation of oxy-fuel cutting gas by utilizing propane and acetylene respectively in the configuration of the VVC nozzle and VAX nozzle (HARRIS Calorific). Laser cutting is widely used for cutting ferrous material thicknesses below 40 mm whereas Plasma and OFC are generally preferred for thicknesses above. Thus the research objectives of the study will be as follows:

- To evaluate the influence of fuel gases on beading of 8 mm and 16 mm mild structural steel EN 10025-2 S355JR+AR
- To determine the effect of the heat-affected zone on the optimal cut quality
- To evaluate or determine composition, phase, and morphology examination on the slag
- To contrast the two fuel gases, evaluate the surface profile (roughness) and cut face concavity with varying OFC parameters (nozzle standoff and cutting speed) resulting in non-adherent slag.

This report presents the background and significance of the study, reviews relevant literature, outlines the research objectives and methodology, and discusses the expected outcomes and implications of the findings. Through a systematic examination of slag adherence variation in OFC, this research endeavours to contribute to the advancement of cutting technologies and their applications in a variety of industrial settings.

Chapter 2 - Literature review

2.1. Overview

The atmospheric air contains 78% Nitrogen gas, 21% Oxygen gas and 1% Argon gas as the bulk and the rest are trace gases, water vapour, krypton, helium, neon, xenon, carbon dioxide, methane, ozone and nitrous oxide, less than 500 ppm each (Cox & Arthur, 2002). Pure Oxygen was first prepared in 1774 by a chemist, Priesley (Slotman & Edward, 1951) and it is used for various purposes including health and industrial applications. In OFC, the oxygen is used to burn the metal to be cut and to expel the slag from the kerf and to provide a higher flame temperature to the flame surrounding the oxygen cutting jet. The combustion of pure oxygen at a minimum purity of 99.5% (namely N25 as Air Liquide reference) and a fuel hydrocarbon is used in OFC resulting in higher flame temperature than one with air.

The first commercial industrial application of an OFC process was described in 1888 by Thomas Fletcher of the Society of Chemical Industry in Liverpool (Slotman & Edward, 1951). It was explained that when pure oxygen is passed through an iron pipe, it ignites at the tip of the pipe. The combustion energy can then be used to cut and or pierce through dense metals.. In 1901, oxygen lancing was patented for its use in the tapping of blast furnaces. Acetylene, which was discovered in 1837 by Davy, was first commercially produced by Wilson in 1892 (Slotman & Edward, 1951). In the same year, Fouche and Picard developed a cutting torch capable of safely combusting pure oxygen and acetylene (Slotman & Edward, 1951). Again, in the same year, Jottrand first locally heated a spot on a steel plate by combusting pure hydrogen and oxygen and using a cutting torch that was a variation of Fouche and Picard's welding torch, then shut off the hydrogen and increased the oxygen flow to make incremental cuts (Slotman & Edward, 1951). Jottrand subsequently added another copper tube on the welding torch to introduce cutting oxygen and instantaneously enable preheating and cutting; the modern cutting torch evolved from this concept. Although OFC was not widely industrialised, it was still undergoing basic development during the First World War and became the primary cutting technique during World War II (Slotman & Edward, 1951).

The cut front of the kerf or the surface at the plate must locally remain above the ignition temperature during cutting. This is enabled by having base materials melting temperature

combustion products being lower than the ignition temperature and the heat generated being greater than heat losses by material being removed from the bottom of the kerf as well as thermodynamic heat losses. Base materials with ignition temperatures close to or below their melting temperatures e.g. aluminium, copper as well as those with high temperature metal oxides e.g. chromium and silicon cannot be processed using OFC as they either melt prior to cutting or the high temperature metal oxide prevents further cutting by forming a solid barrier. Base materials that have high heat conductivity e.g. Copper are also not processed by OFC as they are unable to localise heat during preheat to reach the ignition temperature. The specific heat, thermal conductivities and melting points of the base metal and its metal oxides determine the susceptibility to OFC (Charles & Chater, 1978).

Figure 2 is an illustration of how the OFC process unfolds. Once the kindling temperature has been reached and the cutting oxygen jet released, the jet reacts from the surface of the cut just below the nozzle to the bottom of the plate. As shown in Figure 2 the jet reacts with the metal to form slag and expand both this slag and molten steel from the kerf. With increasing travel speed the cutting oxygen jet seizes to be vertical and begins to incline at an angle causing the jet to create turbulence with the slag, impurities and liquid metal. This results in a concave cut face.

At a minimal cutting drag condition, the cutting oxygen gas jet is in contact with the slag and the slag is in contact with the molten metal. All are separate and join at the respective interfaces where they create a gaseous boundary layer. Going deeper into the kerf from the top surface, both the slag layer and interface (gaseous boundary layer) become thicker. The impurity content of the gaseous boundary layer can be increased should the preheat flame react with the oxygen jet or new combustion products form. Should the slag become thicker than the stable slag thickness then the force upon the slag results in it being moved behind the cutting oxygen jet and settling on the sidewalls below the cut. The periodic movement of the slag to the sidewalls and behind the cut results in dragline formation on the cut face (Charles & Chater, 1978).

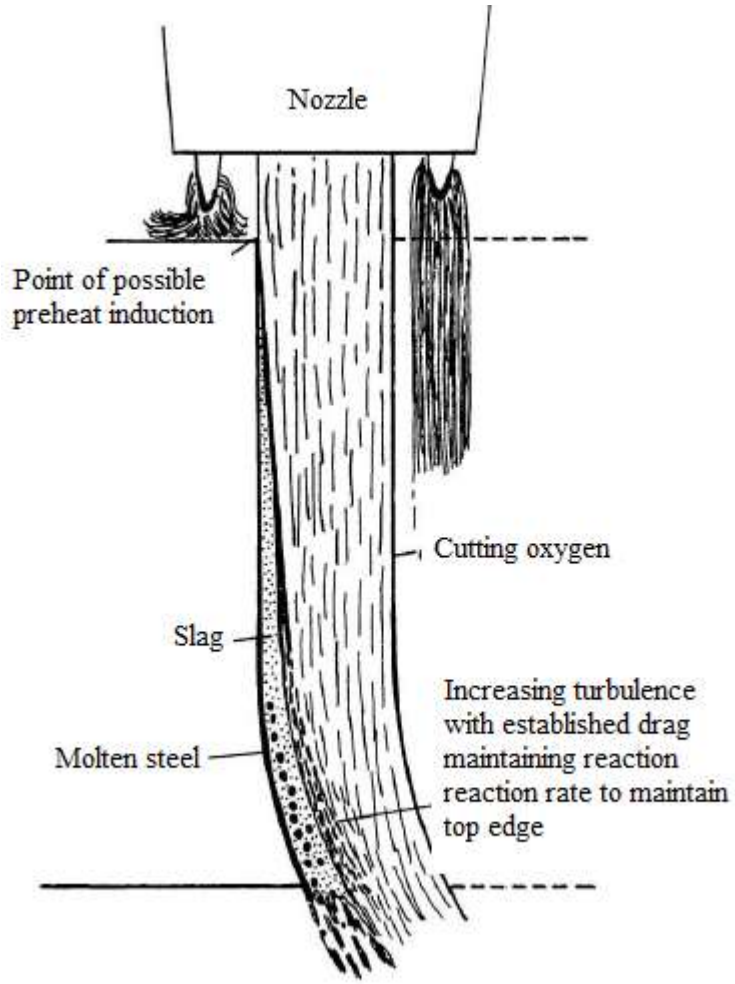


Figure 2. Representation of the OFC process (Charles & Chater, 1978)

The ratio of the total amount of oxygen supplied to the actual oxygen used by the slag is termed the "Oxygen efficiency". High cutting speeds are synonymous with a greater inclination of the cut front and result in high oxygen efficiency and more free iron in the slag. The cutting speed increases with increasing pressure and or increase in nozzle size, however this reaches a maximum beneficial threshold. The increase in cutting speed is more effective when increasing the pressure of smaller nozzle size than to increase the nozzle size at a lower pressure. The design of a nozzle entails adapting the nozzle to a higher pressure in order to increase the kinetic energy for the same quantity of oxygen, the resulting kerf is narrower, for the same rate of burnt metal, the cutting speed will be higher thus, benefits in gas consumption and productivity (Charles & Chater, 1978).

2.2. Background

Muñoz-Escalona et al. (2006) claimed that using propane as fuel gas resulted in less dragline inclination, a narrower kerf width, less adherent slag, and lower surface hardness as opposed to cutting with acetylene. This investigation was subject to pre-selected nozzles and parameters.

Abdulateef et al. (2010) evaluated the effect of cutting parameters (cutting speed, preheat time, and plate thickness) on cut quality (surface roughness and hardness). It was established that for 20 mm thick ASTM, BN1323 a preheat time of 20 seconds followed by a cutting speed of 300 mm/min resulted in improved cut quality

Harish and Babu (2017) used Grey relational analysis together with the Taguchi technique to evaluate the kerf width and surface roughness of mild steel cut with oxy-LPG flame. It was concluded that the minimum surface roughness and kerf width were obtained using 3 bar gas pressure, 300 mm/min travel speed, and 13 mm standoff. Surface roughness is directly proportional to all three process parameters whereas kerf width is directly proportional to gas pressure but inversely proportional to nozzle standoff and cutting speed. Of these three process parameters, the gas pressure is the most impactful.

Jokiaho et al. (2019) investigated the effect of residual stress and cracking of 20, 40, and 60 mm thick steel cut with oxy-propane flame. Due to the concentration of heat, during cutting the OFC flame results in the reversal of optimal heat-treated microstructure by forming a heat-affected zone (HAZ) and generating thermal tensile residual stresses which can result in cracking. The HAZ is apparent on the surface of the cut edge with hardness values decreasing with increasing distance from the cut edge and ultimately reaching the base material value

2.3. Oxy-Fuel Flame Characteristics

The OFC “Flame” is a result of the combustion of a fuel gas and an oxidant (Slotman & Edward, 1951). This flame differs from traditional combustion processes in that it is used as a tool with the OFC torch. The combustion ratio equation (*2.3.1)* is expressed as the ratio of

the flow rate of oxygen to the flow rate of fuel gas, also called the oxygen-to-fuel ratio, in analogy with the air-fuel ratio (AFR).

$$a = \frac{Oxygen\ flow\ rate}{Fuel\ Gas\ flow\ rate} \qquad (2.3.1)$$

The combustion ratio depends on the desired characteristics of the flame i.e. carburizing, neutral or oxidizing flame. The stoichiometric ratio ($n+m/4$) refers to the amount of oxidant (O_2) required to burn all the hydrocarbon (C_nH_m) to produce carbon dioxide (CO_2), water vapour (H_2O) and heat which is driven by equation (2.3.2).

$$CnHm + (n + m/4)O_2 \rightarrow nCO_2 + (m/2)H_2O + Heat \qquad (2.3.2)$$

where n is the carbon molecular volume and m is the hydrogen molecular volume.

For OFC, oxygen gas is the oxidizer and several fuel gases or mixtures can be used. The selection of such a fuel gas is based on regional and local factors including the sourcing conditions, price competitiveness, legislation frameworks, and availability of duly certified equipment.

Upon preheating, the kindling temperature of the base material is approximately 1350 ℃ (Glizmanenko & Yeveseyev, 1961). Previous research has demonstrated that the type of fuel gas , amount of cutting oxygen, and cutting speed have an influence on cut face quality. Optimal cutting parameters are desirable and result in a smooth sound surface to minimize post-cutting activities such as fettling, grinding, and machining to remove irregularities on the cut face (Munoz-Escalona et al., 2006).

The kindling temperature with oxygen determines if a steel can be cut. For OFC to be practical, this temperature needs to be below the melting point of steel. Increasing carbon content results in a decrease in the melting point and an increase in the kindling temperature. The resulting slag of ferrous metals with high carbon content is richer in unoxidized iron which causes the slag to be adherent. In addition to the carbon content, the following factors determine the metal cutability (Glizmanenko & Yeveseyev, 1961):

- The base metal's oxide melting temperature must be below both the melting point of the metal and the cutting temperature.

- The combustion process heat of the oxidation of the base metal should be the majority of cutting energy required to drive the cutting process and the balance supplied by the preheating flame
- The base metal must have low thermal conductivity to allow minimal heat absorption that can detour the initiation and propagation of the cutting process
- The metal oxide formed must have low viscosity to allow seamless flow of the slag through the kerf during cutting
- The base metal must contain minimal impurities which form oxides that hinder the cutting process and or increase its hardenability

The equivalence ratio, also called combustion richness, is the combustion ratio of the fuel gas normalized by its stoichiometric value. The combustion richness is only used for specific concerns and related techniques. A premixed oxy-fuel flame is suitable for welding and cutting applications, and it consists of a two-stage reaction:

A **primary combustion** where the fuel reacts with the oxygen intake to produce heat, carbon monoxide, and hydrogen gas. For acetylene combustion as shown in equation (2.3.3), the peak temperature is obtained at the tip of the inner cone (Abdulateef etal, 2010) .

$$2C_2H_2 + 2O_2 \rightarrow 4CO + 2H_2 + heat \qquad (2.3.3)$$

A **secondary combustion** where the carbon monoxide and hydrogen react with the oxygen of the ambient air to produce carbon dioxide and water vapour (equation (2.3.4)).

$$CO + H_2 + O_2 \rightarrow CO_2 + H_2O \qquad (2.3.4)$$

The primary reaction takes place in the inner cone and the secondary combustion in the plume. When the secondary combustion cannot take place, a large amount of carbon monoxide forms the plume, producing a reducing atmosphere. It is conveniently reminded that carbon monoxide should be controlled due to safety concerns. The normal or standard flame refers to a combustion ratio in accordance with usual working conditions. A **neutral flame** is obtained when the oxygen intake is necessary and sufficient to complete the primary combustion, thus producing a reducing atmosphere. Solely applicable to acetylene combustion, the neutral flow rate ratio of oxygen to fuel gas is almost one-to-one.

A **carburizing flame** is obtained when the combustion ratio is lower than the neutral ratio, thus producing a reducing atmosphere containing free carbons, in addition to the carbon monoxide and hydrogen. An **oxidising flame** is obtained when the combustion ratio is higher than the neutral ratio. The atmosphere contains more and more oxidant compounds (American Welding Society, 2001). Figure 3 below presents three flames, according to the AWS 3.0 American Standard (American Welding Society, 2001).

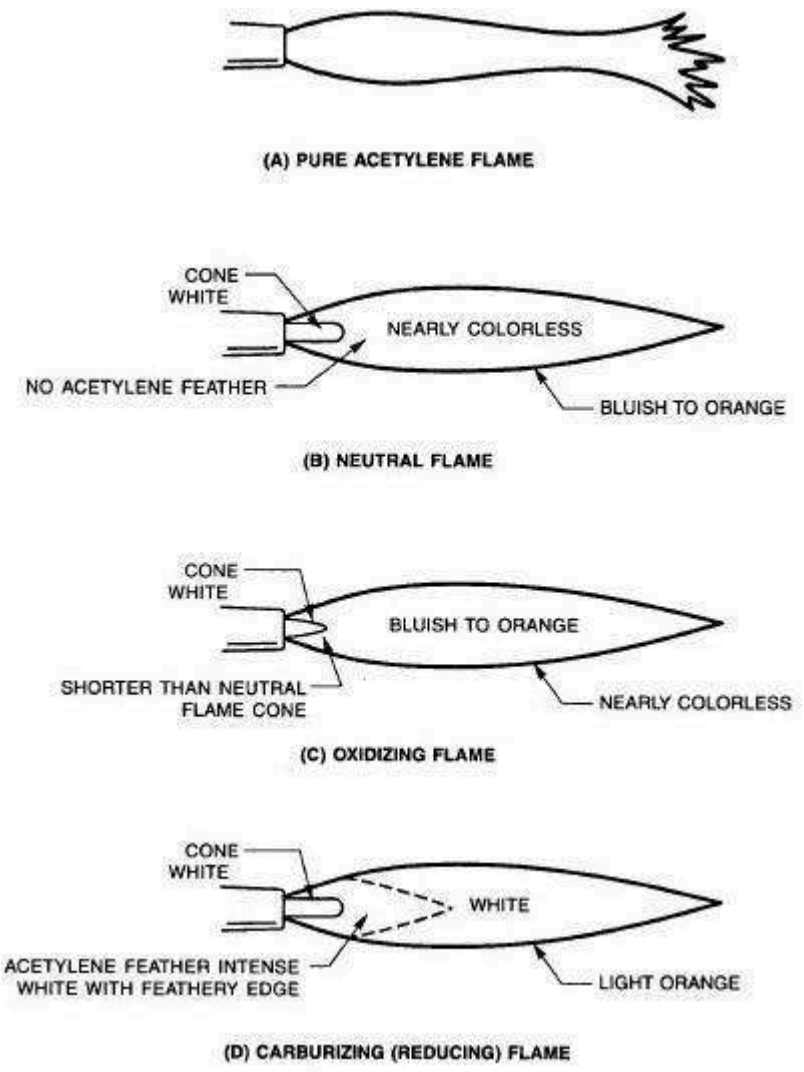


Figure 3. Oxy-acetylene flame (American Welding Society, 2001)

The low heat values (LHV) of the propane and acetylene (acetylene) are 24.03 kW.hr/m^3 and 14.78 kW.hr/m^3, respectively. Applying equation (2.3.5) yields a corresponding fuel gas preheat flow rate of 0.33 m^3/hr for propane and 0.54 m^3/hr for acetylene for 8 mm thick

plate. For 16 mm thick plate, the calculated flow rates are 0.67 m^3/hr and 1.08 m^3/hr for propane and acetylene, respectively (Suzan, 2014)

$$Flow\ Rate\ (m^3/hr) = \frac{t\ (mm)}{LHV\ (kW.hr/m^3)} \qquad (2.3.5)$$

where t is the plate thickness.

Equation (2.3.6) gives the heating power required for heating 0 - 50 mm up to the kindling temperature and is estimated to be 7 kW for the 8mm and 8 kW for the 16mm plate (Suzan, 2014).

$$Heating\ Power\ (kW) = a.t^m \qquad (2.3.6)$$

where a and m are constant values of 4.0735 and 0.2262 respectively. t is the plate thickness.

2.4. Industrial Oxy-Fuel Flame Processes

The oxygen-fuel flame process can be utilised for various industrial applications. The table below categorises the main processes and typical applications thereof:

Table 1: Industrial flame processes (Suzan, 2014)

Category	Process	Typical Application
Joining	Welding	Craftsman
	Brazing	Air Conditioning, Boilers
	Braze-Welding	Cycles
Cutting	Straight Cutting	Parts and Metal furniture
	Bevel Cutting	Weld preparing (Windmills)
	Gouging	De-seaming (ship repairing)
	Manual Cutting	Beam cutting (Public works)

Category	Process	Typical Application
Shaping	Hot Spinning	Gas cylinder manufacturing
	Straightening	Hull (shipyards)
	Dist. Removal	Deck flattening (shipyards)
	Hot Bending	Stiffeners (shipyards)
Surface Treatment	Flame Spraying	Anti-corrosion coatings
	HVOF	Tribological coatings (crankshaft)
	Hardening	Bumpers (railway)
	Granite Flaming	Surface roughening (Public works)
Heating	Welding Preheat	Boiler Fabrication
	Welding Post-heat	Boiler fabrication
Miscellaneous	Iron Powder Cutting	Mould feeders removal (foundry
	Scarfing	Flaw removal (foundry)
	Thermal Lancing	Metal recycling (foundry)
	Jet Piercing	Stone cutting (Quarry)

2.5. Industrial Gas Cutting Methods

Oxy-fuel cutting (OFC), plasma cutting, and laser cutting are the main thermal cutting processes used to process various types of engineering materials used in various sectors such as construction, power generation, and steel manufacturing just to name a few. These three processes differ mainly in the method used to melt the metal. OFC uses a cutting torch which delivers a mixture of the fuel gas and oxygen via a nozzle to firstly preheat the material to its kindling temperature thereafter an oxygen jet is activated to blow away the melted material through the kerf. Plasma cutting uses an inert gas blown at high speed

through a nozzle combined with an electric arc to ionize the gas at about 2500℃ thereby impacting the surface to be cut, removing material and blowing it away through the kerf. Compressed air plasma gas is inexpensive for carbon and low alloy steels and forms an iron oxide that drives an exothermic reaction which results in minimal distortion, a narrower heat-affected zone than OFC, and no slag or dross on the cut face. Laser cutting uses a high-power laser beam to melt the surface of the material, which is then blown away by an assist gas which is generally either oxygen for ferrous materials and nitrogen for stainless steels and non-ferrous materials.

Both laser and plasma cutting are far more productive than OFC, four to fivefold for plasma cutting. However, there are certain limitations regarding the practicality and cost of the laser and plasma-cutting equipment, resulting in the OFC process being the most widely adopted. OFC is the traditional thermal cutting process, and it is being replaced by the more productive Laser and Plasma Cutting which can also cut parts with very intricate geometries with high precision, as shown in Figure 4, whereby the cut faces of each method are contrasted.

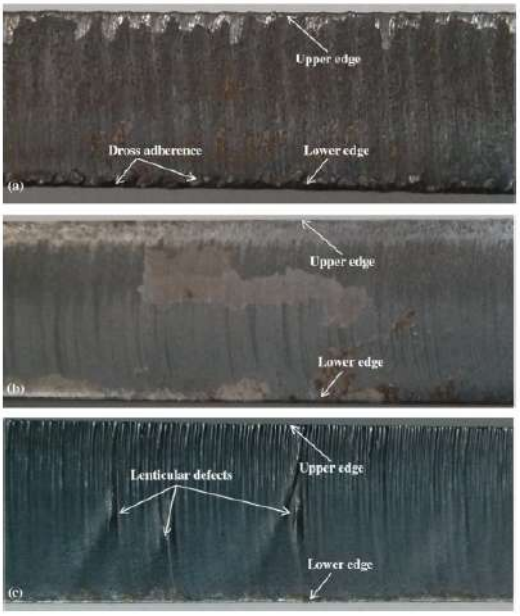


Figure 4. Cut faces of 15 mm thick mild steel: (a) OFC; (b) plasma cutting and (c) laser cutting (Cicero et al., 2016)

The cut quality of the three processes varies even with the respective optimal cutting parameters. As shown in Figure 4, the study by Cicero et al. demonstrated that the cut face is smoother with plasma cutting, followed by laser cutting, and lastly OFC. OFC has a

rough surface with adherent slag and the laser cut has draglines and some unoxidized metal at the bottom of the cut. During fatigue testing, the initiation sites are mostly on the slag-adherent areas with OFC. Figure 5 shows a micrograph of the cut face wherein the HAZ of the OFC varies from 1 - 4 mm and that of the laser cut face is less than 0.5 mm.

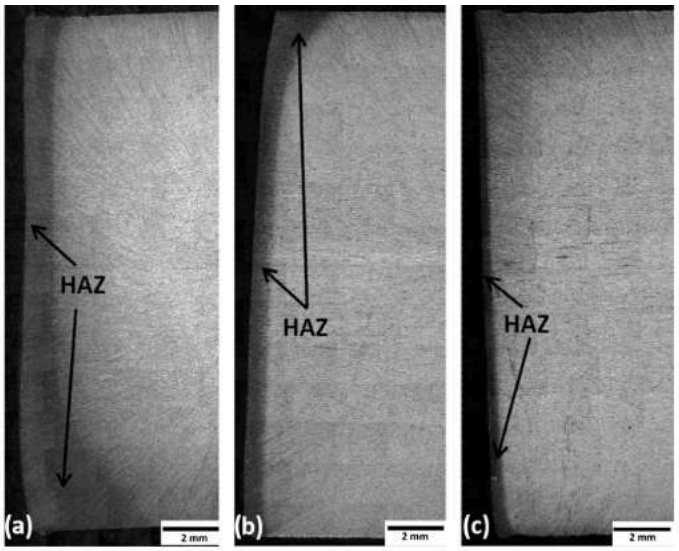


Figure 5. HAZ of 15 mm thick mild steel: (a) OFC; (b) plasma cutting and (c) laser cutting (Cicero et al., 2016)

Due to combustion-related similarities to OFC, laser oxygen cutting is prone to dross adherence if the cutting parameters are not sufficiently optimized. The oxygen-assisted gas nozzle cutting pressures may vary from 0.5 to 5.0 bars, and to avoid excessive combustion, the pressure is reduced and the nozzle diameter increases with increasing plate thickness (Wandera, 2006).

In OFC the metal is heated using a flame to reach its ignition temperature of approximately 1350 °C. Upon reaching this temperature, the cutting oxygen jet is applied at a pressure of 3 - 10 bar to pierce and oxidise the metal, forming a slag and kerf and removing the metal material (Harish & Babu, 2017). The OFC process involves the utilisation of a blow torch to deliver the fuel gas and industrial oxygen that produce heat through combustion. The mixture passes through a cutting nozzle to establish a cut in three steps (Ramakrishna, Raghuram & Avinash Ben, 2018):

- Preheat is to heat the metal up to its ignition temperature but below its melting point. At this point, a bright orange colour is visible with sparks flying in different directions.
- A jet of oxygen is then applied to initiate the cut thereby generating energy (heat), forming and blowing away the slag through the kerf. The slag melting point must be below the surrounding base metal so it can remain viscous to be blown away.
- Once the ignition temperature is reached, the oxidation reaction maintains it.

Laser cutting is the most widely used thermal cutting process for thin gauge / sheet metal materials, ceramics and composites. The laser beam is focused on the material at a spot which allows localised melting which is followed by flushing of the material with a pressure assist gas jet which is inert (mainly nitrogen) or active (mainly oxygen) depending on the material being cut. The inert gas serves to protect the cut face from further oxidation and is used for materials that are sensitive to oxidation such as stainless steels and the active gas is used to facilitate in the combustion exothermic reaction to melt thicker sections and or increase cutting speeds of mainly mild and low alloy steels. The energy released by the latter exothermic reaction is in similar order of magnitude to the power of the laser beam. These two sources of energy in laser cutting of low carbon steels result in two cutting fronts, that of the laser beam and that of the exothermic reaction which both determine the quality of the cut face and if the latter dominates it results in side burning and poor cut quality (Genna, Menna & Tagliaferri, 2020).

Some drawbacks of the laser-cutting process include the formation of draglines, heat-affected zone, and adherent slag. The rate at which heat can be dissipated from the kerf and surrounding base material is a critical factor during laser cutting. At a high rate, the melting of the metal is sluggish, resulting in insufficient energy to cut, a tapered edge due to cooling by the bottom of the cut, and the formation of slag (Genna, Menna & Tagliaferri, 2020).

Laser cutting uses the power density of a laser beam to form a kerf on the base material and steam of pressurised gas to flush out the processed material. Figure 6 illustrates the thermal cutting process whereby the laser beam is focused on the spot of a material at a predetermined focal length to provide sufficient energy to melt the material (Wandera, 2006).

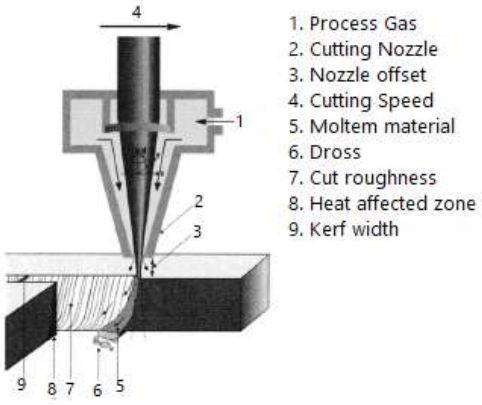


Figure 6. Laser Cutting Surface Characteristics (Wandera, 2006)

There are three types of laser cutting processes types which are determined by the main transformation process (Wandera, 2006):

Laser Beam Inert Gas cutting, as shown in Figure 7, is a thermal cutting process whereby the laser beam melts the material. The high pressure gas jet (nitrogen or argon) blows the material out of the kerf, and shields the melted material from oxidation and protects the laser optics. The process is used on mainly stainless steels and non-ferrous materials and aims to minimise adherent dross at the bottom of the kerf.

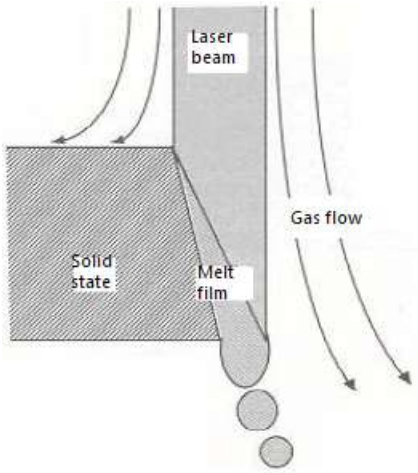


Figure 7. Laser Beam Inert Gas Cutting (Wandera, 2006)

Laser Oxygen Cutting is a thermal cutting process that utilises oxygen as an assist gas which serves to enhance the exothermic reaction, enabling faster cutting speeds than laser fusion cutting. The oxygen gas blows out the molten material and protects the laser optics. This technique is used for mild and low alloy steels and results in an oxidised cut face which may require further post process cleaning activities if the oxide is not restricted. The

metal oxide cutting front has higher laser absorption than a pure metal front and improves metal blow out of the kerf by reducing the viscosity and surface tension of the molten material.

Laser vaporisation cutting, in Figure 8, uses a relatively higher laser power density and slower cutting speeds compared to the previous laser cutting processes. These operating conditions locally heat the material beyond its melting temperature and vaporise it. Similarly, the assist gas is used to blow the vapour material out of the kerf. This cutting process is used on non-metallic materials such as wood, leather, paper, acrylic, some ceramics and polymers

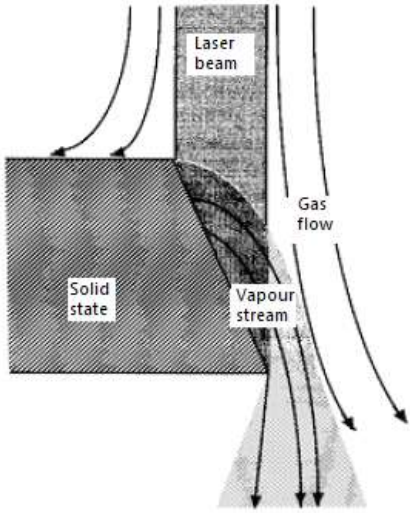


Figure 8. Laser Vaporisation Cutting (Wandera, 2006)

Oxygen laser cutting parameters are the assist gas type and flow rate, base material composition and laser beam power (Golnabi & Bahar, 2008). The material composition, the laser beam power and the travel speed determine the width of the heat-assisted zone . A reasonable cut quality is achieved with oxygen laser cutting at a power of 170 kw, 1 - 6 oxygen bar pressure, and a minimum cutting speed of 7 mm/sec. The exothermic reaction of oxygen determines the oxide formation and resulting dross or slag. The dross formation is independent of laser power. Fibre and CO_2 lasers have wavelengths of approximately 1 micrometer and 10.6 micrometres, respectively. The quality of a laser-cut face is mainly determined by the amount of dross and surface roughness. A smooth surface with no dross is the most desirable during laser cutting (Golnabi and Bahar, 2008). In general, the surface

roughness increases with cut material thickness as shown in Figure 9. At a given thickness, the fibre laser has a rougher surface than the CO_2 laser.

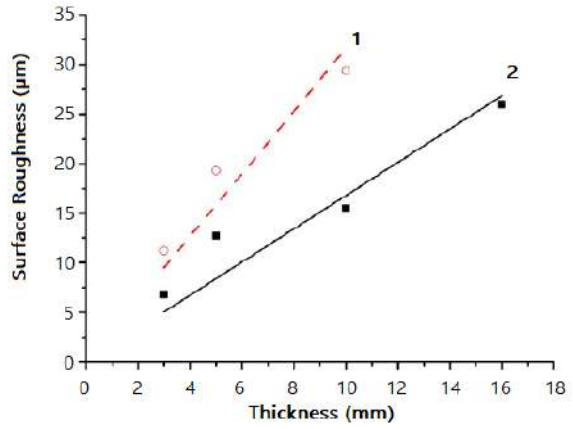


Figure 9. Roughness value versus cut sheet thickness (1- fibre laser, 2 - CO_2 laser) (Orishich, Shulyatyev & Golyshev, 2016)

Figure 10 shows that the surface roughness reaches an optimal value, then tends to rise upon further increasing the cutting speed. Increasing cutting speed reaches a point where the material does not separate and the kerf channel seals. Figure 11 illustrates that the maximum thickness during laser cutting of low-carbon steel is 40 - 50 mm. The fibre laser has uncontrolled localised burning at lower cutting speeds, and the optimal cutting speed decreases with increasing thickness (Orishich, Shulyatyev & Golyshev, 2016). The fibre laser technology has since improved, resulting in the development of a machine with a capacity of 135 kW cutting 400 mm carbon steel (Weike, 2024).

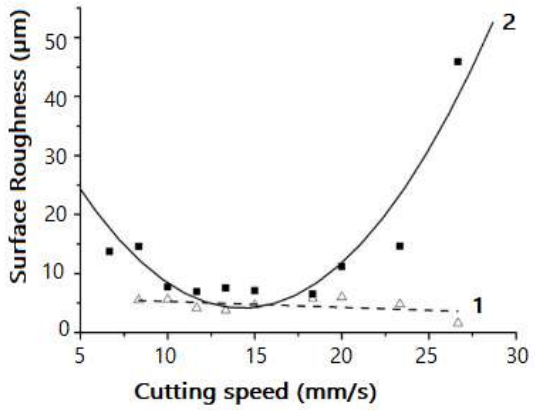


Figure 10. Surface roughness 1 (upper) 2 (lower) vs Cutting Speed of low carbon steel sheets with 1 kw fibre laser (Orishich, Shulyatyev & Golyshev, 2016)

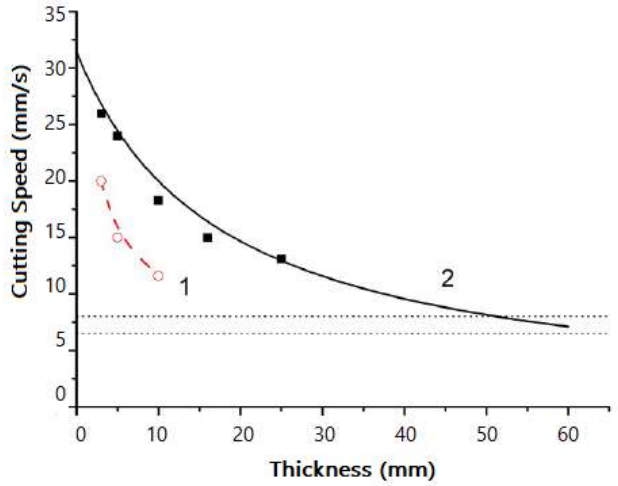


Figure 11. Optimal cutting speed versus cut sheet thickness (1 fibre laser, 2- CO_2 laser) (Orishich, Shulyatyev & Golyshev, 2016)

Nitrogen has low chemical activity, and it is cheaper than completely inert gases such as helium and argon (Figure 12). High assist gas pressures are applied to minimise the adherence of dross to the bottom of the kerf due to the high viscosity of the molten material as well as striations on the cut face (Wandera, 2006).

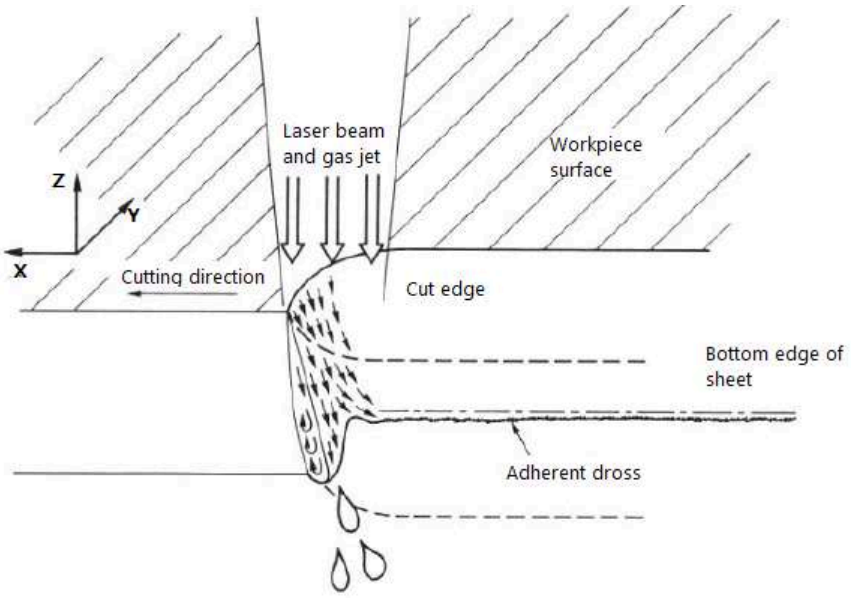
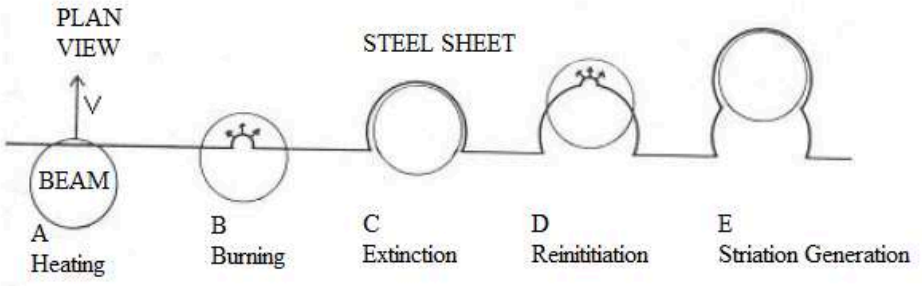


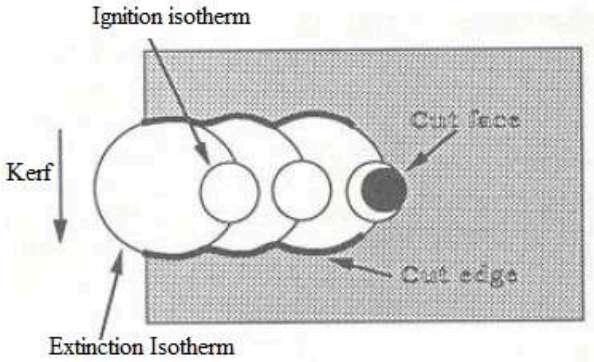
Figure 12. Cut Zone of Stainless Steel Laser Cutting (Wandera, 2006)

Draglines in laser cutting are a result of the metastable state of the process and are a function of sideways burning, liquid layer oscillation at the surface and variation in the

absorbed power due to surface plasma. Together with the temperature gradients, the thickness of the molten material fluctuates causing oscillations in the front of the cut which cause coarse striations at the bottom of the kerf. Figure 13 shows how laser oxygen cutting generates a circular pulsed wave at the surface of the kerf forming periodic striations of the cut face. Subsequent to the localised melting of the laser beam, the melt front proceeds ahead of the laser beam cooling and extinguishing the moving beam. As the beam interacts with unprocessed material, it re-ignites and the process continues forming a pattern of striations of the cut face. If the cutting speed is faster than the oxidation reaction then the laser beam and molten material front move at the same speed. The striations are formed due to slower cutting speed and the molten metal front moving in all directions after ignition. A faster speed, which is generally preferred, results in finner striations that are adjacent to the top surface.



(a) A schematic showing how striations can be generated



(b) Striation formation due to sideways burning

Figure 13. Oxygen cutting striations (Wandera, 2006)

During laser cutting, burrs are produced at the bottom of the cut face due to the molten metal solidifying faster than it can be removed. Burrs are metal oxides (slag), and their

formation is prone to materials with a low viscosity and high surface tension. Dross can be removed by an additional gas jet directed toward the bottom of the workpiece or mechanical means after cutting. The heat-affected zone for laser-cut materials increases with increasing thickness and heat input and slowing the laser travel speed (Wandera, 2006).

2 kW lasers can cut low carbon - mild steels up to 15 mm yielding the desired surface quality, however, the cut of more than 15 mm thickness requires higher-powered lasers. The applied gas pressure of the oxygen is lower (less than 1 bar) for thicker section steels and higher (more than 1 bar) for thinner section steels. This aims to minimise side burning of the steel resulting in gouges and a rough surface on the cut face. The higher the carbon content of the steel the less prone it is to side burning and the thicker the steel the more likely it is to have side burning (O'Neill & Gabzdyl, 2020).

FeO constitutes the main oxide product composition at about 97.6% (wt%), and the balance is Fe_2O_3 and Fe_3O_4. Assuming iron is only combusted into FeO, the reaction can be written as $Fe + 0.5O_2 = FeO$, and it is exothermic with a reaction thermal energy of 4600 kJ/kg. This exothermic power increases with material thickness, which aids the cutting process. This reaction requires large amounts of oxygen, posing a challenge of side burning for thicker sections. Figure 14 shows both the laser beam and oxygen jet delivered via a nozzle that houses a lens that focuses the laser beam at a focal point. The reaction generates a plate temperature above 1000 °C which is initiated by the laser beam. The surface reacting with the oxygen jet must be above this temperature to ensure complete combustion of the iron at the gas front and minimal dross. Unlike Nitrogen-assisted cutting, oxygen combustion drives the reaction at the depth of the cut and not the laser beam.

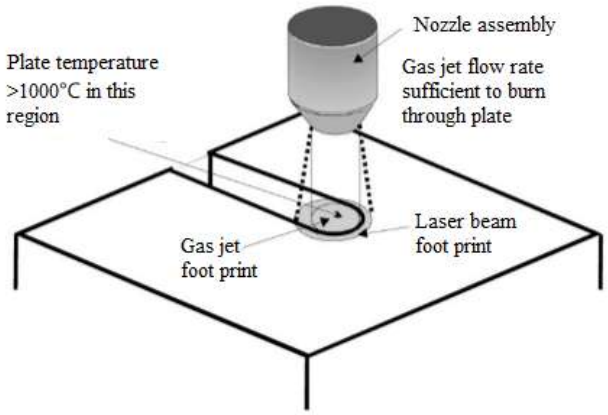


Figure 14. Oxygen-assisted laser cutting (O'Neill & Gabzdyl, 2020)

Some advantages of laser oxygen cutting to OFC are (O'Neill & Gabzdyl, 2020):

- No preheating time for oxygen laser cutting is required.
- OFC has non-localised heating, resulting in a larger HAZ than oxygen laser cutting
- Laser oxygen cutting requires no fuel gas
- Laser oxygen cutting has no top-edge melt
- Laser oxygen cutting utilises simpler nozzle designs

In recent times, Fibre lasers have been widely adopted at the demise of CO_2 and Nd: YAG lasers. This is due to the following advantages (Lai et al., 2017):

- Better beam adsorption
- Good beam quality
- Good cutting reliability
- Strong flexible light effect
- Low cost

The cut quality is affected by several variables including cutting speed, focal length, assist gas pressure, laser output power, and nozzle diameter. Figure 15 shows the relationship between dross adherence and the cutting pressure of stainless steel. The slower the cutting speed the more adherent dross and the faster the speed the same outcome prevails thus an in-between optimal value is generally preferred. Figure 16 shows that excessive or insufficient assist gas pressure leads to the adherence of dross. The former is associated with an insufficient blowout of material where low pressure and a vortex are formed on the

material surface, starving the kerf of enough pressure to remove melted material (Lai et al., 2017).

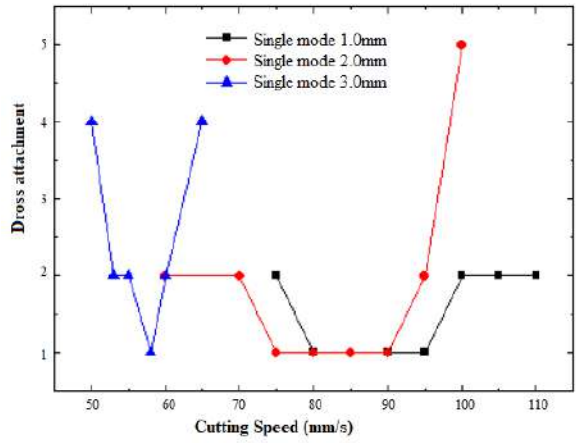


Figure 15. Dross attachment vs cutting speed for stainless steel LBC (Lai et al., 2017)

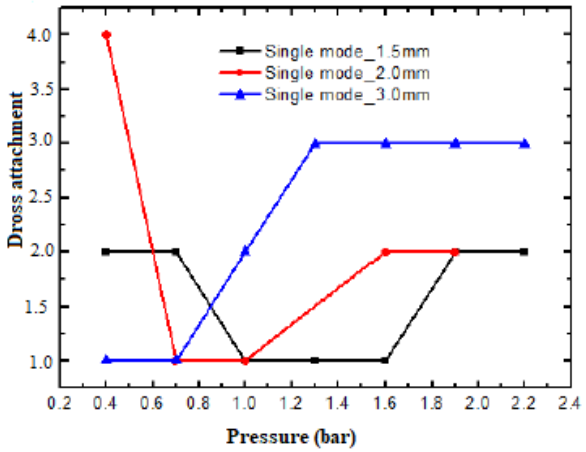


Figure 16. Dross attachment vs gas pressure for stainless steel (Lai et al., 2017)

2.6. Oxy-Fuel Cutting Process Gases

Before the discovery of acetylene by Turner and Wilson in 1892, hydrogen was used as fuel gas for welding and cutting. OFC is the most utilised industrial thermal cutting process due to its versatility of thickness range, low-cost equipment, adaptability to manual or mechanised methods, and range of fuel gas and nozzles that can be selected (Abdulateef, Mustafa & Salman, 2010). In practice, the most commonly used fuel gases are acetylene, propane (and its base variants e.g. LPG), propylene, and natural gas. The nature of the

flame and the heat distribution within the inner and outer cones of these fuel gases determine the process variables such as flame temperature, preheat time, cutting speed, and surface cut quality. The values of process parameters corresponding to different fuel gases are listed in Table 2.

Table 2 - Fuel gas characteristics (Abdulateef, Mustafa & Salman, 2010)

Fuel Gas	Maximum Flame Temperature (℃)	Oxygen to fuel gas Ratio (vol)	Heat distribution (kJ//m^3)	
			Primary	**Secondary**
Acetylene	3,160	1.2 : 1	18,890	35,882
Propane	2,810	4.3 : 1	10,433	85,325
Mapp	2,927	3.3 : 1	15,445	56,431
Propylene	2,872	3.7 : 1	16,000	72,000
Hydrogen	2,834	0.42 : 1	-	-
Natural Gas	2,770	1.8 : 1	1,490	35,770

The nature of fuel gas influences the time required for ignition, whereas the amount or flow rate of oxygen required during cutting is determined by the diameter of the cutting nozzle. This diameter subsequently influences the necessary pressure and the width of the kerf. The kerf width increases with increasing thickness of the material. In comparison to propane, acetylene was reported to be more expensive and less safe and to contain contaminants that are harmful to cutting operators (Munoz-Escalona et al., 2006).

The oxygen utilised for OFC is an industrial grade of 99.5% purity with generally, a maximum of 0.5% (5000 ppm) impurities. Depending on the type and density, the impurity has a detrimental effect on the cutting speed as shown in Figure 17 (Charles & Chater, 1978). The larger the relative density of the impurity the larger the effect. Krypton has the highest effect while hydrogen presents the lowest effect on the cutting speed. The cutting speed can be determined using equation (2.6.1).

$$y = a - k\,log(1 + bx) \qquad (2.6.1)$$

whereby y is the cutting speed (ft/h). a and b are constants related to the steel thickness. k is the constant related to the impurity and x is the concentration of the impurity in vol. %.

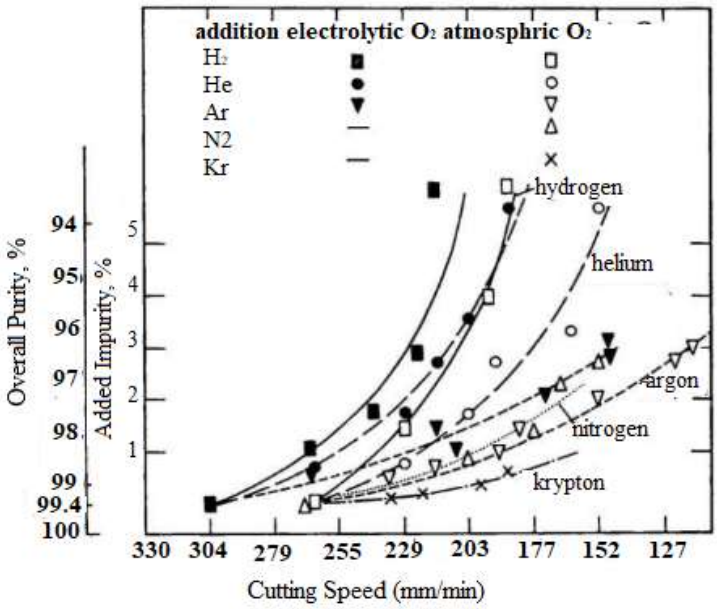


Figure 17. Effect of impurity of cutting oxygen on cutting speed (Charles & Chater, 1978)

As mentioned above the impurity forms an interface (gas boundary layer) between the cutting oxygen and the slag which increases in thickness toward the bottom of the cut. It is assumed that the combustion rate is greater than the rate of diffusion. It is evident that the denser the impurity at the interface the lower the combustion rate of oxygen and the slower the cutting speed. The oxygen supplied at the top is purer than at the bottom, due its contamination by the combustion products of the metal. Thus the combustion rate at the bottom of the plate is slower than at the top. However, as the draglines incline, the dynamics of the jet can have a better effect in expelling the slag. The presence of draglines during cutting results in turbulence or mixing of the oxygen with the impurities (Charles & Chater, 1978).

For the same cutting conditions, using acetylene as fuel gas results in similar cutting speeds as the propane, however, the latter is preferred for cutting thick sections. The combustion ratio of propane is higher than that of acetylene, which requires more oxygen to facilitate preheating and takes longer to preheat than acetylene. This can affect the cutting oxygen stream and slow down the reaction rate. Propane has a higher equivalence ratio than

acetylene and provides less localisation of heat and a lower flame temperature. The use of propane also results in less carburizing on the base material surface adjacent to the cut face. Carburizing occurs at 5 to 10 microns in the adjacent cut face material and through a gain of carbon in the steel which in turn increases the hardenability. The carbon originates from the liquid base metal in the kerf and not from the combustion of the hydrocarbon. Iron oxide slag preferentially nucleates over carbon forming the gas molecule. The molten steel on the surface of the cut face is supersaturated with the carbon arising from the dissociation of the carbon dioxide and solidifies on the cut face creating the carburized layer. Faster cutting speeds are achieved when the preheat flame is closer to the oxygen-cutting jet. However, if the preheat flame is too close then the cutting speed decreases due to contamination of the oxygen jet by the combustion products of the preheat flame (Charles & Chater, 1978). As shown in Figure 18, the cutting speed increases with an increase in the metal temperature. Above 600 °C, phase transformations inhibit cutting.

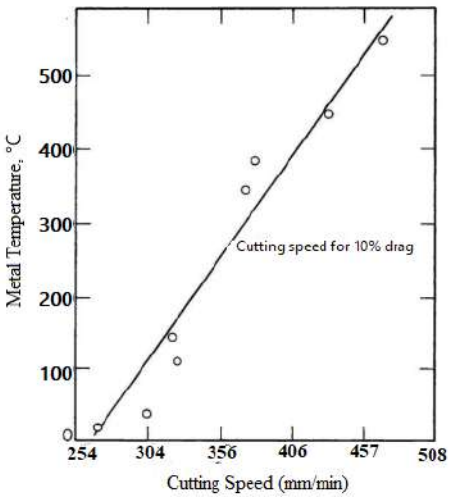


Figure 18. Effect of metal temperature on cutting speed for 28.5mm mild steel thick plate (Charles & Chater, 1978)

The purity of the oxygen is a key parameter in the OFC process. The minimum oxygen purity required is 99.5%, this enables the desired cutting speed and surface quality to be achieved. It has been demonstrated that a decrease of 1% in purity (from 99.5% to 98.5%) results in a decrease in cutting speed by 25%, and consequently an increase in oxygen consumption of the same order (Abdulateef, Mustafa & Salman, 2010).

2.7. Oxy-Fuel Cutting Process Equipment

In principle, the design of OFC torch tips includes numerous spaced openings (which are usually circular for acetylene and triangular for alternate gases) for delivering the preheat mix of fuel gas and oxygen that surround a central larger hole that delivers cutting oxygen as shown in the two-piece acetylene nozzle in Figure 19. The smaller preheat holes form the inner cone and have the function of cooling the nozzle during cutting and preventing flashback into the cutting system. The hole in the centre of the cutting tip is an outlet for cutting oxygen (Harish & Babu, 2017). The cutting oxygen is activated to enable the removal of material through rapid oxidation and flushing of the ferrous materials through the kerf. Both the preheat and cutting oxygen provide the energy required to sustain the cut (Pond & Martin, 2020).



Figure 19. Two-piece oxy-fuel cutting nozzle - (a) two pieces (b) nozzle assembly (Pond & Martin, 2020).

Alternative designs of the cutting nozzles were developed to optimise the cutting of thicker materials. To achieve satisfactory quality, materials can be cut at relatively slow cutting speeds, and the velocity of the oxygen jet tends to decrease at the bottom of the cut face. The development of divergent cutting nozzles was able to mitigate this decrease in velocity by restricting the flow of cutting oxygen gas exiting the nozzle, thereby increasing the velocity of the gas. This resulted in faster cutting speeds and reduced the consumption of cutting oxygen in comparison to traditional cutting nozzles (Davis, 2024).

2.8. Oxy-Fuel Cutting Process Parameters

Figure 20 demonstrates the three stages of a preheat flame applied in an OFC process, including an inner cone as a blue bright flame and an outer cone which relative to the inner cone flame is a clearer transparent flame. The three sequential stages of the process are

preheat whereby the flame is applied to the base material surface with the inner cone tangent to an outer cone flowing over it thereby raising the material surface to its kindling temperature. Followed by piercing whereby the cutting oxygen is activated to establish a kerf by rapidly oxidising and blowing away the material. Lastly, the cutting takes place and the flame which is now a combination of (i) and (ii) above is moved along the base material surface to cut through and along the desired section.

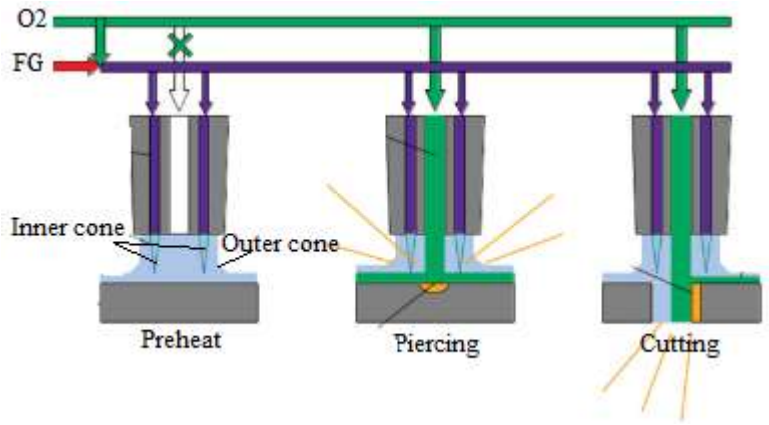


Figure 20. Three stages of the OFC process (Pond & Martin, 2020)

If the piecing stage is done without sufficient preheating and the cutting oxygen jet is activated prematurely, the oxygen jet will then act to cool the surface of the material and prevent ignition. Excessive cutting speed results in a higher proportion of unoxidised versus oxidised material in the kerf, which results in the cut being interrupted (Pond & Martin, 2020).

Optimal cut quality can be achieved by firstly establishing and maintaining the cutting speed which should allow a feed rate that enables the material to oxidise. This is followed by sufficient standoff which facilitates adequate heat input and reduces spatter which may damage the cutting tip. Finally adjusting the combustion ratio which varies with the FG and should be established such that the inner cone is simultaneously stabilised to the torch tip. Manual OFC process has shortcomings due to no vigorous methods to ascertain that kindling temperature has been achieved or detecting an extinguished cut. Similarly, the inner cone standoff cannot be sufficiently maintained. If the standoff is too close, it can result in base material distortion and a crash event. In addition, too far a standoff can lead to loss of cut (Pond & Martin, 2020).

The preheat temperature is 700 - 900 ℃. The four conditions for the process to take place are as follows (Abdulateef, Mustafa & Salman, 2010):

- The base metal must have a kindling temperature below its melting point
- The melting point of the base metal oxide must be lower than the surrounding material
- The ignition temperature must be sustained by the reaction of the cutting oxygen jet with the base metal
- The cutting oxygen must be protected by the process of combustion gases.

Increasing the cutting speed results in a rounded bottom edge, undercutting of the edge, and concavity. Decreasing the cutting speed results in an unstable process and gouges on the surface of the cut. Increasing oxygen pressure results in a wider cut and less oxygen for combustion whilst decreasing oxygen pressure results in gouging and adherent slag. Utilising an oversized nozzle can result in a tapered cut face as the cutting oxygen expands and removes more metal at the bottom of the cut. Conversely, utilising a smaller nozzle at slower cutting speeds to cut thicker gauge material can result in good cut face quality (Abdulateef, Mustafa & Salman, 2010). Narrower kerf widths with the fastest oxygen jet allow for faster cutting. The critical area is at the bottom of the cut where there is minimal cutting oxygen (Charles & Chater, 1978).

2.9. Mild Steel Metallography

Plain carbon steels contain minimal alloying elements and can be fabricated with ease. These steels consist mostly of the ferrite phase which is soft and the harder pearlite phase. Plain carbon steels contain carbon ranging from 0.10 % to 1% and other alloying elements such as manganese, silicon, nickel, chromium, molybdenum, boron, and aluminum. During the microstructural examination, the ferrite phase can be seen as a light phase coexisting with a darker phase pearlite as shown in Figures 21 and 22 (Benscoter & Bramfitt, 2004) . Depending on the thermal treatment, the morphology of the ferrite may be equiaxed with pearlite islands as shown in Figure 21. This represents a hot rolled structure at a temperature above the recrystallisation temperature (hot working). Hot rolling at temperatures below the recrystallisation temperature (cold working) produces a

microalloyed high strength low alloy (HSLA) steels where the ferrite phase is finer with elongated grains as shown in Figure 22.

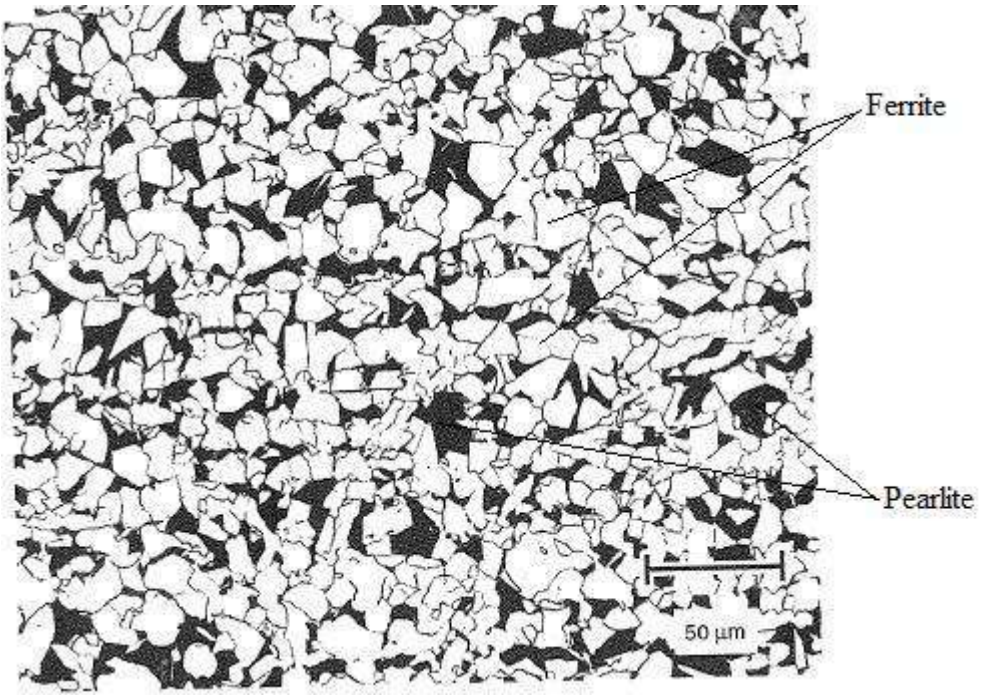


Figure 21. Microstructure of mild steel equiaxed ferrite and pearlite islands (Benscoter & Bramfitt, 2004)

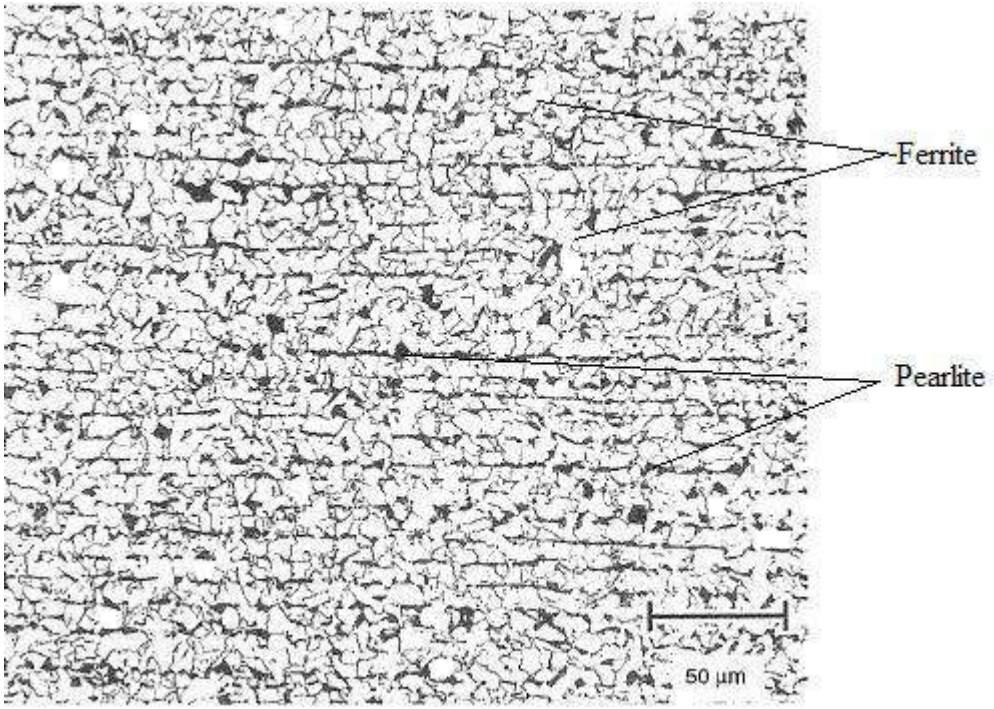


Figure 22. Microstructure of HSLA steel with elongated microstructure (Benscoter & Bramfitt, 2004)

For plain carbon steels, the ferrite phase has a maximum of 0.005% carbon and is essentially iron (Fe) and the excess carbon forms cementite (Fe_3C) which is a compound of iron and carbon. The ferrite volume fraction content of these steels is greater than the pearlite content. As shown in equation 2.91, pearlite is a combination of ferrite and cementite.

$$Fe + Fe_3C \rightarrow Pearlite \qquad (2.9.1)$$

Care should be taken in the preparation of microstructures of these steels as they contain the soft phase, ferrite which is susceptible to cold work during the micro sample preparation process. This can lead to a distorted appearance and interpretation of the structure resembling elongated grains and in some cases scratches. Ferrite is soft and can be mechanically cold-worked during sample preparation. Mechanical cold work can lead to serious issues ranging from a sloppy appearance of the microstructure to an artefact that can result in a complete misinterpretation of the metallographic features (Benscoter & Bramfitt, 2004).

2.10. Oxy-Fuel Cut Quality

2.10.1. Post-Cutting Characterisation

There are three types of cuts, either straight or beveled depending on the torch angle as shown in Figure 23.

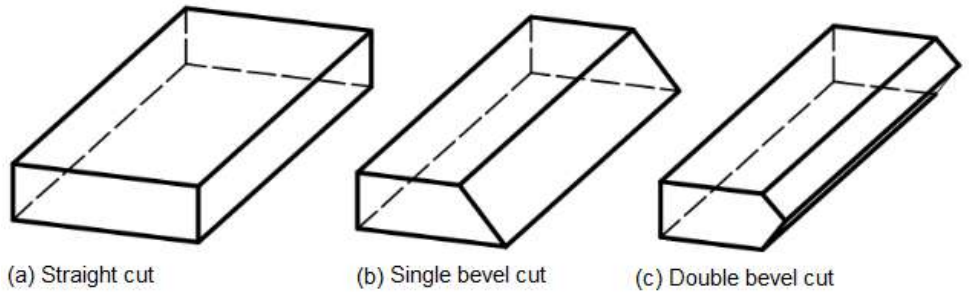


Figure 23: Three types of cuts

During post-cutting characterisation, the cut may be examined for the following:

- Dross (see definition), is the metal oxide that remains on the cut face and or edge

- Draglines (Figure 24), (n) is the distance between two points on a dragline, and (f) is the pitch of the drag, measured in the cutting direction

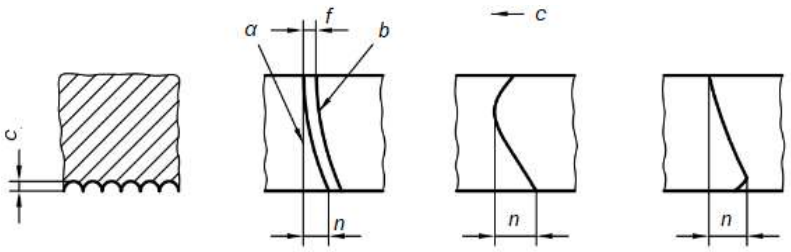


Figure 24. Dragline - (a) reference line (b) dragline (c) advance direction (ISO, 2006)

- Concavity (Figure 25) measurement, (U) is the peak distance between two protruding points on a cut face

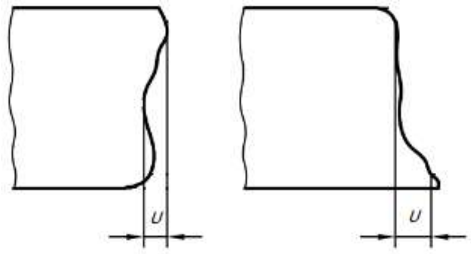


Figure 25. Concavity (ISO, 2006)

- Surface roughness, Ra (Figure 26) is a measurement of the sum of the height of the peak and depth of the valley points on a cut face and can be quantified by the average of five outlying single measured distances Rz5.

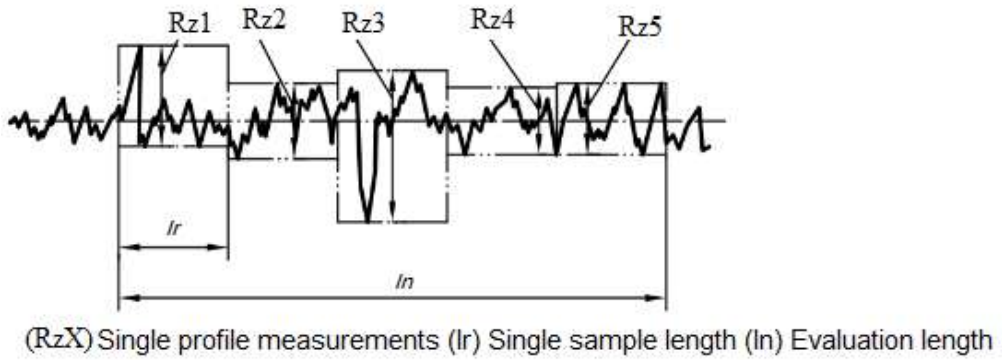


Figure 26. Surface roughness (ISO, 2006)

- Top edge melting (Figure 27), (*r*) is a qualitative assessment of the form of the cut face which may be either a sharp, molten, or overhang top edge

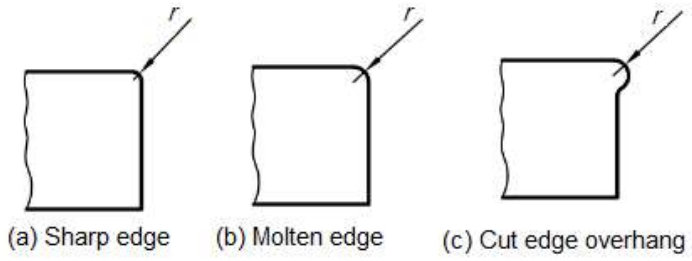


Figure 27. Top edge melting (ISO, 2006)

- Gouging (Figure 28), is an examination of the gouges which are irregular sized grooves or scourings of removed material appearing on the cut face

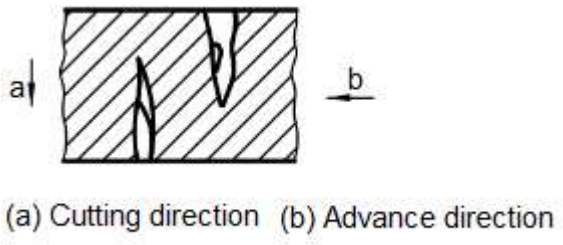


Figure 28. Gouging (ISO, 2006)

The gouging and concavity of the cut face increase with increasing thickness of the base material, cutting speed, and oxygen pressure. The top edge melting occurs during the preheat phase. In the preheat gas flow, the selection of the cutting nozzle and the nozzle-to-plate distance are important considerations (Slotman & Edward, 1951). Appendix C provides an additional visual guide to post-cut face quality considerations (The Harris Products Group, 2015).

Heat-treated steel sections have non-uniform mechanical properties in the thickness direction due to segregation. Due to the relatively high heat input energy required, thick plates are often separated using OFC. As a result of the concentration of heat, during cutting the OFC flame results in the reversal of the optimal heat-treated microstructure by forming a heat-affected zone. This generates thermal tensile residual stresses which can

cause cracking in the HAZ area. The HAZ is apparent on the top plate surface where preheat and initiation of the cut is undertaken. The hardness decreases from the top plate surface with increasing distance through the plate thickness, and ultimately reaching the base material hardness value. For a wider HAZ, the hardness can reach a maximum with increased alloying elements (Jokiaho et al., 2019.

In general, the HAZ comprises three regions, martensite (Figure 29), mixed region with martensite and the tempered base metal phase (Figure 30), and tempered base metal phase (Figure 31). The mixed phase region has a higher proportion of martensite with decreasing thickness and cutting speed. The base material is that of a wear resistant steel with carbon equivalent of 0.3 (Jokiaho et al., 2019)

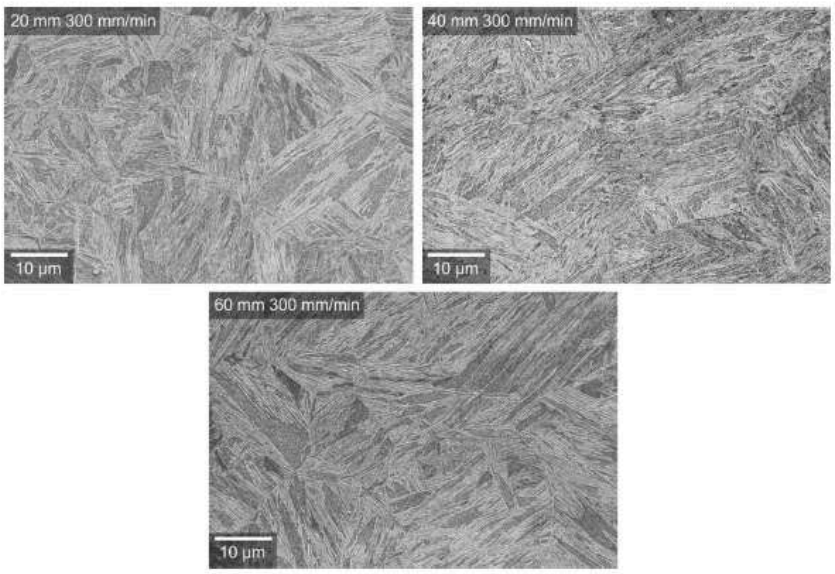


Figure 29. The HAZ martensite region (Jokiaho et al., 2019)

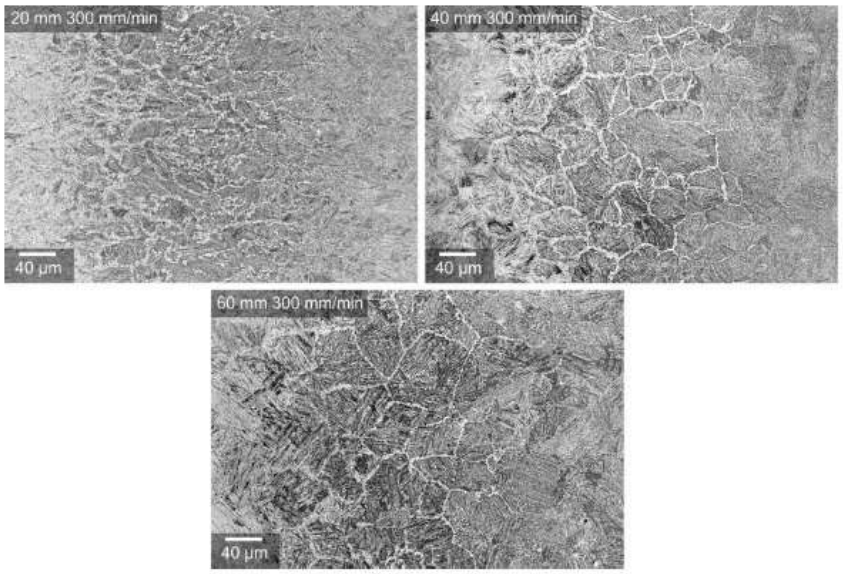


Figure 30. The HAZ mixed phase region (Jokiaho et al., 2019)

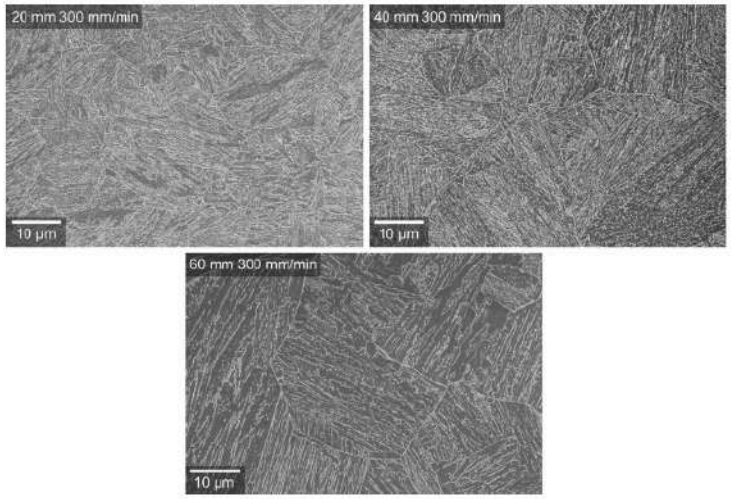


Figure 31. The HAZ tempered base metal region (Jokiaho et al., 2019)

2.10.2. Effect Of Cutting Speed On The Post-Cutting Surface Quality

The variation of cutting speed determines the surface quality of the cut, which also depends on the nature of the fuel gas (Munoz-Escalona et al., 2006). The heat distribution for the oxy-acetylene flame shows that one-third of the heat is concentrated in the inner cone primary flame whereas that of the oxy-propane is one-tenth (add references). As a result, the surface of the oxy-propane cuts have some concavity whilst that of the oxy-acetylene

cut tends to exhibit flakes at the surface of the top edge which are generally easy to remove. Figure 32 shows the flakes at various cutting speeds, 100, 150, 250, and 300 mm/min.

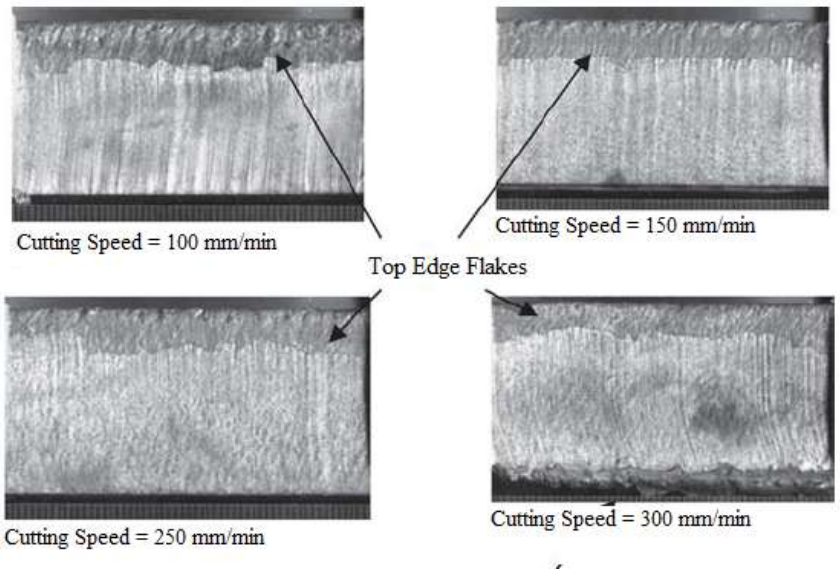


Figure 32. Specimens cut with oxy-acetylene (Munoz-Escalona et al., 2006)

Munoz-Escalona et al. (2006) reported that the surface roughness of oxy-propane cuts is smoother than that of the oxy-acetylene cuts, and this roughness diminishes at the optimal cutting speeds of 200 - 300 mm/min for a 25 mm thick plate of AISI 1045 steel (Figure 33). The surface roughness of the oxy-acetylene cuts decreases with increasing cutting speed. For oxy-propane cuts, the roughness decreases to its lowest value (minimum) at the nominal cutting speed, thereafter it increases.

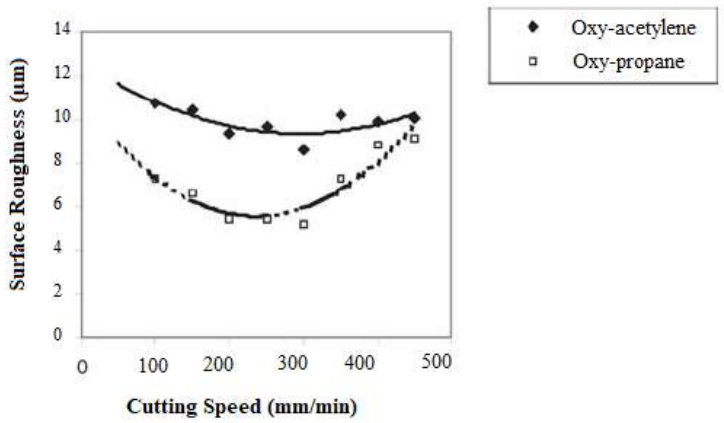


Figure 33. Mild Steel Surface roughness vs cutting speed of oxy-acetylene and oxy-propane (Munoz-Escalona et al., 2006)

Further investigations by Munoz-Escalona et al. (2006) found that the cut dragline displacement rises proportionally to the cutting speed cutting speeds as shown in Figure 34. This is due to less oxygen at the bottom of the cut with increasing cutting speed and the nature of the oxy-propane flame which is less inclined than the oxy-acetylene flame.

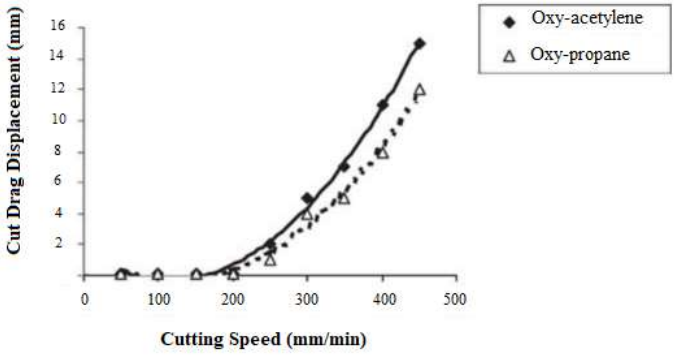


Figure 34. Cut Drag Displacement vs Cutting Speed of oxy-acetylene and oxy propane (Munoz-Escalona et al., 2006)

Due to localised heating which depends on the nature of the flame and travel speed, the surface hardness of AISI 1054 steel is suggested to be altered during oxy-fuel gas cutting (Munoz-Escalona et al., 2006) As shown in Figure 35, this effect diminishes through the thickness of the cut piece for cutting speeds of 100 mm/min (a) to 400 mm/min (d). In general, the oxy-acetylene flame which has a more concentrated heat distribution has a higher variation in hardness, particularly at cutting speeds below 300 mm/min compared to the oxy-propane flame. The hardness values correlate well with the microstructures for both the oxy-propane and oxy-acetylene cuts. At a certain depth within the cut face, no microstructural change is observed. Oxy-propane cuts present a reduced surface hardening effect compared to oxy-acetylene cuts for specific cutting speeds . This is due to the nature of the flame of each respective flame and the decrease in temperature gradient at the cut face.

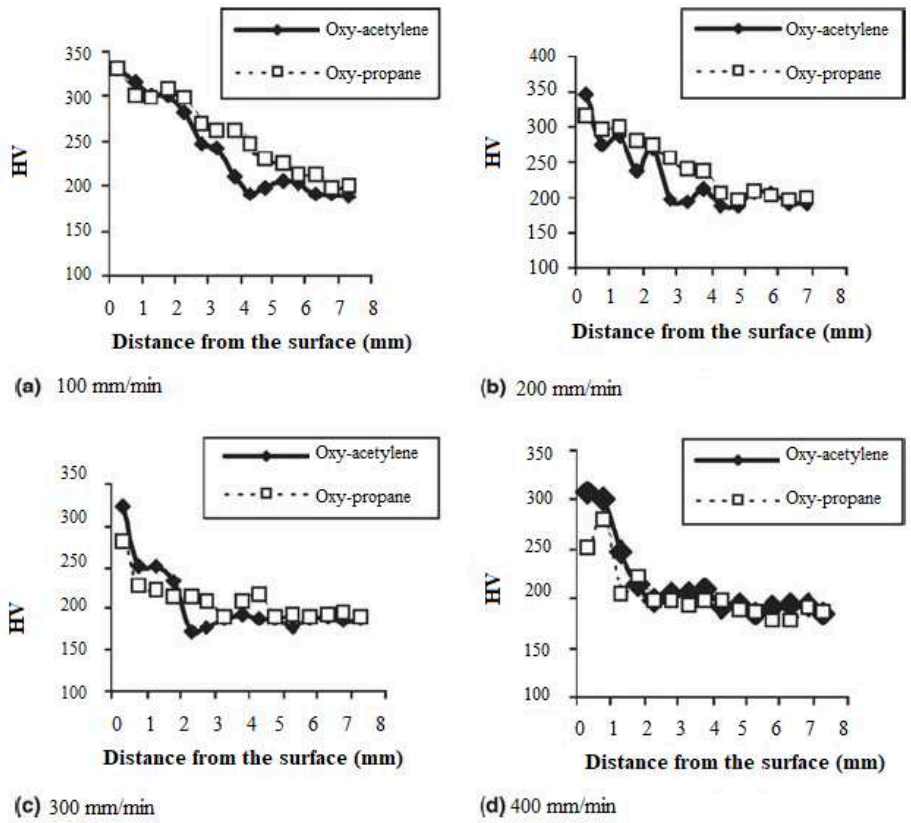


Figure 35. Surface Hardness vs Distance from the surface of oxy-acetylene and oxy-propane cut samples (Munoz-Escalona et al., 2006)

2.11. Oxy-Fuel Cutting Slag

Machine cutting has a consistent tip-to-workpiece distance and travel speeds compared to manual cutting, thus the slag tends to be less adherent with machine cutting. The greater the proportion of oxides to free iron the easier it becomes to remove slag. The formation of iron oxides is favoured by rust on the plate, sufficient cutting oxygen, and low heat input during the cutting process. Very thin materials have relatively higher heat input while very thick materials have slag impeding the advancement of the heat at the bottom of the cut.

Slag composition is affected by the plate thickness, cutting speed, oxygen pressure, oxygen purity, and the type of material cut (Slotman & Edward, 1951). Free iron causes beading which is a tendency of the slag to adhere to the bottom of the cut. Beads are rich in metallic iron and are difficult to remove. The higher the percentage of free iron the more adherent the slag. Free iron decreases with increasing material thickness, decreasing the cutting speed and a lower purity of oxygen. This results in higher percentages of combined hematite (Fe_2O_3) and magnetite (Fe_3O_4) than wustite (FeO) (Slotman & Edward, 1951).

Slag is visible with both the oxy-propane and oxy-acetylene cuts on Figure 36. In comparison to the oxy-acetylene, the lesser concentrated heat distribution of the propane mitigates the slag formation and impacts the slag adherence. The slag also provides thermal energy which can cause distortion of the workpiece and localised heating of the cut face in the vicinity of the slag. Figure 36 below shows the heat tint, resulting from localised heating on the cut face of the oxy-acetylene and oxy-propane samples (Munoz-Escalona et al., 2006).

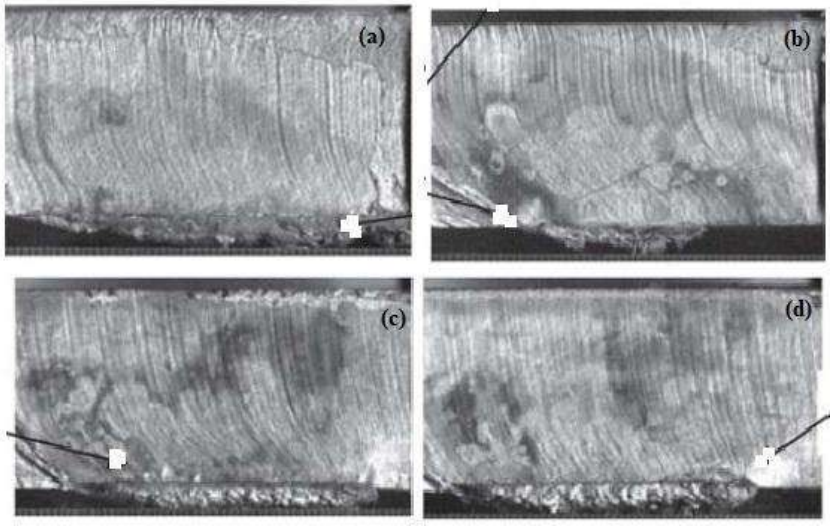


Figure 36. Heat tint on 25 mm thick plate cut faces - (a) oxy-acetylene at 350 mm/min; (b) oxy-acetylene at 450 mm/min; (c) oxy-propane at 400 mm/min; (d) oxy-propane at 450 mm/min (Munoz-Escalona et al., 2006)

Figures 37 and 38 show the effect of preheat time on the hardness and surface roughness at various cutting speeds. With the exception of an excessive preheat of 25 seconds, increasing the cutting speed from 100 - 250 mm/min shows an initial gradual decrease in both the hardness and surface roughness values. Further increasing the speed beyond 250 mm/min results in an optimal roughness and hardness value and thereafter further increasing the cutting speed results in a decrease in the hardness and surface roughness of the cut face (Abdulateef, Mustafa & Salman, 2010).

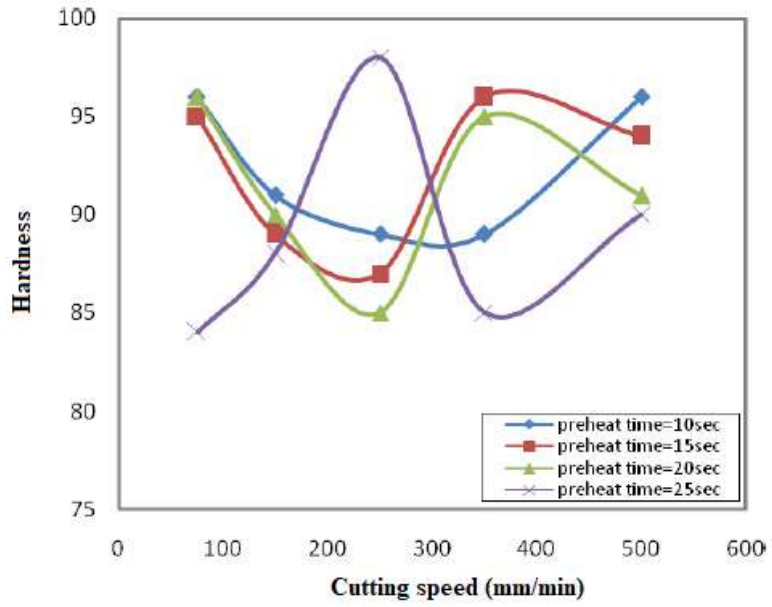


Figure 37. Variation of hardness with cutting speed for 20 mm mild steel plate (Abdulateef, Mustafa & Salman, 2010)

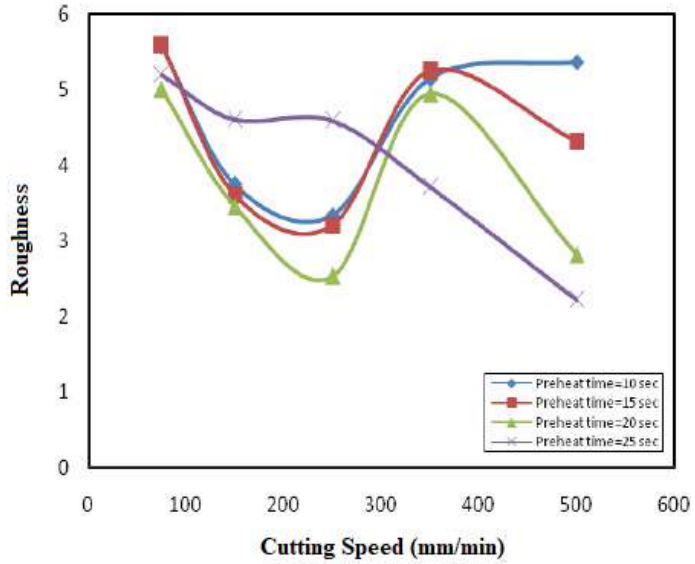


Figure 38. Variation of roughness with cutting speed for 20 mm mild steel plate (Abdulateef, Mustafa & Salman, 2010)

Chapter 3 - Experimental Procedure

To evaluate, contrast, and characterise the adherence of the OFC slag, two fuel gases propane and acetylene were used to cut the 8 mm and 16 mm mild steel plate test pieces at the predetermined cutting parameters described in this section.

3.1. Raw Materials and Equipment

Table 3 presents a list of equipment and consumables used in this research. The equipment consists of items needing regular upkeep and are non perishable, while consumables are periodically used up during operation.

The equipment used in this study consisted of cutting machines and laboratory analytical instruments such as Harris Plus Portable Cutting System, Scanning Electron Microscope coupled with Energy Dispersive Spectroscopy (SEM-EDS), Hardness Tester, Optical Microscope, Roughness Tester, and Stereo Microscope. The consumables principally included fuel gases (propane and acetylene), cutting tips, and mild steel samples.

Figure 39 shows the Harris Plus portable cutting system which is a straight-line cutting machine mounted with a cutting torch Model 198-4F and three tubes attached to it. Each of the three tubes supplies fuel gas, preheat oxygen, and cutting oxygen, respectively. The cutting machine is connected to the cylinders via the hoses. The inlet pressure is controlled using pressure regulators and flashback arrestors to prevent the flame from returning into the houses and eventually cylinders.

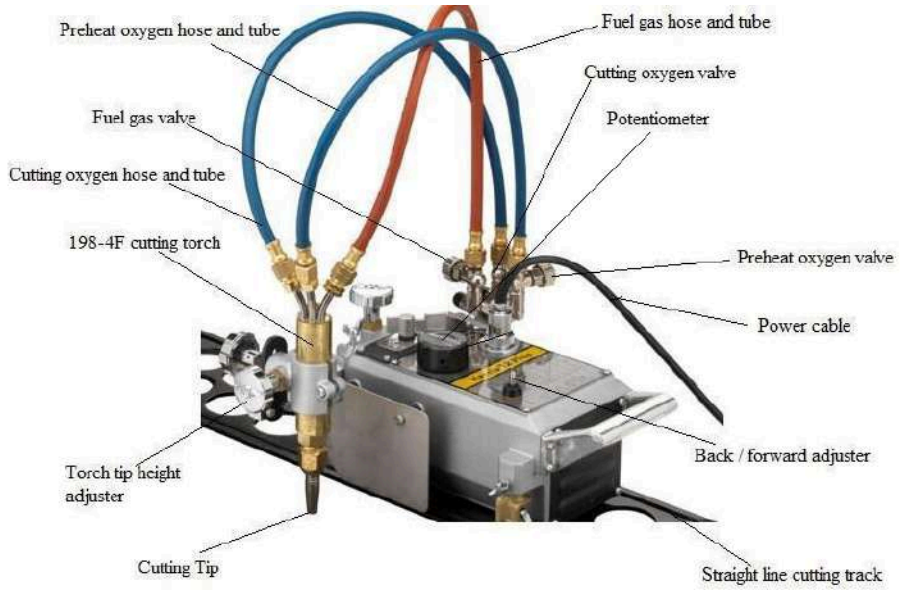


Figure 39. Harris Plus Portable Cutting System (The Harris Products Group, 2015)

Table 3: List of equipment and consumables

Description	**Specification**
Equipment	
Straight Line Cutting Machine	Portable Cutting System - Harris Plus Model - 220 V (See Appendix A)
3-meter Straight Line Cutting Track	Harris Straight Line Cutter Track 900057
Cylinder Pressure Regulators	Harris Regulator 801 Oxygen 3/8" Harris Regulator 801 Acetylene 3/8" Harris Regulator 801-4-LP 9/16"
Hardness Tester	Vickers Hardness at 300 gf and 10 sec. dwell time
SEM & EDS	Zeiss, EHT = 20.00 kV, Aperture = 60.00 µm
Optical Microscope	Olympus Model GX41F
Roughness Tester	SRT-6210 Digital Portable Roughness Tester
Stereo microscope	Nikon SMZ 745T
Consumables	

Description	Specification
Fuel Gases	-Propane (126 L/48 kg) -Acetylene (50 L/25 B/8.6 kg)
Oxidiser	Oxygen (50L/200B/14kg)
Cutting Tips	Harris Cutting Tip 6290-00 VVC LP Harris Cutting Tip 6290-3/0VVC LP Harris Cutting Tip 6290-2 VAX (See Appendix B)
Gas Delivery Hoses	Rubber 02/Oxy Blue Hose 8mm Orange LPG neoprene hose 8mm Rubber acetylene/red hose 8mm
Flashback Arrestors	Harris FBA 188TRGB Oxy RM 3/8" Harris FBA 188-1GBR8 Oxy TM 3/8" Harris FBA 188TLGB Acet RM 3/8" Harris FBA 188-1GBL8 Fuel TM 3/8"
Hose Clips	Double Ear "O" Clip 13-15 mm
Mild Steel Plate Material	EN10025-2 S355 JR+AR 400x600x8 mm 400x600x16 mm

3.2. Cutting Pre-Trials

The cutting operation requires a careful selection of various components to be integrated into the cutting machine to ensure optimal performance. In practice, cutting pre-trails are recommended to facilitate the determination of appropriate cutting parameters and components, including cutting nozzles, cutting pressure, nozzle standoff, and cutting speed. The guidelines for nozzle cutting parameters are detailed in the original equipment manufacturer (OEM) as described in Appendix B (The Harris Products Group, 2015).

3.2.1. Cutting Nozzles

The cutting nozzles were selected as follows:

- 6290-2VAX for oxy-acetylene cutting of both the 8 mm and 16 mm mild steel plate
- 6290-3/0VVC for oxy-propane cutting of the 8 mm mild steel plate
- 6290-0VVC for oxy-propane cutting of the 16 mm mild steel plate

3.2.2. Cutting Pressure

Appendix B stipulates that the cutting oxygen pressure should be 5 bar for the 6290-2 VAX and 6290-3/0 VVC nozzles and 6 bar for the 6290-0VVC nozzle. The fuel gas and cutting oxygen pressures were set at 1 bar and 6 bar, respectively, as shown in Figure 40. This approach was necessary to normalise the cutting pressure, limit the number of experimental parameters, and standardise test parameters during this study.

		
Oxygen pressure 600 kPa / 6 bar	Acetylene pressure 100 kPa / 1 bar	Propane pressure 100 kPa / 1 bar

Figure 40. Experimental cutting pressures

3.2.3. Nozzle Standoff and Flame

The optimal cutting nozzle standoff has the tip of the inner cone approximately 1 mm above the surface of the plate being cut. For a standard flame with an inner cone length of approximately 5 mm, a 6 mm and 15 mm standoff values were used. Figure 41 shows the two experimental nozzle standoffs and oxy-fuel flames.

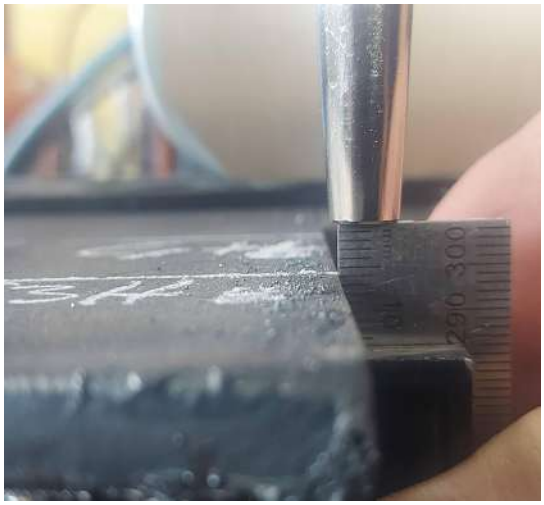
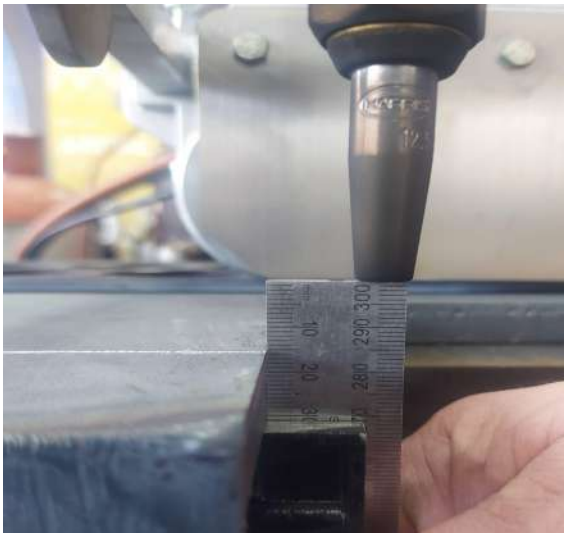
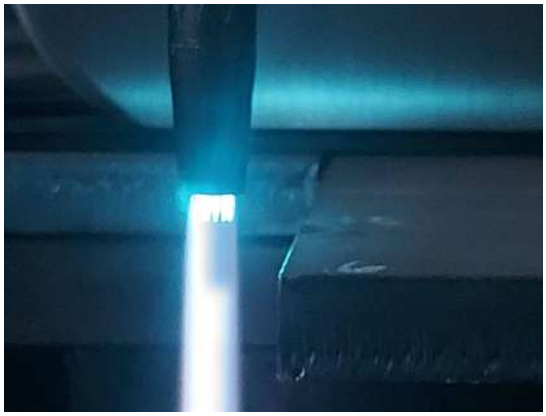
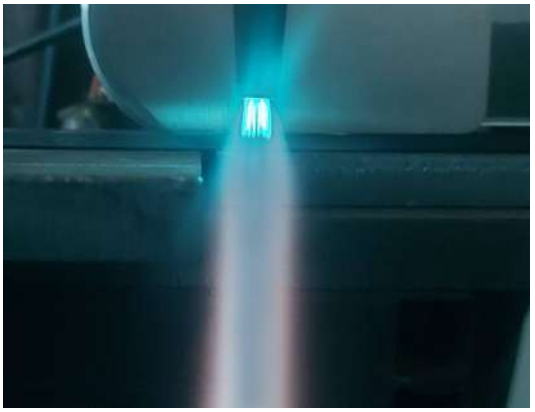
	
6 mm nozzle standoff	15 mm nozzle standoff
	
Acetylene Flame	Propane flame

Figure 41. Experimental nozzle standoff and flames

3.2.4. Cutting Speed

The cutting speed determines the quality of surface cuts. From the chart cutting speed specifications, an extrapolation approach was necessary to calculate a 'nominal average' of cutting speed for three nozzles recommended for oxy-fuel cutting of 8 mm and 16 mm plate samples. A standard deviation of plus or minus 20% was considered for each average cutting speed, determining a maximum and a minimum cutting speed, as given in Table 4.

Table 4: Cutting speed estimation

Extrapolated Cutting Speed					
Plate Thickness (mm)	Chart Cutting Speed (mm/min) VVC	Chart Cutting Speed (mm/min) VAX	Nominal Average Cutting Speed (mm/min)	Nominal Min. Cutting Speed (mm/min)	Nominal Max. Cutting Speed (mm/min)
8	647	600	623	499	748
16	613	600	607	485	728

A potentiometer was used to determine dials corresponding to nominal, minimum, and maximum cutting speeds. A calibration of the 4 - 10 potentiometer dials at 0.5 intervals was undertaken by measuring the time taken to cover a calibration distance of 200 mm for each dial setting. For instance, 10 potentials were recorded after 15.9 s, resulting in a cutting speed of 755 mm/min, as shown in Table 5.

Table 5: Potentiometer calibration

Potentiometer Dial Setting	Time (sec)	Speed (mm/min)
10	15.9	755
9.5		717
9	17.7	678
8.5		640
8	19	632
7.5		592
7	22	545
6.5	23.8	504
6	25.7	467
5.5		428
5	30.6	392
4.5		353
4	40.5	296

The selected potentiometer cutting speeds for the 8mm plate are shown in red, and those for the 16mm plate are shown in blue, Table 6 shows that the cutting speeds are within five percent of nominal cutting speeds according to OEM recommendations.

Table 6: Nominal cutting speed deviation

Plate Thickness (mm)	Chart Cutting Speed (mm/min) VVC	Chart Cutting Speed (mm/min) VAX	Nominal Average Cutting Speed (mm/min)	Nominal Min. Cutting Speed (mm/min)	Nominal Max. Cutting Speed (mm/min)
8	647	600	623	499	748
		Deviation (%)	-1%	-1%	-1%
16	613	600	607	485	728

Plate Thickness (mm)	Chart Cutting Speed (mm/min) VVC	Chart Cutting Speed (mm/min) VAX	Nominal Average Cutting Speed (mm/min)	Nominal Min. Cutting Speed (mm/min)	Nominal Max. Cutting Speed (mm/min)
		Deviation (%)	2%	4%	2%

3.3. Cutting Trial Samples

The mild steel received plate samples were cut along the 600 mm length of the plate, first beginning with the lower nozzle standoff (6 mm) and slowest cutting speed for 200 mm intervals on each of the three speeds and gradually increasing the speed to the maximum. The same was done for the higher nozzle standoff (15 mm) on a separate line of the plate which is not affected by the heat input of the cutting at a distance of 50 mm from the initial cut. Figure 42 below shows an example of the plate marking up for samples 1 to 6.

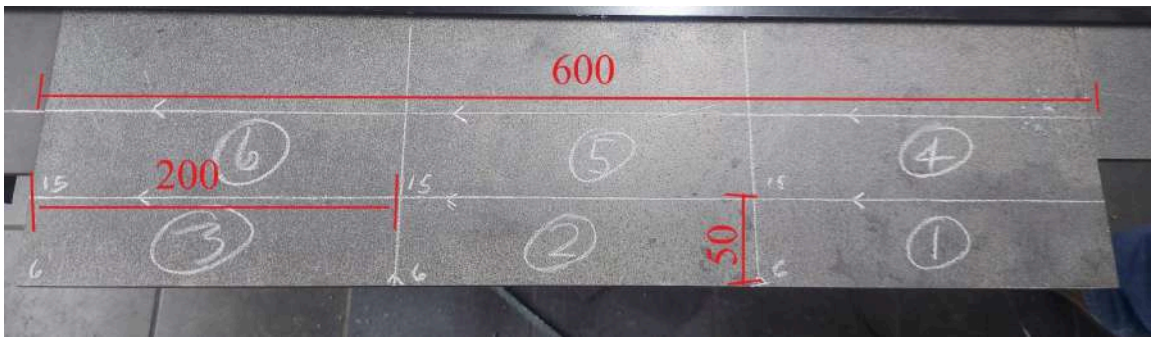
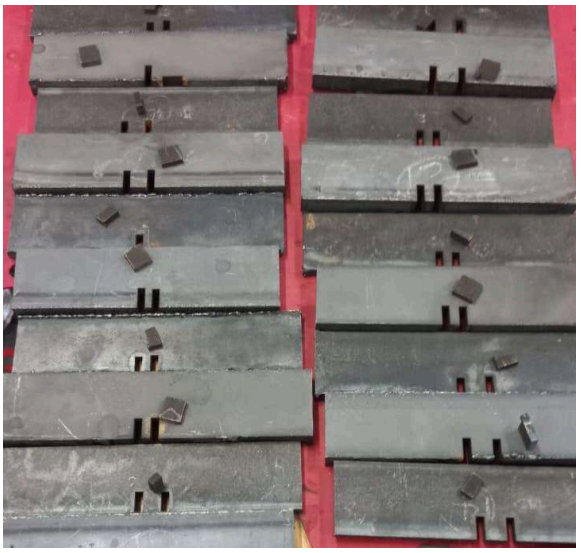


Figure 42. Sample preparation example for 8 mm thick plate for the 6 mm (No 1-3) and 15mm (No. 4 - 6) nozzle standoff

The as-cut samples (Figure 42, No 1-2-3 samples, for instance) were further cut to separate the three test pieces, obtained at varying cutting speeds, using a bandsaw machine, as shown in Figure 43. Each test piece to be analysed was 200 x 50 x thickness (8 mm & 16 mm). The total number of coupons was 24 rectangular section pieces (Figure 43, right).





Bandsaw mechanical cutting machine	200 mm x50 mm x 8 or 16 mm test pieces

Figure 43. Sample preparation - Bandsaw

Table 7 summarises the parameters used to prepare samples, namely 1 - 12, which were cut with oxy-acetylene. 6 samples of each thickness (8 mm and 12 mm) were considered for cutting experiments. The width and length of steel samples remained constant for consistency purposes.

Table 7: Oxy-acetylene sample cutting parameters

Sample Number	Thickness (mm)	Fuel Gas	Nozzle type	Nozzle standoff (mm)	Cutting Speed (mm/min)	Oxygen Pressure (bar)	Fuel Gas Pressure (bar)
1	8	Acetylene	6290-2 VAX	6	504	6	1
2	8	Acetylene	6290-2 VAX	6	632	6	1
3	8	Acetylene	6290-2 VAX	6	755	6	1
4	8	Acetylene	6290-2 VAX	15	504	6	1

Sample Number	Thickness (mm)	Fuel Gas	Nozzle type	Nozzle standoff (mm)	Cutting Speed (mm/min)	Oxygen Pressure (bar)	Fuel Gas Pressure (bar)
5	8	Acetylene	6290-2 VAX	15	632	6	1
6	8	Acetylene	6290-2 VAX	15	755	6	1
7	16	Acetylene	6290-2 VAX	6	467	6	1
8	16	Acetylene	6290-2 VAX	6	592	6	1
9	16	Acetylene	6290-2 VAX	6	717	6	1
10	16	Acetylene	6290-2 VAX	15	467	6	1
11	16	Acetylene	6290-2 VAX	15	592	6	1
12	16	Acetylene	6290-2 VAX	15	717	6	1

Similarly, 6 samples of each thickness, 8 mm and 16 mm were prepared for oxy-propane cutting. Table 8 shows the oxy-fuel cutting parameters for sample numbers 13 - 24.

Table 8: Oxy-propane sample cutting parameters

Sample Number	Plate Thickness (mm)	Fuel Gas	Cutting Nozzle	Cutting Nozzle standoff (mm)	Cutting Speed (mm/min)	Oxygen Pressure (bar)	Fuel Gas Pressure (bar)
13	8	Propane	6290-3/0 VVC	6	504	6	1
14	8	Propane	6290-3/0 VVC	6	632	6	1
15	8	Propane	6290-3/0 VVC	6	755	6	1
16	8	Propane	6290-3/0 VVC	15	504	6	1
17	8	Propane	6290-3/0 VVC	15	632	6	1
18	8	Propane	6290-3/0 VVC	15	755	6	1
19	16	Propane	6290-0V VC	6	467	6	1
20	16	Propane	6290-0V VC	6	592	6	1
21	16	Propane	6290-0V VC	6	717	6	1
22	16	Propane	6290-0V VC	15	467	6	1
23	16	Propane	6290-0V VC	15	592	6	1
24	16	Propane	6290-0V VC	15	717	6	1

3.4. Characterisation of steel samples

3.4.1. Base Material Composition

The base mild steel material received from the supplier was used in the as-received condition during the cutting experiments. The material was manufactured to comply with the structural steel standard SANS 50025 (South African National Standards for steel) / EN 10025-2. This designation is the standard for technical delivery conditions for non-alloy structural steels. The grade of the studied steel is S355 JR + AR. The breakdown of the steel's grade symbols is S- Structural steel, 355- the minimum yield strength in Mpa, JR- longitudinal charpy v-notch impacts are minimum 27 joules at 20℃, AR - the supplied condition is as rolled.

The test certificate supplied corresponds with BS EN 10204 (British Standard - Engineering), which is the standard for different types of inspection certificates for metallic products. Type 3.1 is an inspection certificate whereby the test results are generated from an actual specific test. In the case of the studied steel, the test certificate references a specific heat and or lot number produced. The test certificate chemical composition is given in Table 9 below and the test report can be found in Appendix F.

Table 9: Base Material Test Report

Chemical Composition (%)															
T (mm)	Heat No.	C	Si	Mn	P	S	Cr	Ni	Cu	V	Ti	Al	Mo	N	B
8	23104493A	0.15	0.3	1.45	0.024	0.005	0.02	0.005	0.01	0.001	0.015	0.029	0.003	0.0037	0.00050
16	J27-14541A	0.16	0.3	1.38	0.016	0.002	0.07	0.010	0.02	0.003	0.011	0.021	0.003	0.0030	0.00003

3.4.2. Cutting Process Visual Examination

The inclination of the cutting oxygen jet was observed for each sample during the cutting process. After sample cutting, a slag detachability test was carried out on the bottom of the cut face which will not be further for the below characterisation techniques. A steel scraper was used for the test on the cut face on the opposite end of the kerf for each of the cut samples. The examinable face on the other end of the kerf was left with the slag for the SEM and EDS evaluation.

3.4.3. Macro Examination

To conduct the metallurgical macro examination, a section of the 200x50x8 mm and 200x50x16 mm samples was examined at 50X magnification using the stereo microscope scope for the macro profile. The as-cut face was also visually examined to assess the extent of gouging, draglines, and slag coverage.

3.4.4. Surface Roughness Testing

The profilometer used to evaluate the surface roughness of the samples employs a contact-based measurement technique where a diamond-tipped stylus is traversed across the sample surface. The profilometer settings were configured with a cut-off length of 15.0 mm. 30000 points were measured across the length at the top, middle, and bottom of each respective cut face to provide an optimal balance between measurement accuracy and surface characteristics. Roughness parameters examined included the average surface roughness (Ra) and the average maximum profile height (Rz), which collectively offered a comprehensive assessment of the surface texture.

3.4.5. Test Piece Sample Preparation

The test pieces were prepared for hardness and metallographic analysis. These samples were obtained by carefully sectioning the 200 x 50 x 8 mm and 200 x 50 x 16 mm rectangular pieces, using a precision wire cutter (Figure 44). The wire-cutting technique was employed to achieve accurate and clean cuts, reducing the potential for mechanical damage or alteration of the microstructure at the cutting edges and most importantly, ensuring the slag at the bottom remains intact for post-analysis.

The sectioned samples were then subjected to further standard metallographic preparation techniques. These samples were hot-mounted in a resin (polyfast) and then ground through a series of progressively finer abrasive papers. The sample cross-sections were finally polished to achieve a mirror-like surface using diamond paste (9 µm, 3 µm, and 1 µm suspension). For metallographic analysis, each sample was further submitted to etching using a suitable reagent, 3% nital (3% v/v nitric acid in methanol), to reveal the microstructural features. Hardness testing did not require the etching of samples.

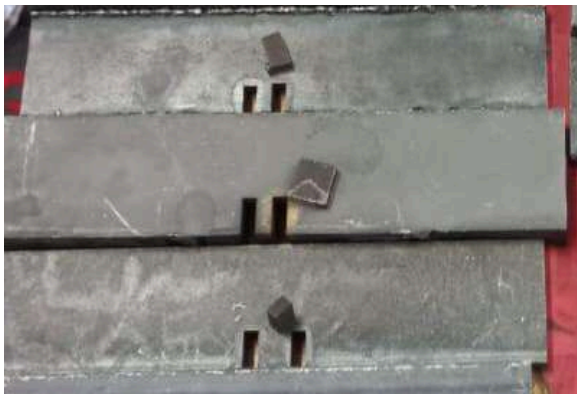
	
Wire cutter mechanical cutting machine	Test pieces cut out
	
Test sample cut	Mounted samples

Figure 44. Sample preparation - Wire cutter and mounting

3.4.6. Hardness Testing

A Vickers hardness survey was conducted on polished samples using a test load of 300 gf and a dwell time of 10 seconds. 10 micro-indentation measurements were taken at constant incremental intervals from the top surface of the sample to a distance of approximately 2 mm into the cut face of the test samples.

3.4.7. SEM and EDS Evaluation

Scanning electron microscopy (SEM) and energy-dispersive X-ray spectroscopy (EDS or EDX) analysis were conducted to obtain detailed information about the microstructure and

elemental composition of the cut samples. The 3 or 4 etched samples were mounted together on a stage in the sample chamber of a scanning electron microscope. An aluminum tap bound all samples to ensure electrical conductivity and prevent charging effects during imaging.

SEM analysis mapping was performed using a Zeiss scanning electron microscope. The microscope was operated at an accelerating voltage of 20 kV, with an aperture of 60 μm, to achieve high-resolution images of the microscopic features. The SEM was utilised to examine structural elements of both the base steel and slag, including defects and adherence of the slag to the bottom of the cut face, at magnifications ranging from 200X, 500X, 1000X, and 2000X, depending on the level of detail required.

For compositional analysis, EDS was conducted using an Oxford Instruments a-act 50 EDS detector attached to the SEM. The analysis focused on identifying and quantifying the elemental composition of different phases or oxides observed in the slag SEM images. Key variables examined included atomic percentages of elements and the distribution of major alloying elements, which were critical for understanding the slag composition and properties. The EDS equipment was later upgraded to the most recent version of which samples 1, 11, 18, 20, 21, and 23 were analysed.

3.4.8. Optical Microscope

An optical microscope equipped with 10x, 20x, and 50x objective lenses and a digital camera for image capture was used for metallurgical optical microscope examination. The cut face of the base material was analysed to determine the morphology of phases and phase distribution.

-

Chapter 4 - Results

4.1. Cutting Process Visual Examination

The cut face of each test piece was visually examined for slag adherence, inclination of the cutting oxygen jet, and gouges. The observations are summarised in Table 10. Sample numbers 9, 12 and 24 were not examined due to termination of the cut as the cutting speed was gradually increased.

Adherent slag is observed in samples 1 - 6, 11, 14, 20 -21 and 23. The rest of the samples have non-adherant slag.

Table 10: Visual examination of the cut face

Sample #	Slag adherence	Oxygen jet inclination	Gouges (Y/N)	OFC Flame	As-cut face
1	Adherent	Forward	N		
2	Adherent	Perpendicular	N		
3	Adherent	Backward	N		

Sample #	Slag adherence	Oxygen jet inclination	Gouges (Y/N)	OFC Flame	As-cut face
4	Adherent	Forward	N		
5	Adherent	Perpendicular	N		
6*	Adherent	Backward*	N		
7	Non Adherent	Forward	N		
8	Non Adherent	Erratic	N		

Sample #	Slag adherence	Oxygen jet inclination	Gouges (Y/N)	OFC Flame	As-cut face
10	Non Adherent	Forward	N		
11	Adherent	Erratic	N		
13	Non Adherent	Forward	N		
14	Adherent	Perpendicular	N		
15	Non Adherent	Backward-erratic	N		

Sample #	Slag adherence	Oxygen jet inclination	Gouges (Y/N)	OFC Flame	As-cut face
16	Non Adherent	Forward	N		
17	Non Adherent	Forward	N		
18	Non Adherent	Backward-erratic	N		
19	Non Adherent	Forward	N		
20	Adherent	Perpendicular-erratic	N		

Sample #	Slag adherence	Oxygen jet inclination	Gouges (Y/N)	OFC Flame	As-cut face
21	Adherent	Perpendicular-erratic	N		
22	Non Adherent	Forward	N		
23	Adherent	Perpendicular-erratic	N		

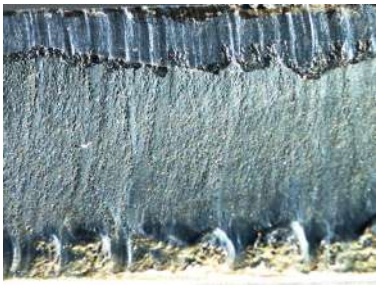
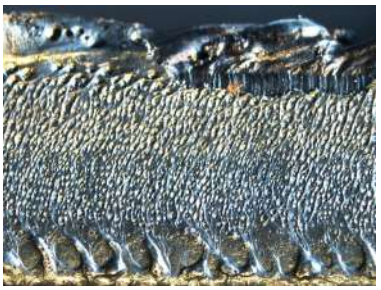
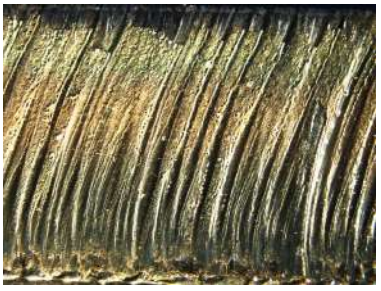
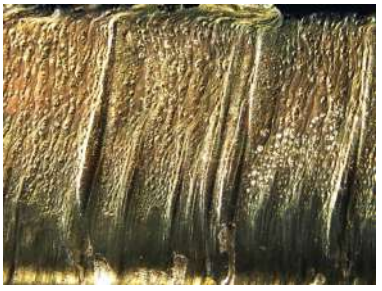
*Flame travelling left to right

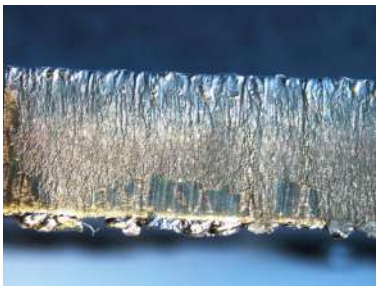
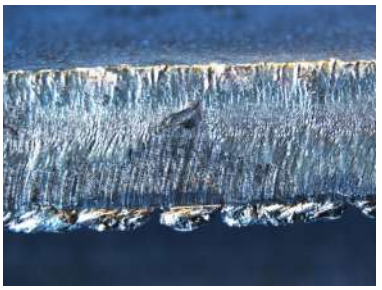
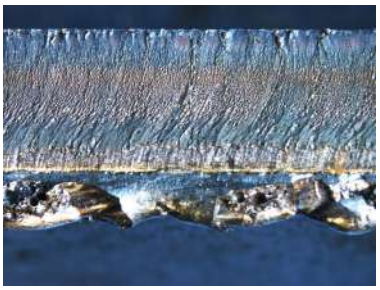
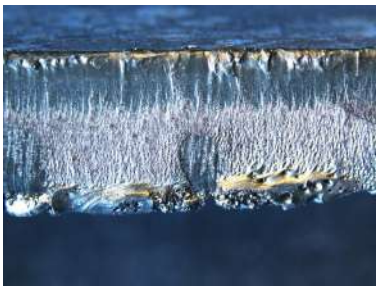
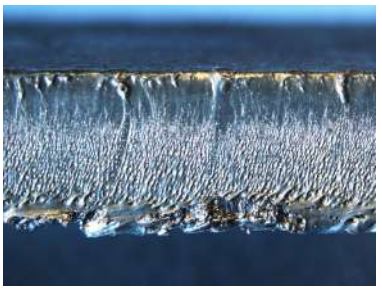
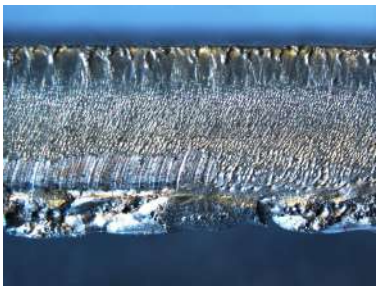
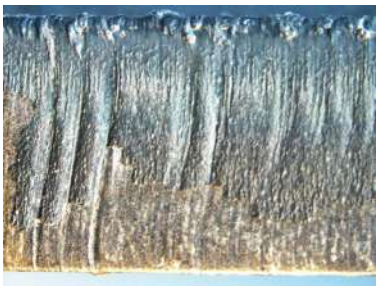
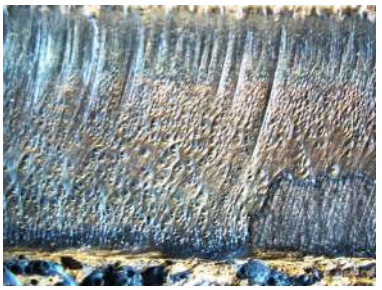
4.2. Macro Examination

Images of the macro examination from the stereo microscope are shown in Table 11. The images are identified by sample number, fuel gas, thickness, standoff, and cutting speed. For nomenclature purposes, SO_1 is the 6 mm standoff. SO_2 is the 15 mm standoff. Vc_1, Vc_2, Vc_3, Vc_4, Vc_5, and Vc6 represent cutting speeds of 504 mm/min, 632 mm/min, 755 mm/min, 467 mm/min, 592 mm/min, and 717 mm/min.

The thinner samples (8 mm thick) have a cut surface that is predominately fibrous whereas the thicker samples (16 mm) show a cut surface with predominantly draglines.

Table 11: Macro examination of the cut face

		
1. acetylene - 8 mm - SO_1 - Vc_1	2. acetylene - 8 mm - SO_1 - Vc_2	3. acetylene - 8 mm - SO_1 - Vc_3
		
4. acetylene - 8 mm - SO_2 - Vc_1	5. acetylene - 8 mm - SO_2 - Vc_2	6. acetylene - 8 mm - SO_2 - Vc_3
		
7. acetylene - 16 mm - SO_1 - Vc_4	8. acetylene - 16 mm - SO_1 - Vc_5	10. acetylene - 16 mm - SO_2 - Vc_4

		
11. acetylene - 16 mm - SO_2 - Vc_5	13. Propane - 8mm - SO_1 - Vc_1	14. Propane - 8mm - SO_1 - Vc_2
		
15. Propane - 8mm - SO_1 - V_3	16. Propane - 8mm - SO_2 - V_1	17. Propane - 8mm - SO_2 - V_2
		
18. Propane - 8mm - SO_2 - Vc_3	19. Propane - 16mm - SO_1 - Vc_4	20. Propane - 16mm - SO_1 - Vc_5
		
21. Propane - 16mm - SO_1 - Vc_6	22. Propane - 16mm - SO_2 - Vc_4	23. Propane - 16mm - SO_2 - Vc_5

4.3. Surface Roughness

The results of the surface roughness test are given in Appendix D and summarised in Tables 12 and 13, showing the Ra and Rz5 parameters. Ra is a measurement of the sum of the height of the peak and depth of the valley points whilst Rz5 represents the average of five outlying single measured distances.

The surface roughness of the oxy-acetylene samples has an Ra value ranging from 27 - 83 µm whereas the oxy-propane is 30 - 98 µm. The Rz5 range is 72 - 161 µm and 57 - 117 µm respectively.

Table 12: Surface roughness (Ra) and (Rz5) - Acetylene

No.	A (Top)		B (Middle)		C (Bottom)		**Sample Average**	
	Ra (µm)	Rz (µm)	Ra (µm)	Rz (µm)	Ra (µm)	Rz (µm)	**Ra (µm)**	**Rz5 (µm)**
1	48	66	10	65	25	85	**28**	**72**
2	17	61	22	81	43	110	**27**	**84**
3	44	83	57	80	38	66	**47**	**76**
4	39	101	17	91	28	50	**28**	**81**
5	127	92	55	84	66	81	**83**	**86**
6	42	78	69	70	115	83	**75**	**77**
7	49	154	60	147	71	169	**60**	**157**
8	36	150	49	164	58	170	**48**	**161**
10	29	123	35	104	48	119	**37**	**115**
11	37	75	64	185	80	169	**60**	**143**

Table 13: Surface roughness (Ra) and (Rz5) - Propane

No.	A (Top)		B (Middle)		C (Bottom)		**Sample Average**	
	Ra (µm)	Rz (µm)	Ra (µm)	Rz (µm)	Ra (µm)	Rz (µm)	**Ra (µm)**	**Rz5 (µm)**
13	62	48	36	59	30	64	**43**	**57**
14	101	54	97	84	97	84	**98**	**74**
15	44	62	44	81	37	80	**42**	**75**
16	39	100	37	86	34	78	**37**	**88**
17	35	92	36	63	21	48	**30**	**68**
18	59	71	29	77	68	98	**52**	**82**

No.	A (Top)		B (Middle)		C (Bottom)		**Sample Average**	
	Ra (µm)	Rz (µm)	Ra (µm)	Rz (µm)	Ra (µm)	Rz (µm)	**Ra (µm)**	**Rz5 (µm)**
19	77	86	72	109	70	106	**73**	**100**
20	58	64	86	131	67	114	**70**	**103**
21	67	114	70	114	43	55	**60**	**95**
22	40	128	18	105	45	120	**34**	**117**
23	13	45	13	45	33	120	**20**	**70**

4.4. Transverse Hardness

For each sample, transverse hardness results are given in Appendix E. Table 14 presents a summary of the maximum, minimum, and average hardness results. The samples have dispersed values of the measured standard deviation. No clear trend can be deduced.

Table 14: Vickers Hardness

Sample No.	Max (HV)	Min (HV)	Avg (HV)	STD (HV)
1	189	122	171	21
2	195	164	185	8
3	191	161	178	8
4	192	125	172	15
5	200	165	187	9
6	188	155	178	9
7	365	220	295	53
8	153	139	145	4
10	375	189	275	66
11	276	182	209	33
13	182	150	173	8
14	186	165	176	5
15	188	137	174	12
16	179	154	168	6
17	184	163	173	5
18	178	130	161	12
19	357	213	291	42
20	337	150	237	46
21	321	158	197	51

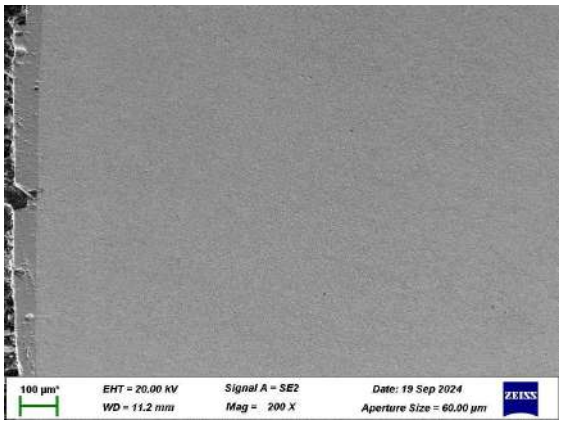
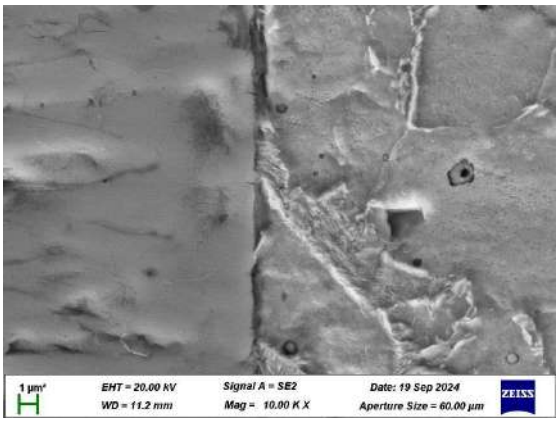
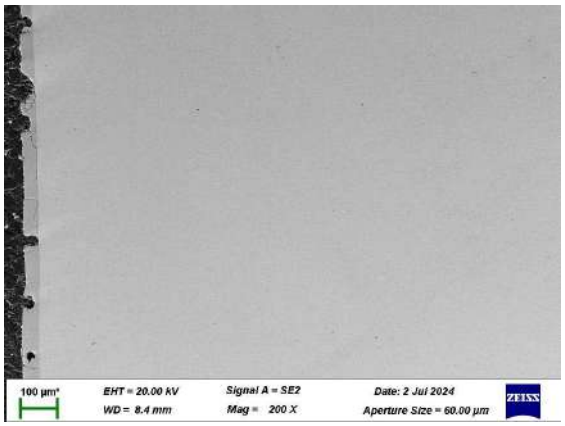
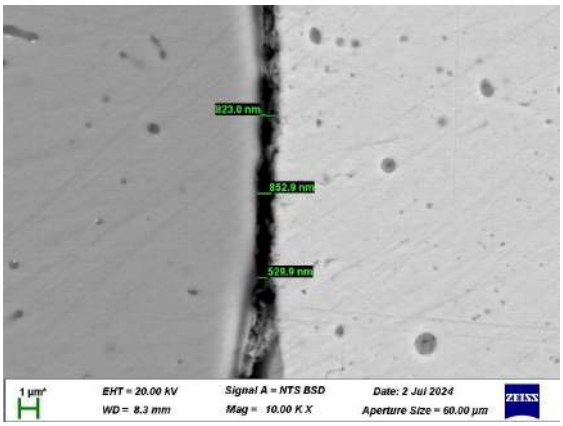
22	189	130	145	15
23	305	153	206	52

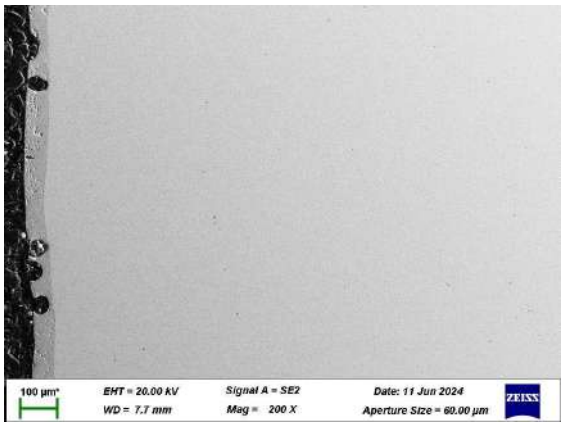
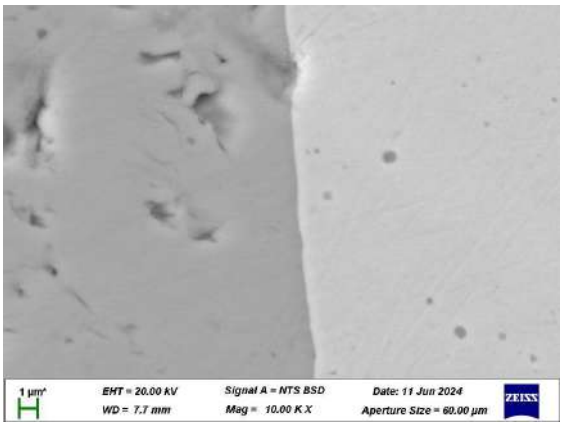
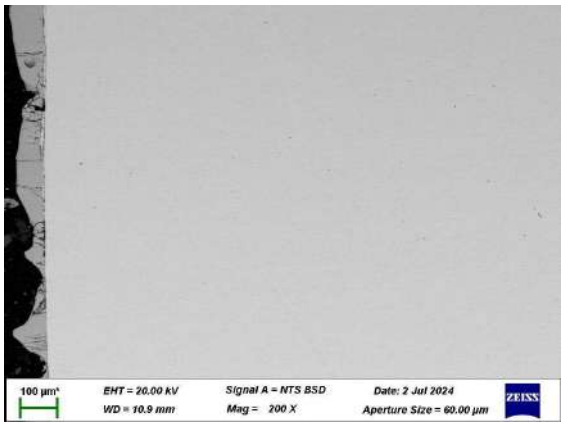
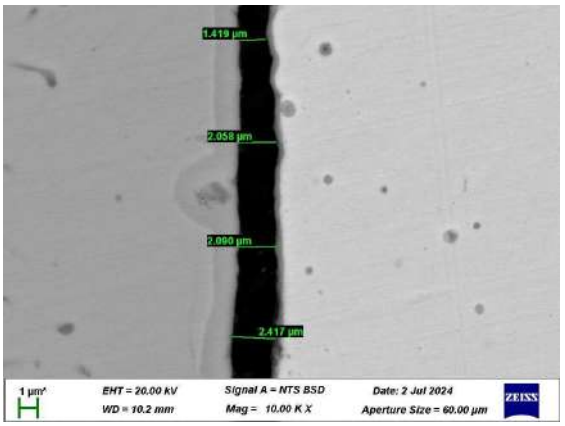
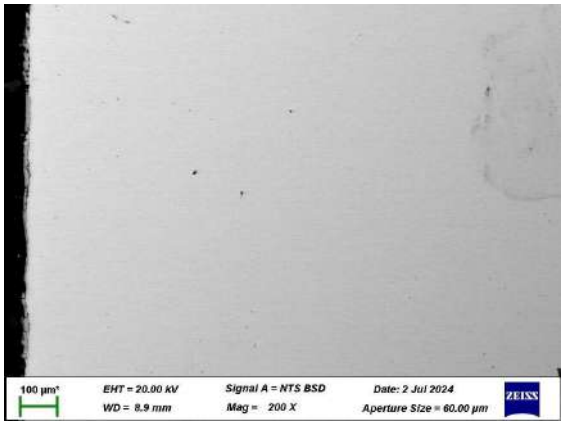
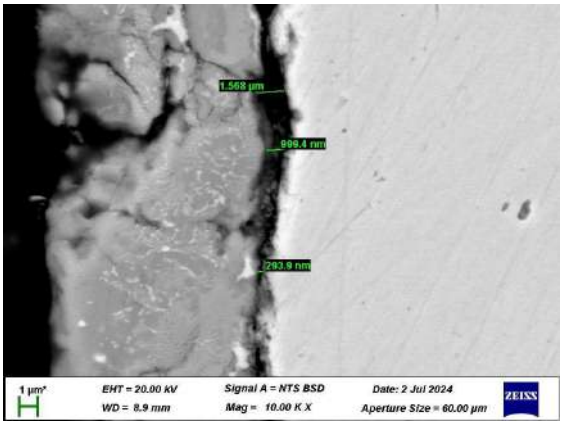
4.5. SEM and EDS Analysis

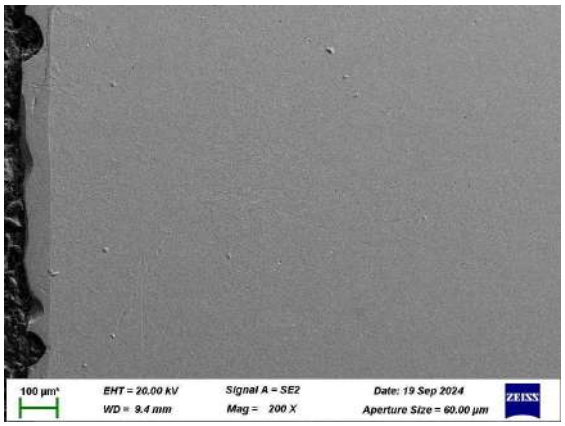
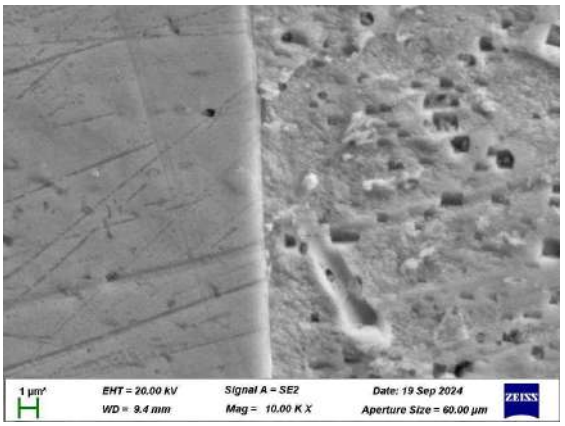
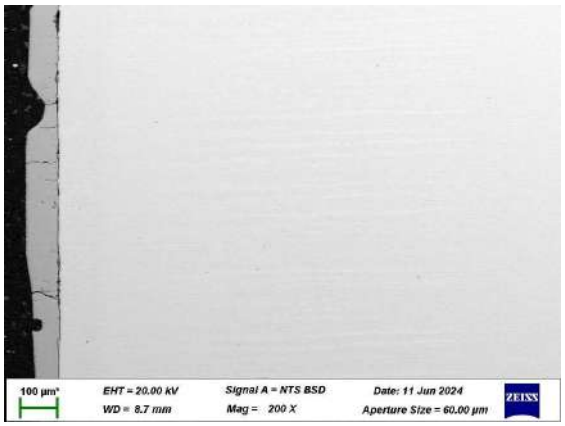
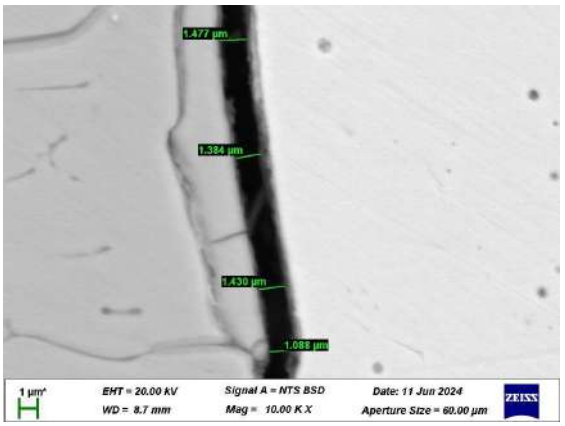
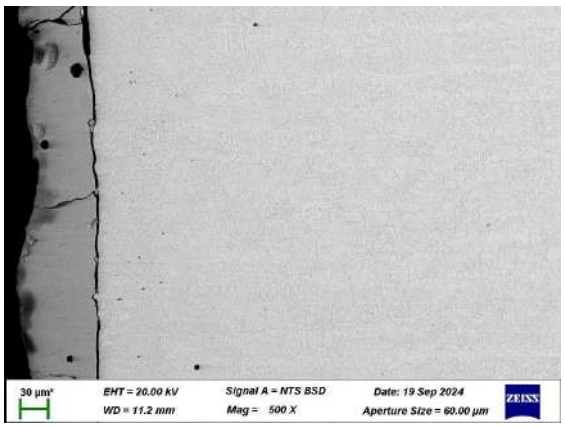
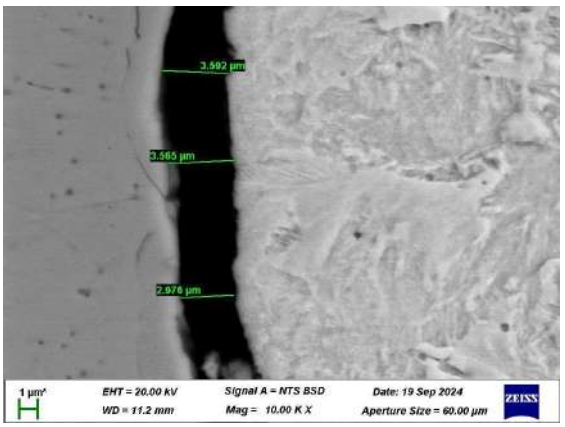
The SEM images taken for each sample number (#) at magnifications of 200X and 10000X, presenting the gap where applicable are shown in Table 15. The elemental composition of slag from EDS analysis is displayed in Table 16 for each sample.

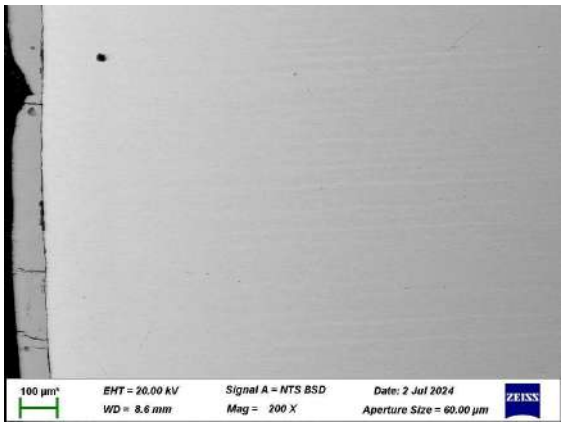
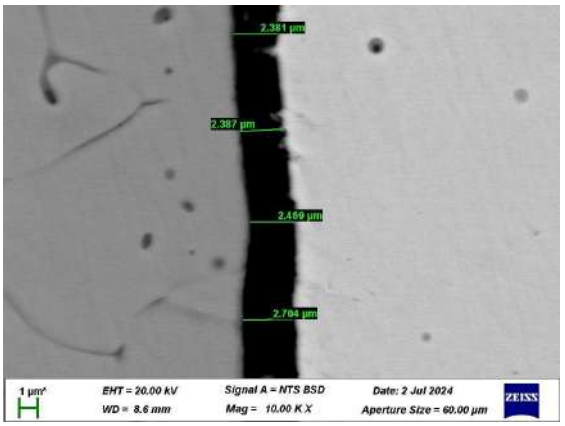
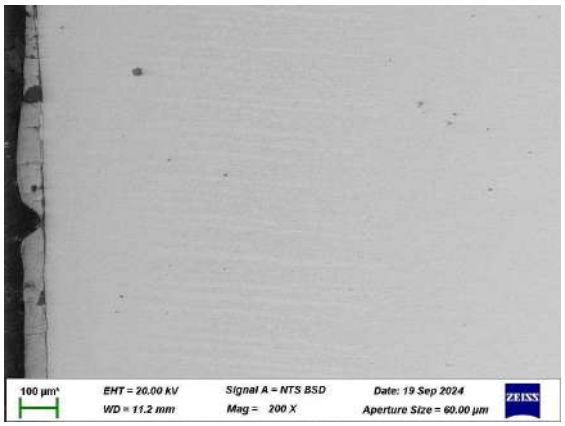
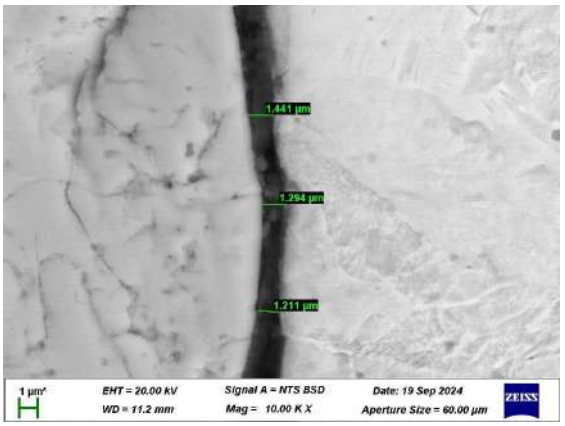
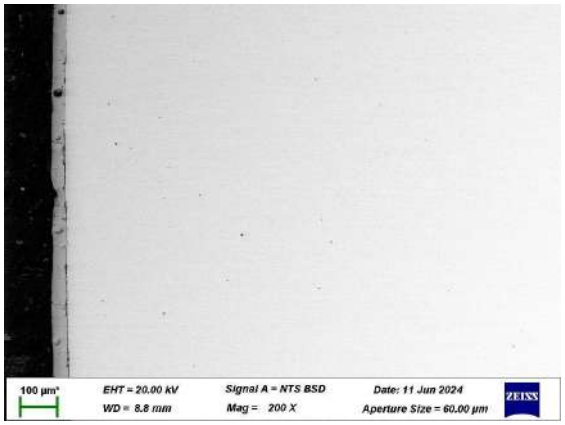
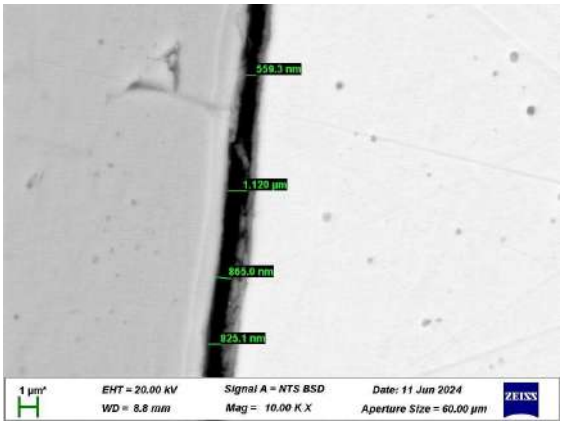
Based on microscopic analysis, adherent slag is observed in samples 1,3, 6, 16, 19 and 22 - 23. The rest of the samples have non-adherant slag. In comparison to the visual observation in Table 1 wherein samples 1 - 6, 11, 14, 20 -21 and 23 were adherent.

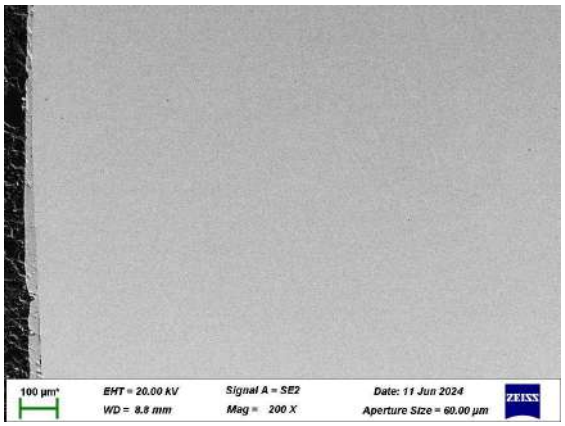
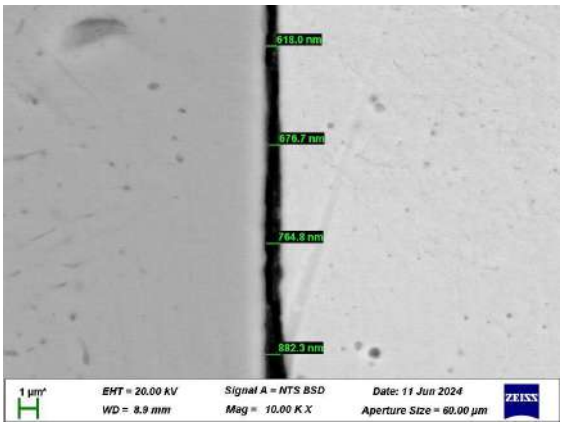
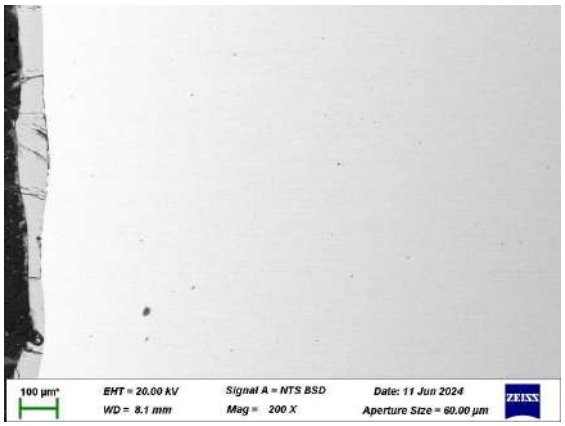
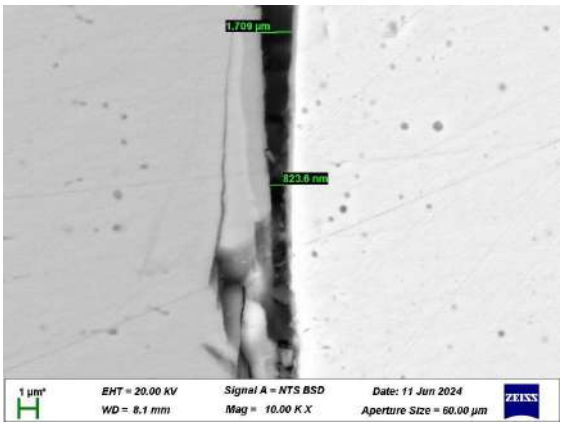
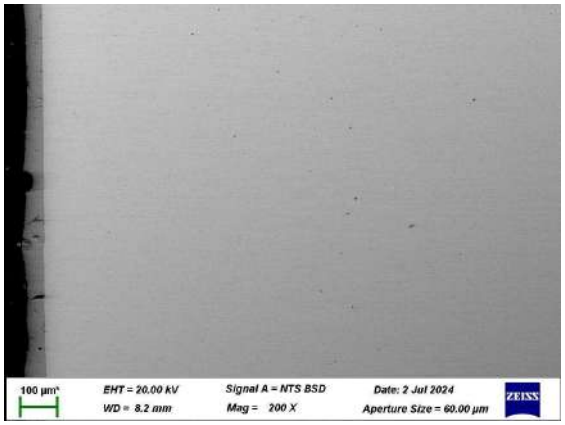
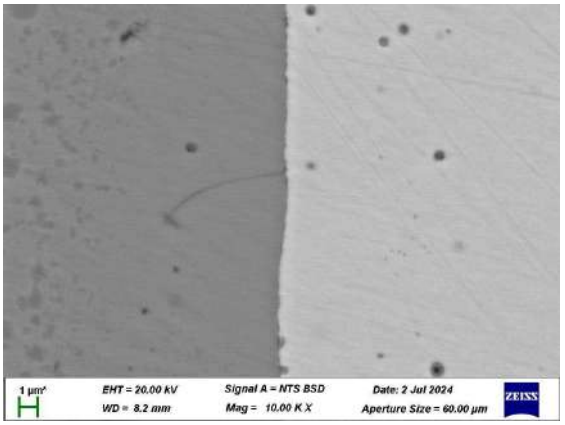
Table 15: SEM Analysis

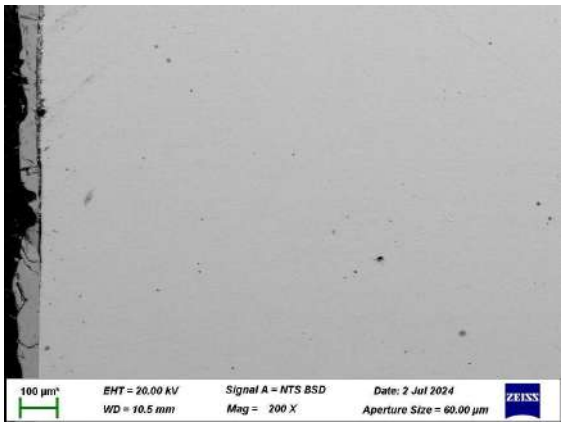
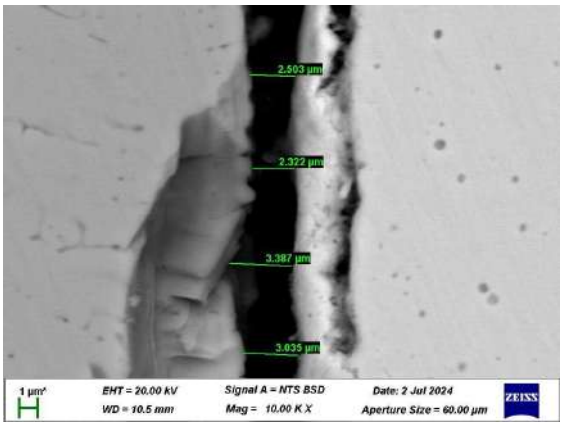
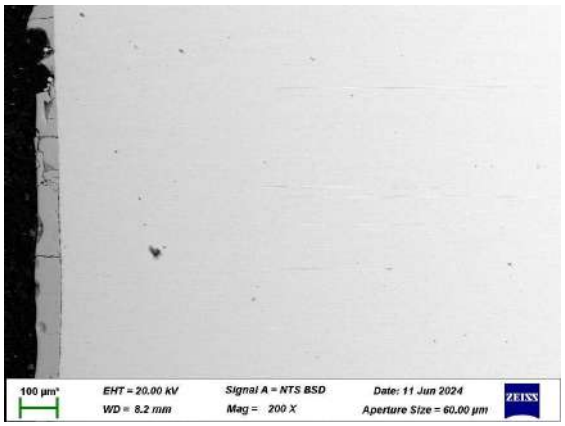
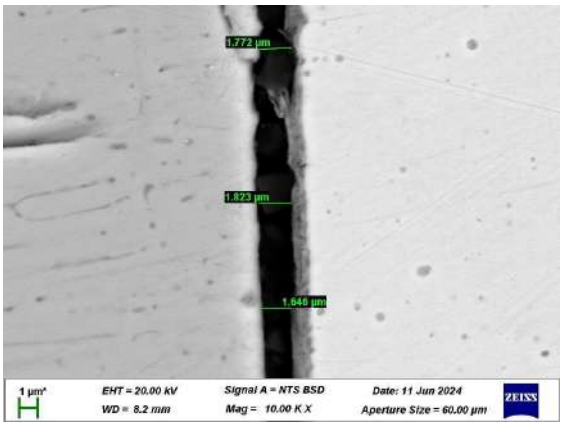
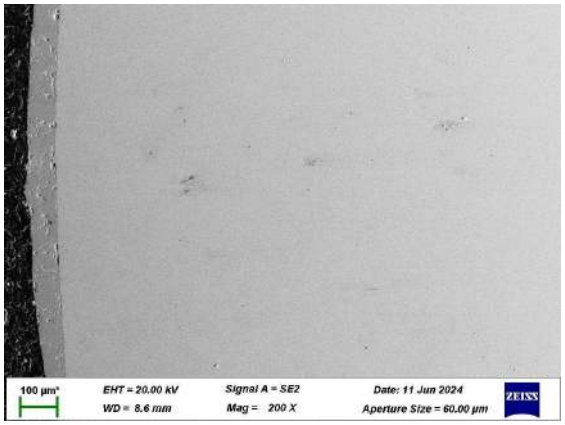
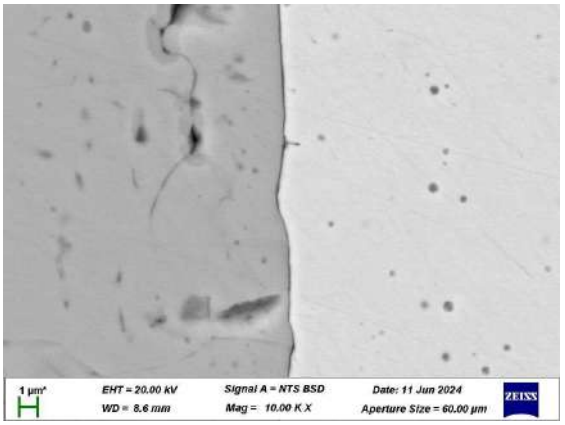
#	Image at 200 X	Image at 10000 X
1		
2		

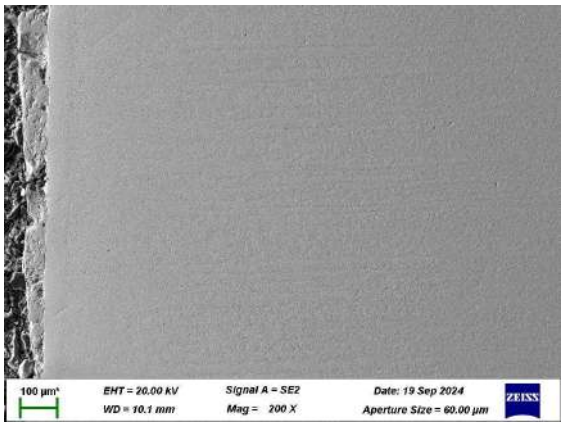
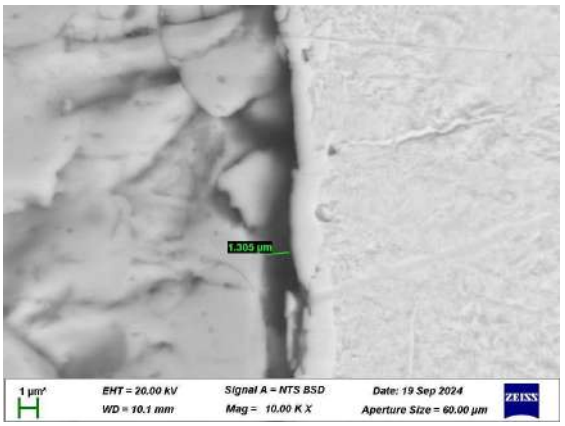
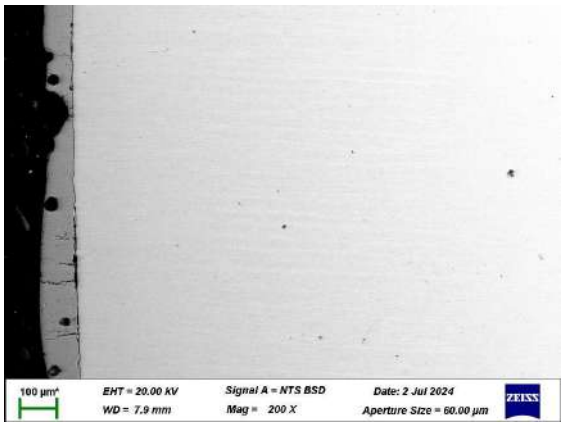
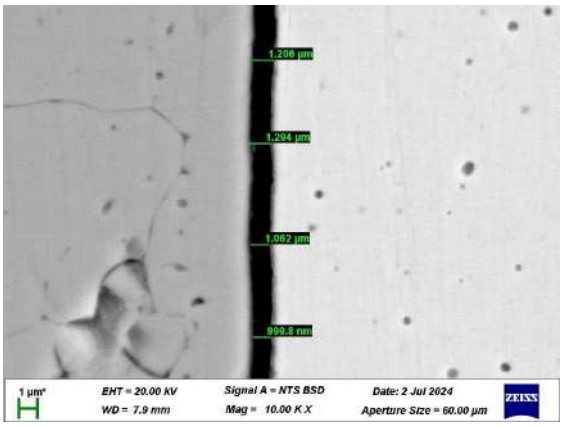
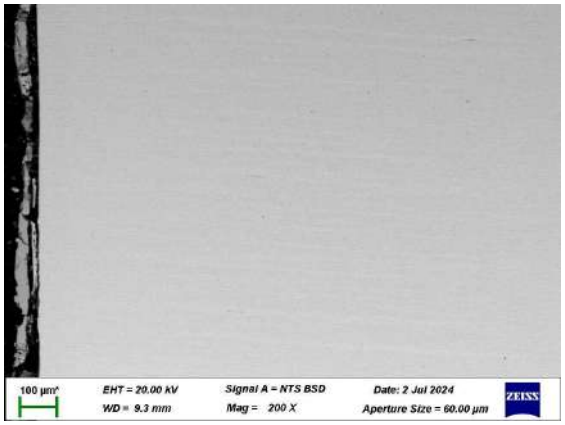
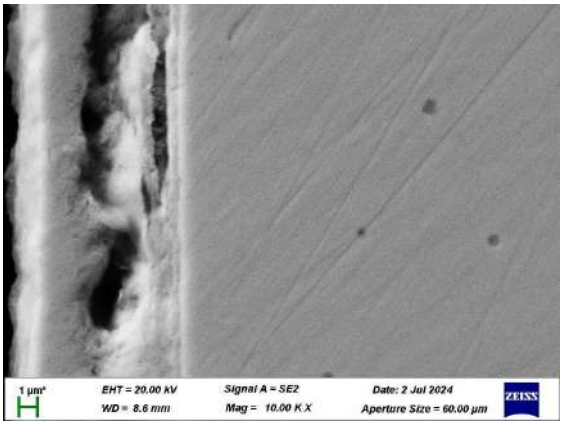
#	Image at 200 X	Image at 10000 X
3		
4		
5		

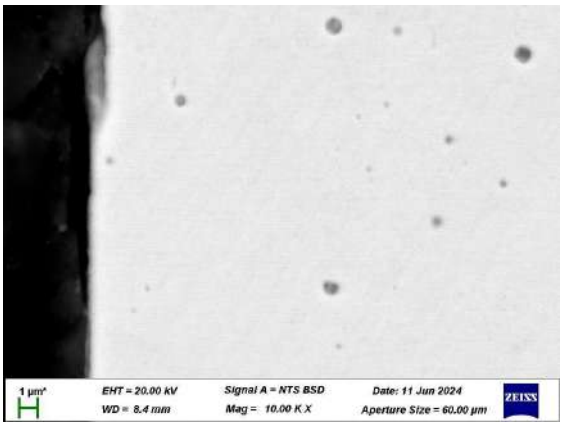
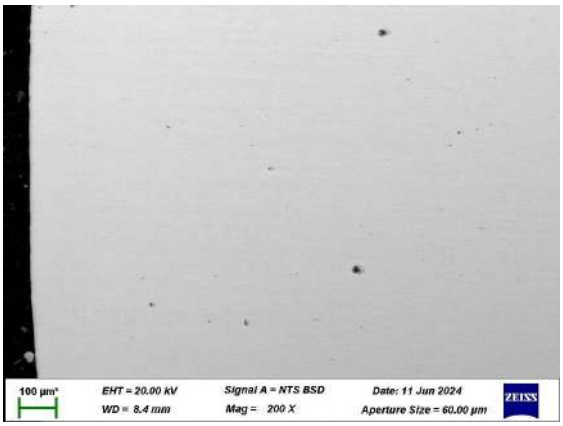
#	Image at 200 X	Image at 10000 X
6		
7		
8*		

#	Image at 200 X	Image at 10000 X
10		
11		
13		

#	Image at 200 X	Image at 10000 X
14		
15		
16		

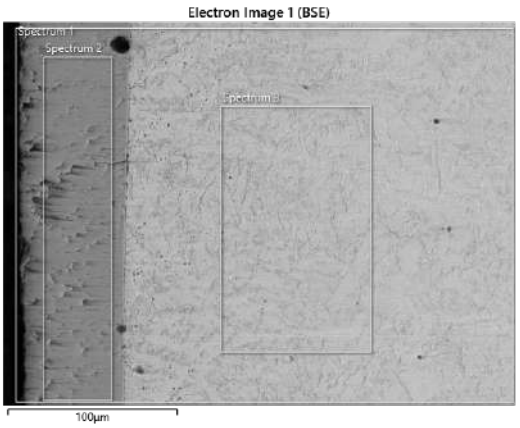
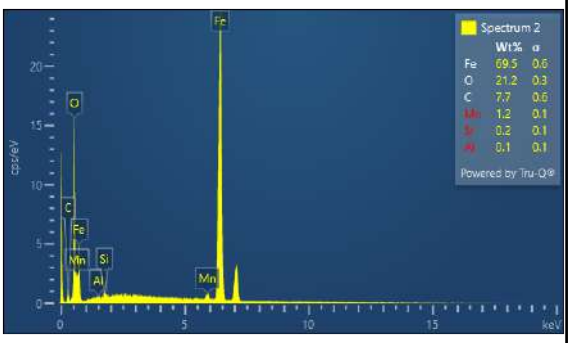
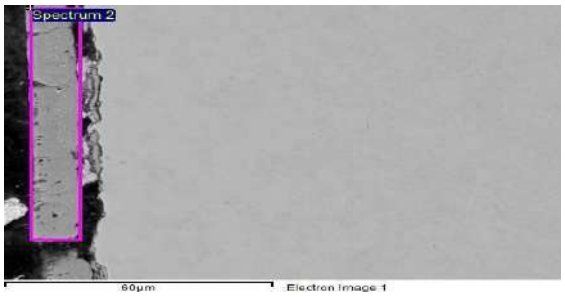
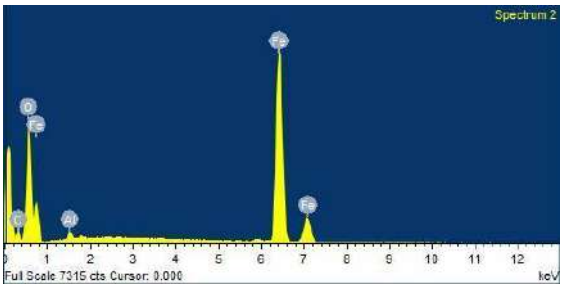
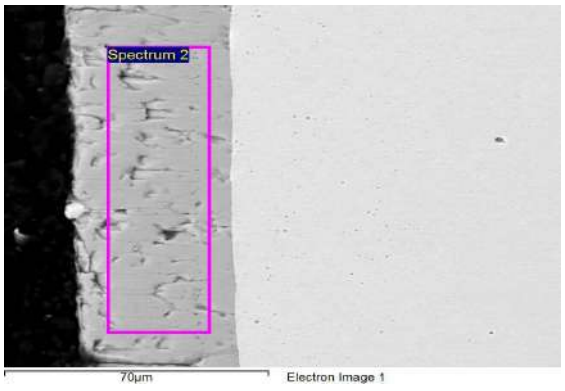
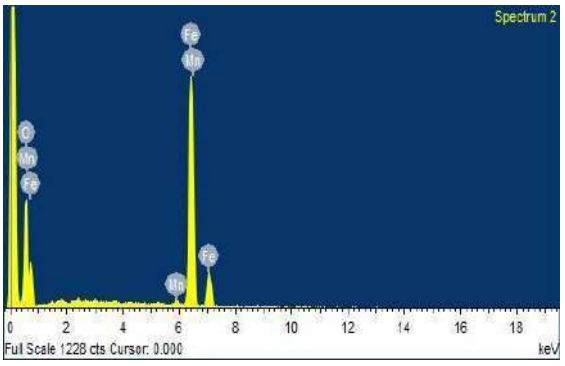
#	Image at 200 X	Image at 10000 X
17		
18		
19		

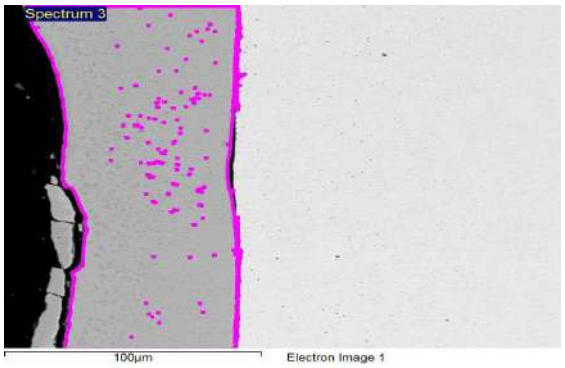
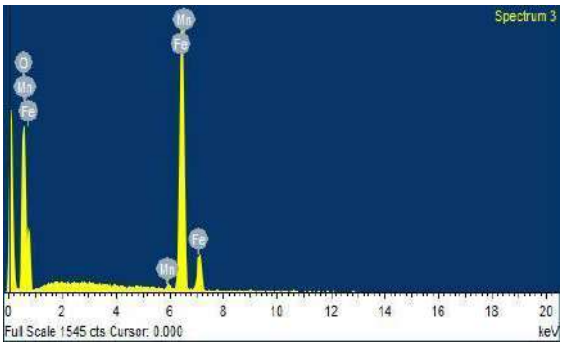
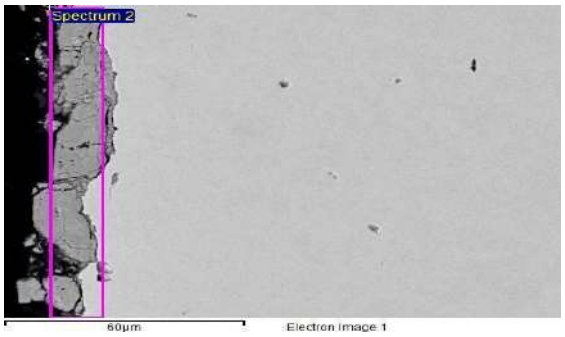
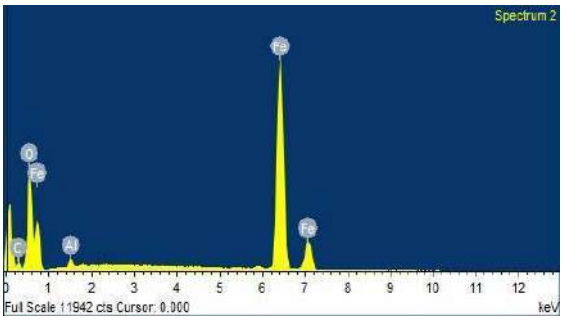
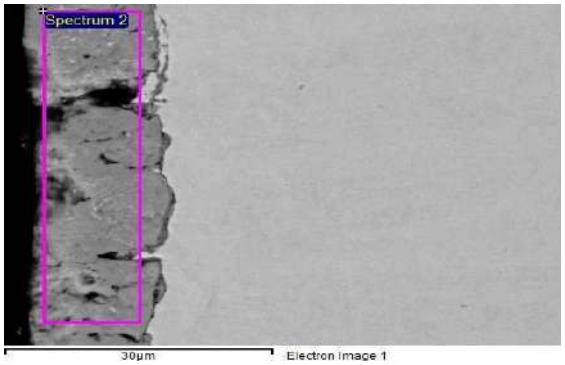
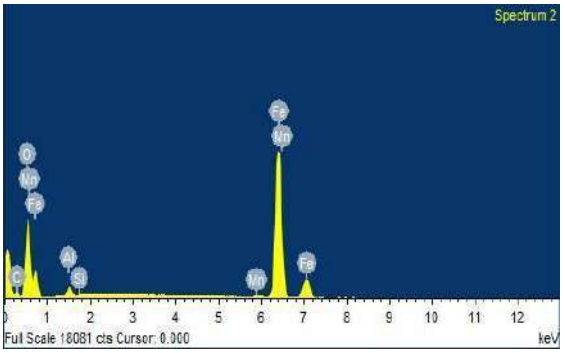
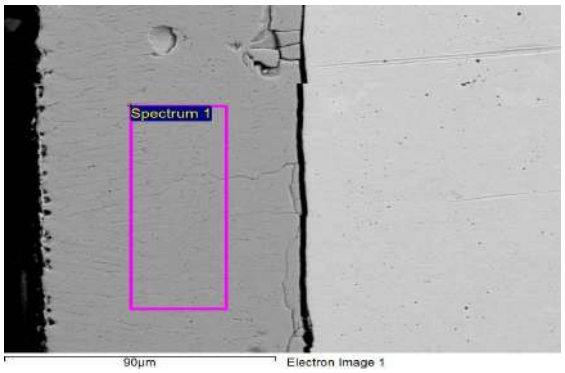
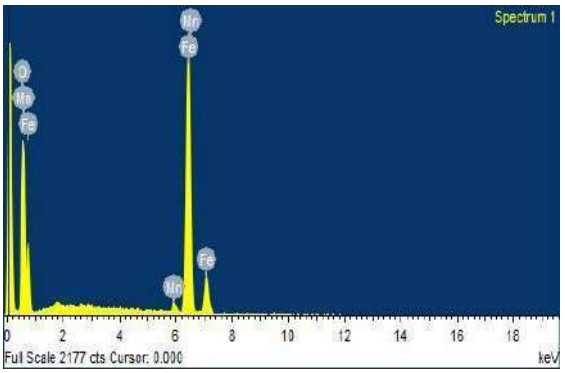
#	Image at 200 X	Image at 10000 X
20		
21		
22		

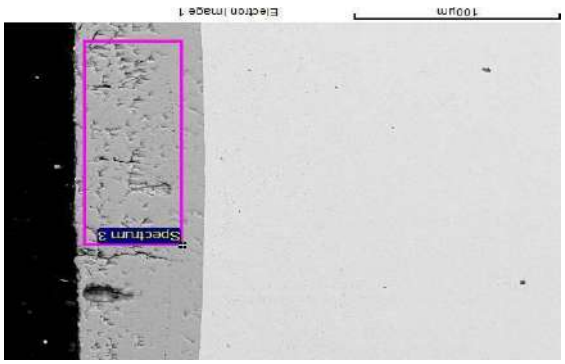
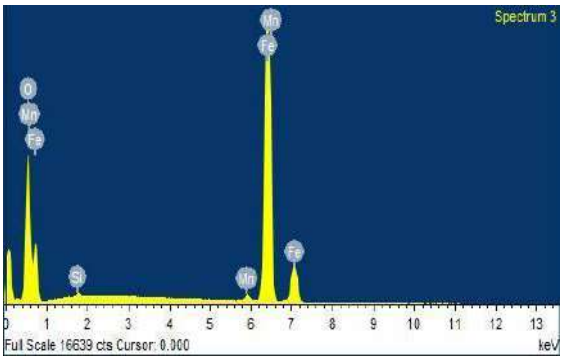
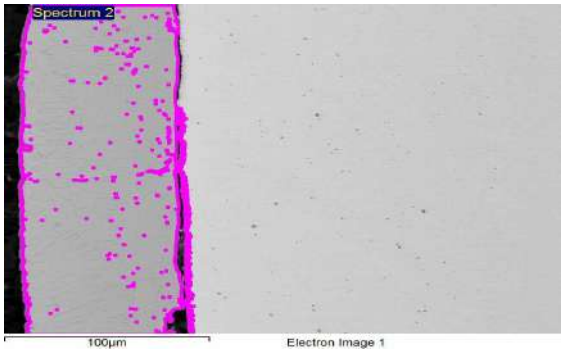
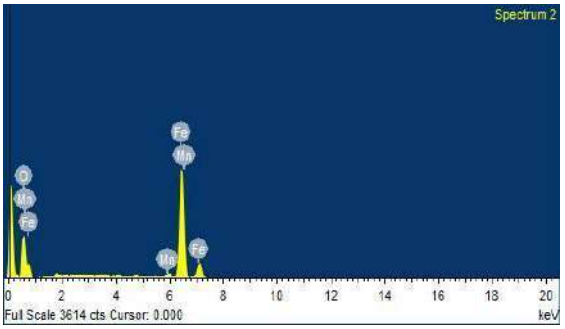
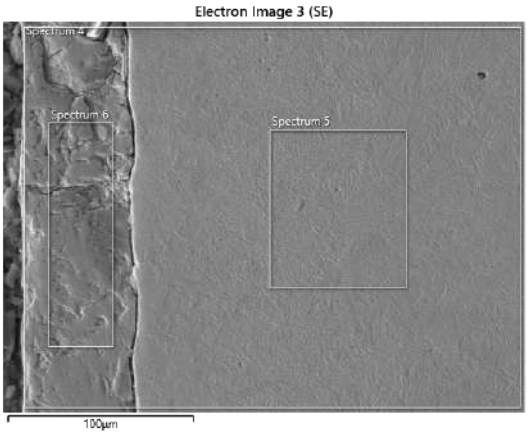
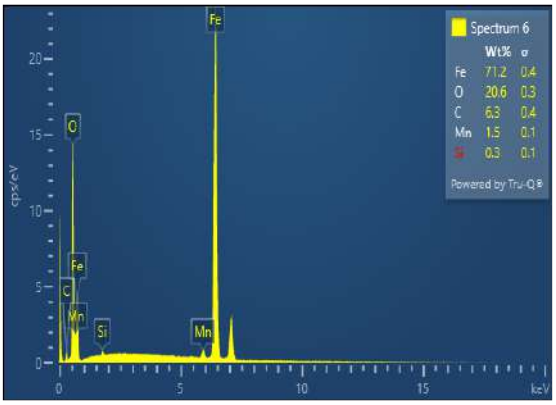
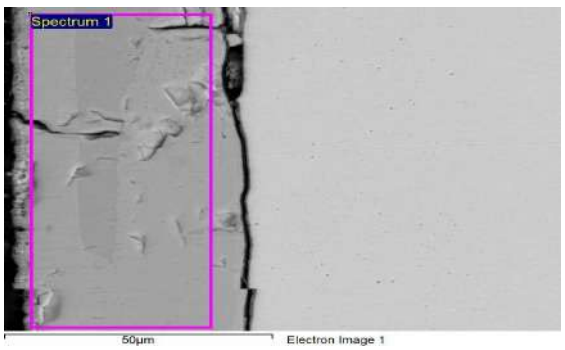
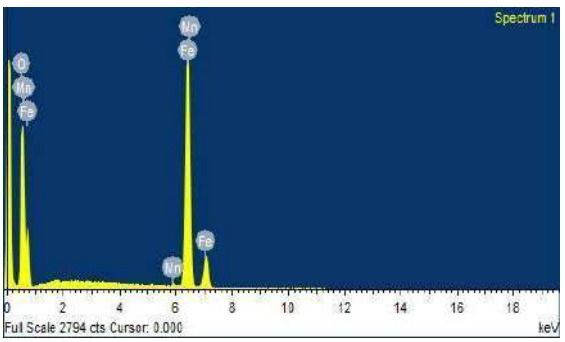
#	Image at 200 X	Image at 10000 X
23		

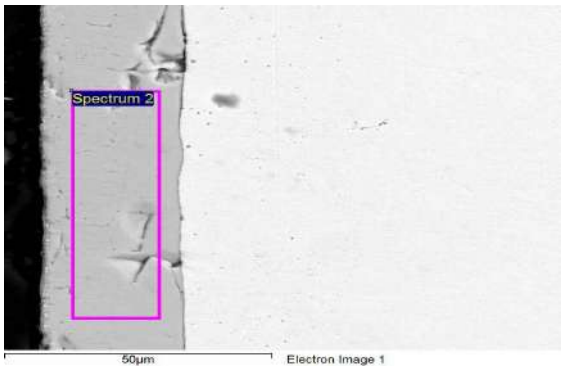
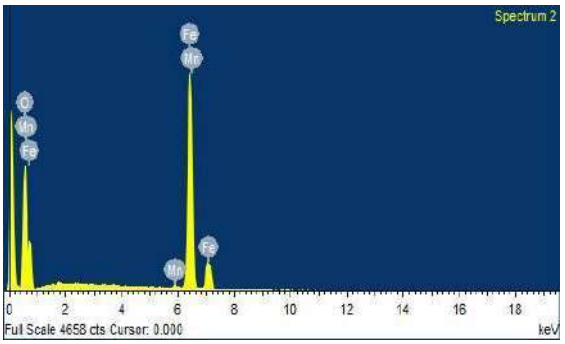
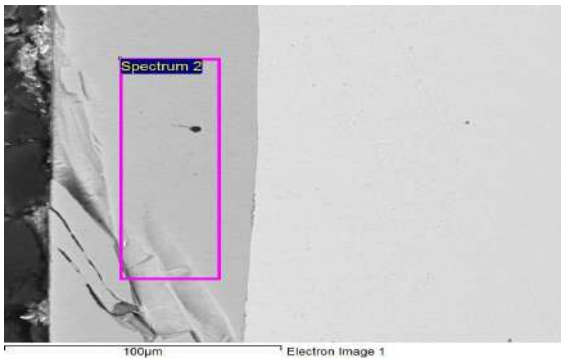
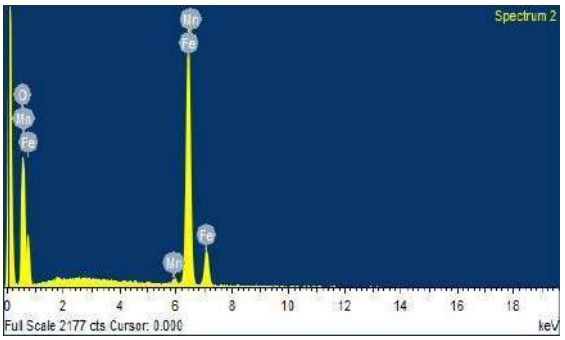
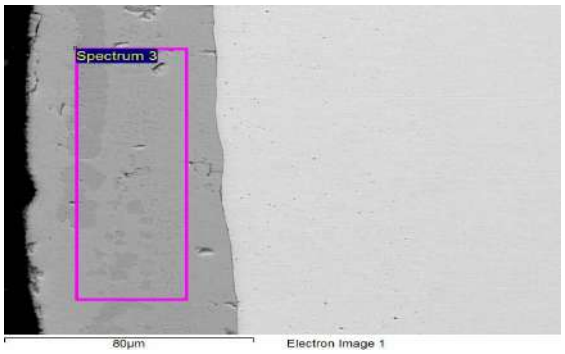
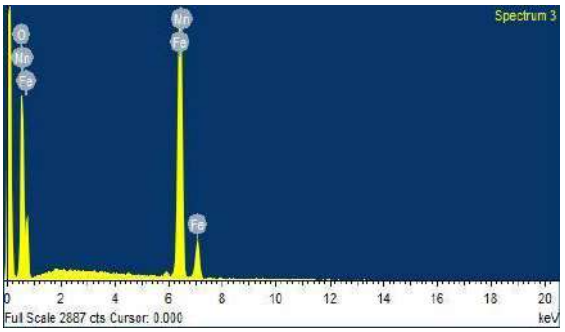
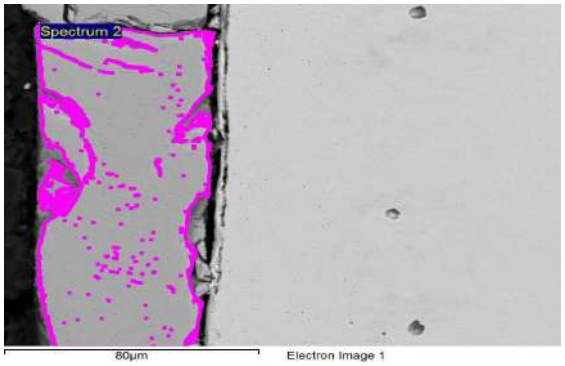
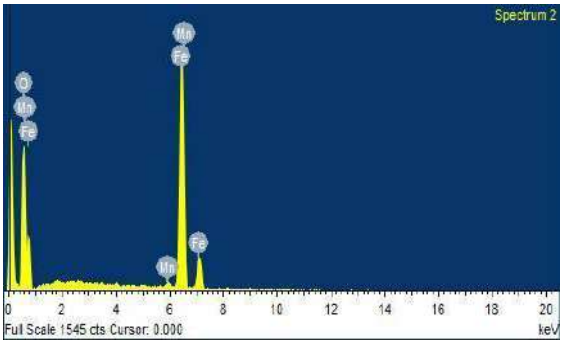
** Magnification at 500X for sample 8.*

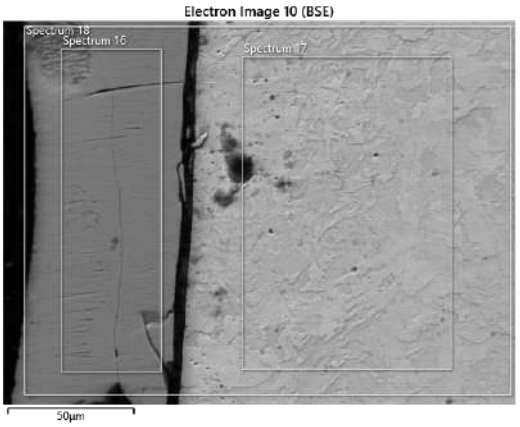
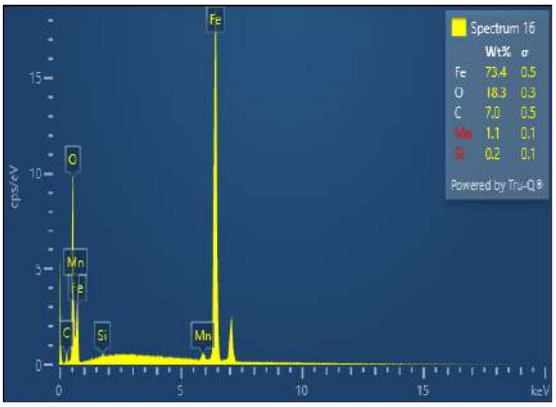
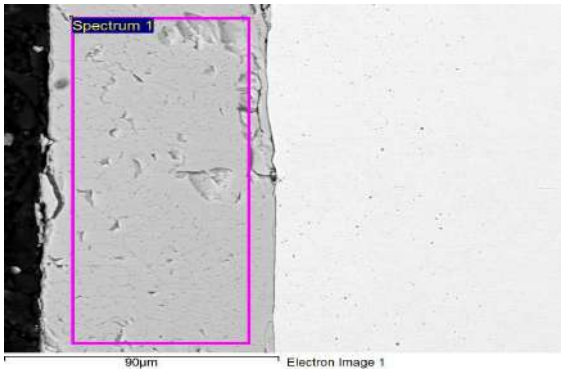
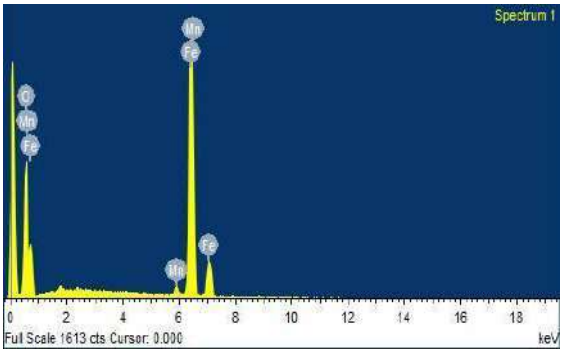
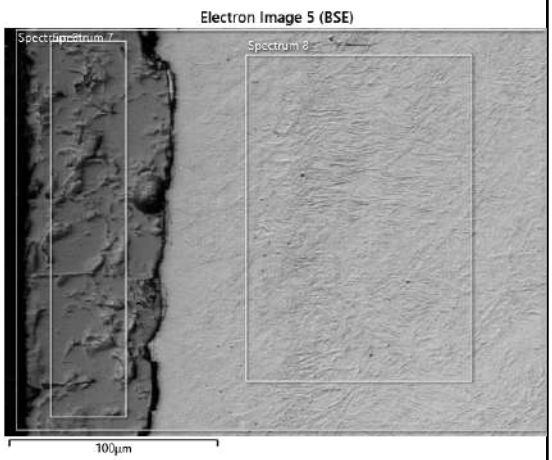
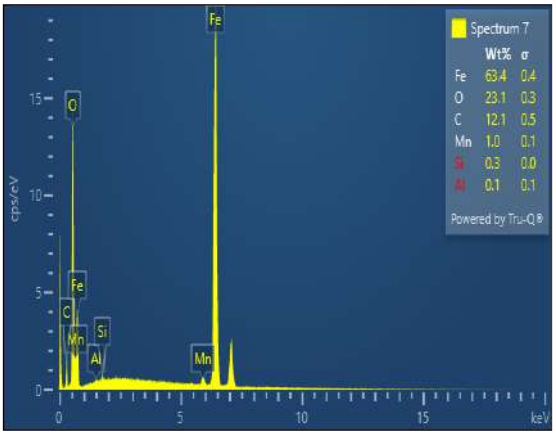
Table 16: EDS Slag Analysis

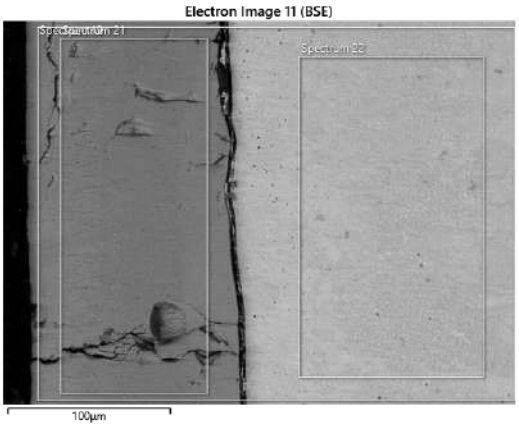
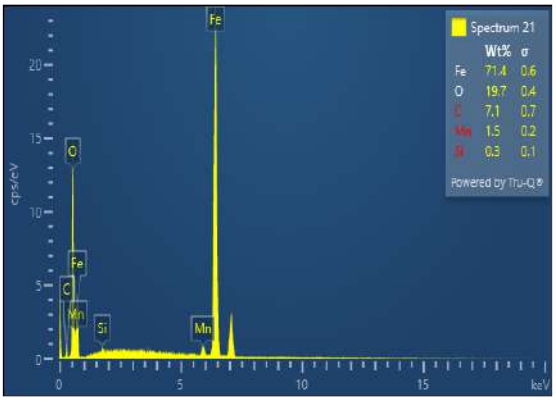
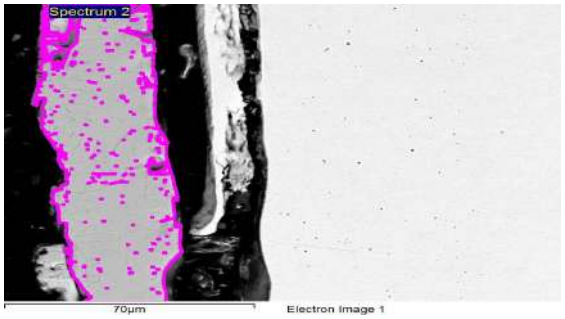
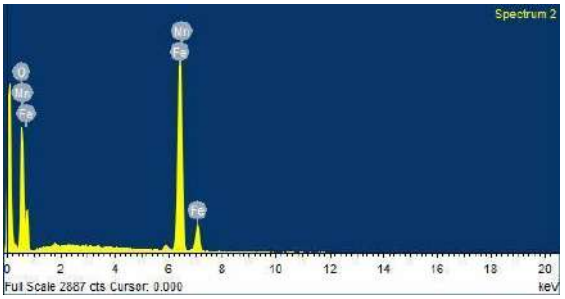
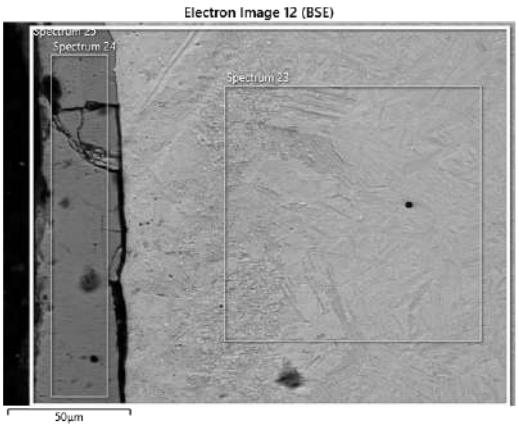
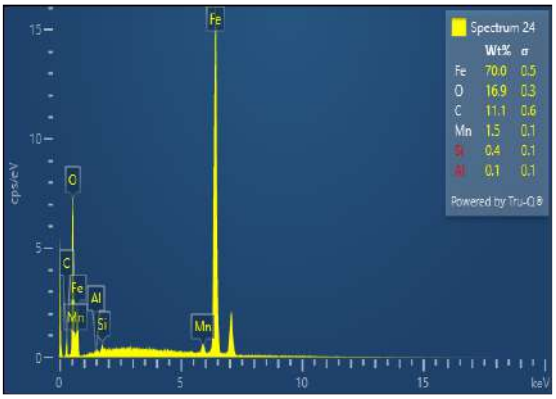
#	Area Analysed	Elemental Composition
1		
2		
3		

#	Area Analysed	Elemental Composition
4		
5		
6		
7		

#	Area Analysed	Elemental Composition
8		
10		
11		
13		

#	Area Analysed	Elemental Composition
14		
15		
16		
17		

#	Area Analysed	Elemental Composition
18		
19		
20		

#	Area Analysed	Elemental Composition
21		
22		
23		

EDS composition of the slag was used to calculate the atomic ratios of iron and oxygen using equations (4.5.1) and (4.5.2), respectively. To match each slag composition to common iron oxides (hematite: Fe_2O_3, magnetite: Fe_3O_4, and wustite: FeO), the atomic ratio of oxygen to iron was calculated using the equation (4.5.3). For stoichiometric iron oxides, oxygen-to-iron atomic ratios are 1.5, 1.3, and 1.0 for Fe_2O_3, Fe_3O_4, and FeO, respectively. Table 17

summarises the atomic ratios of oxygen and iron, and the oxygen-to-iron atomic ratios for each sample.

$$Atomic\ ratio\ (Fe)\ = \frac{EDS\ weight\%\ Fe\ (iron)}{55.845} \quad (4.5.1)$$

$$Atomic\ ratio\ (O)\ = \frac{EDS\ weight\%\ O\ (oxygen)}{15.999} \quad (4.5.2)$$

$$Oxygen\ -\ to\ -\ iron\ ratio\ (Fe_xO_y)\ =\ \frac{x}{y} \quad (4.5.3)$$

The oxygen:iron ratio ranges from 0.8 - 1.6, the values were not coherent with the results from visual and microscopic observation.

Table 17: EDS Slag Composition

	Weight (%)							Atomic Ratio		Iron Oxide Ratio
#	Oxygen	Manganese	Silicon	Aluminium	Carbon	Iron	Total	Oxygen	Iron	Oxygen:Iron
1	21.2	1.2	0.2	0.1	7.7	69.5	99.9	1.3	1.2	1.1
2	29.5	-	-	1.1	6.1	63.4	100	1.8	1.1	1.6
3	23.2	1.1	-	-	-	75.7	100.0	1.4	1.4	1.1
4	27.5	1.2	-	-	-	71.3	100	1.7	1.3	1.3
5	23.4	-	-	1.1	4.9	70.6	100	1.5	1.3	1.2
6	26.2	0.6	0.2	1.6	4.6	66.8	100.0	1.6	1.2	1.4
7	28.1	2.0	-	-	-	69.9	100	1.8	1.3	1.4
8	25.8	1.4	0.3	-	-	72.6	100	1.6	1.3	1.2
10	20.4	2.0	-	-	-	77.5	100	1.3	1.4	0.9
11	20.6	1.5	0.3	-	6.3	71.1	100	1.3	1.3	1.0
13	29.2	0.8	-	-	-	70.0	100	1.8	1.3	1.5
14	26.6	0.8	-	-	-	72.6	100	1.7	1.3	1.3
15	24.7	1.3	-	-	-	74.1	100	1.5	1.3	1.2
16	27.8	1.1	-	-	-	71.0	100.0	1.7	1.3	1.4
17	26.9	1.3	-	-	-	71.8	100	1.7	1.3	1.3

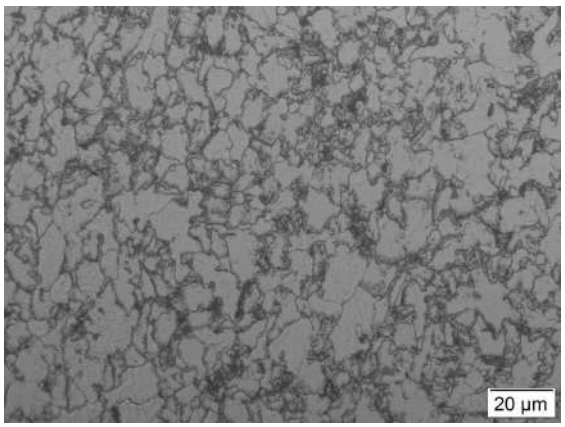
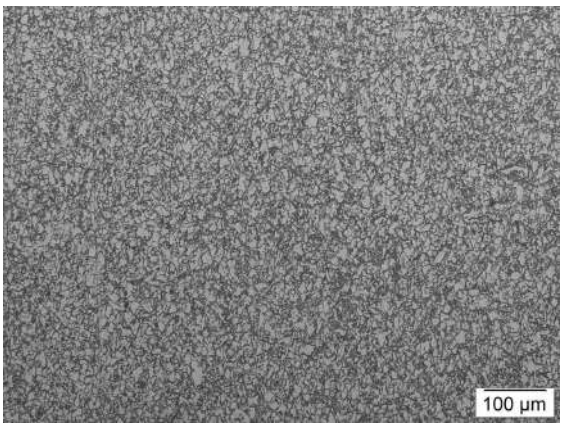
	Weight (%)							Atomic Ratio		Iron Oxide Ratio
#	Oxygen	Manganese	Silicon	Aluminium	Carbon	Iron	Total	Oxygen	Iron	Oxygen:Iron
18	18.3	1.1	0.2	-	7.0	73.4	100	1.1	1.3	0.9
19	24.5	1.9	-	-	-	73.6	100.0	1.5	1.3	1.2
20	23.1	1.0	0.3	0.1	12.1	63.4	100	1.4	1.1	1.3
21	19.7	1.5	0.3	-	7.1	71.4	100	1.2	1.3	1.0
22	27.5	1.4	-	-	-	71.1	100.0	1.7	1.3	1.3
23	16.9	1.5	0.4	0.1	11.1	70.0	100.0	1.1	1.3	0.8

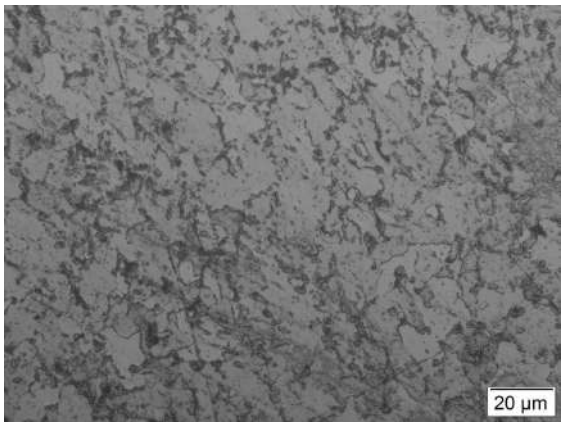
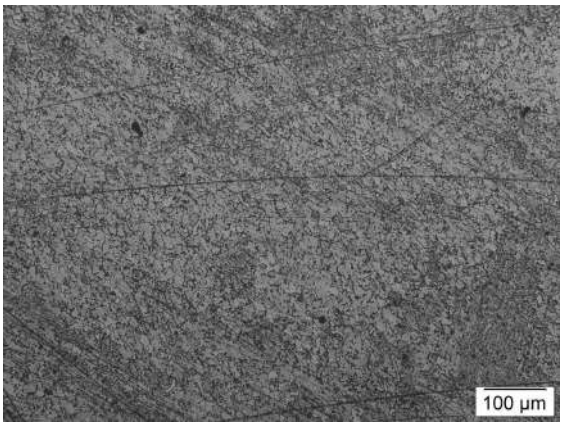
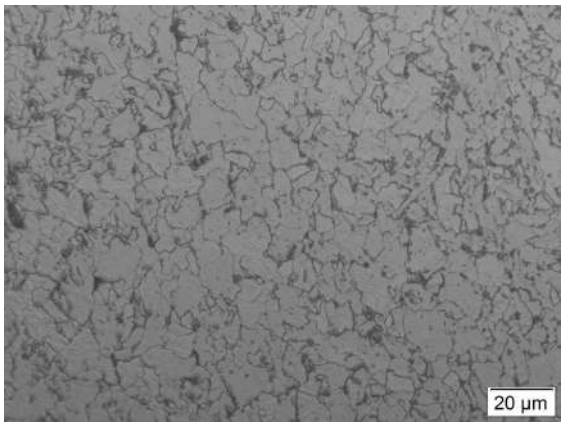
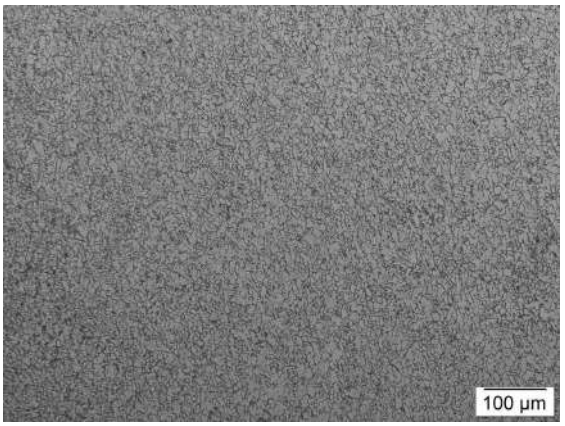
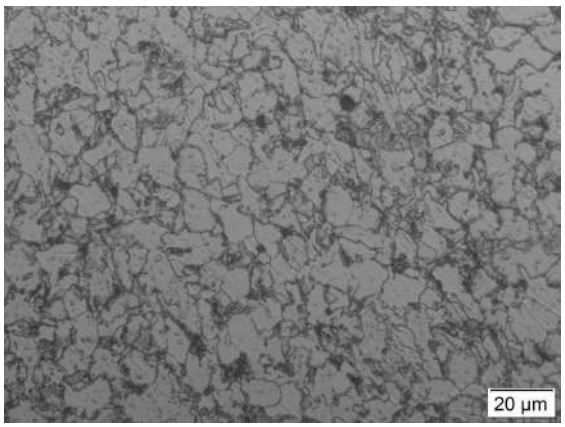
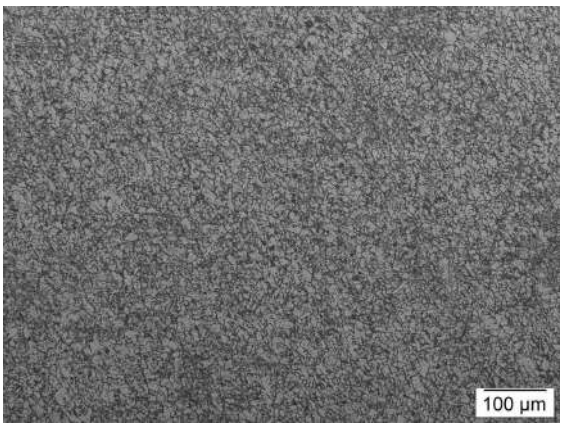
4.6. Optical Microscopy Images

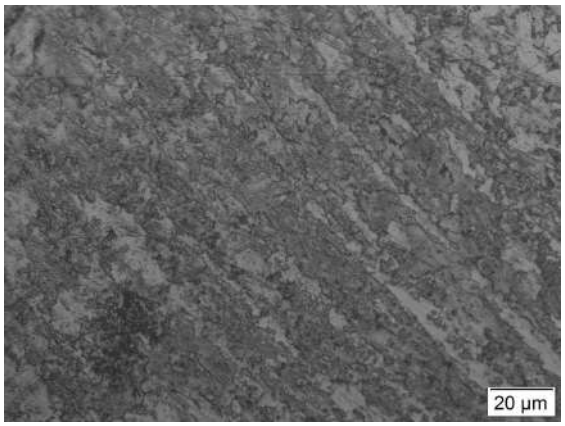
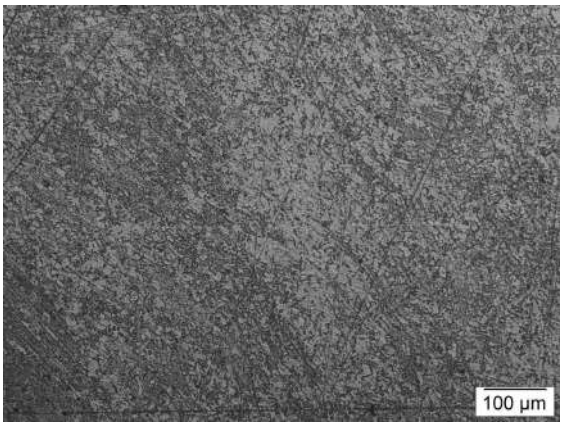
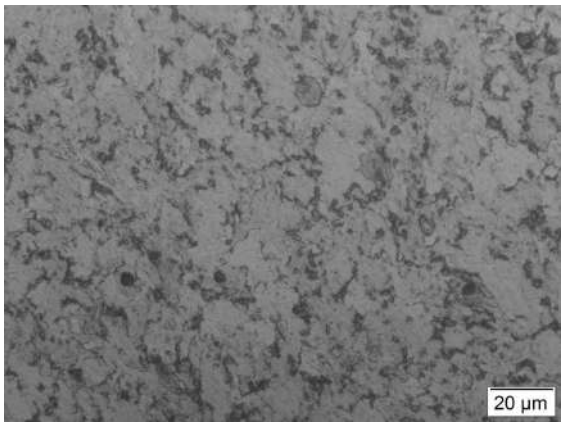
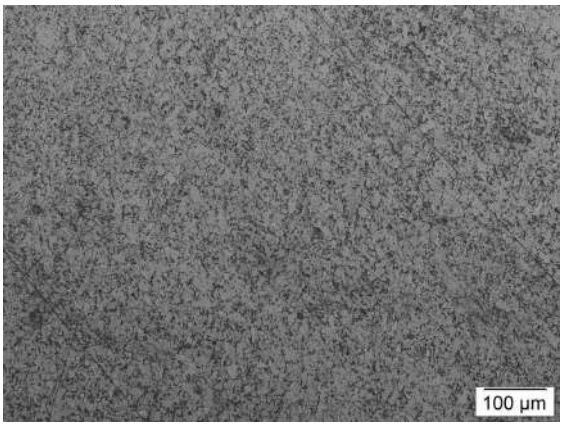
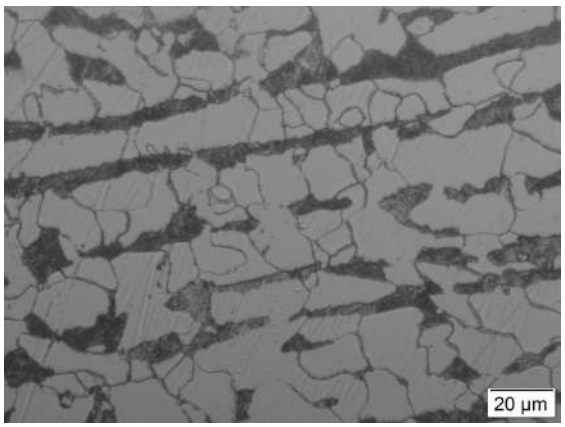
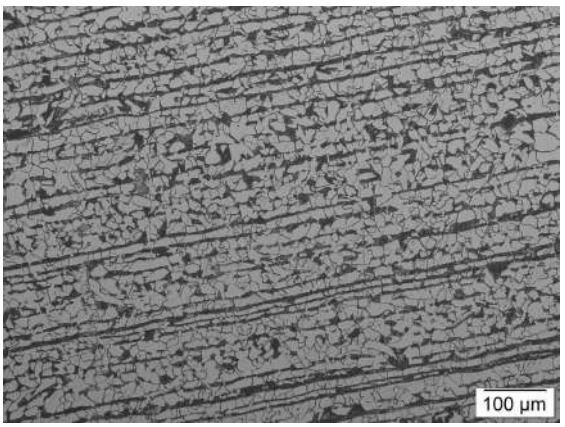
The optical micrograph images taken for each sample number (#) at magnifications of 20 µm and 100 µm are given in Table 18. The lighter phase is ferrite and the darker phase pearlite.

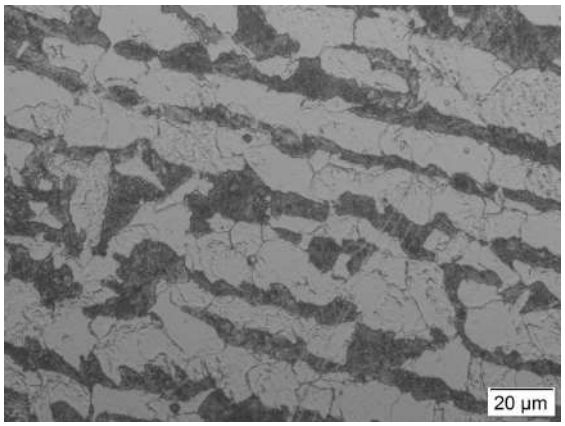
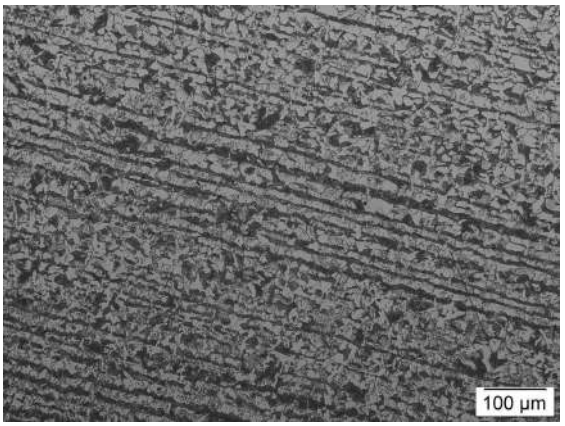
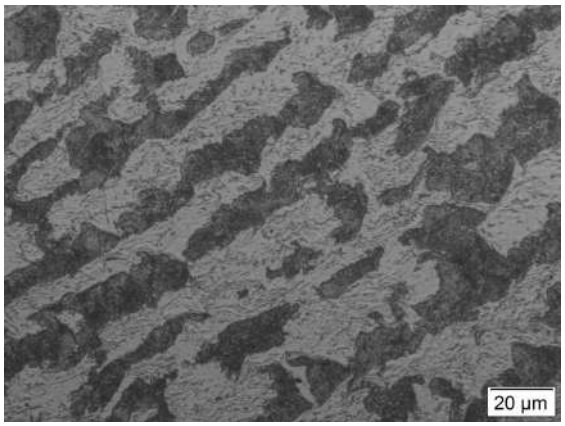
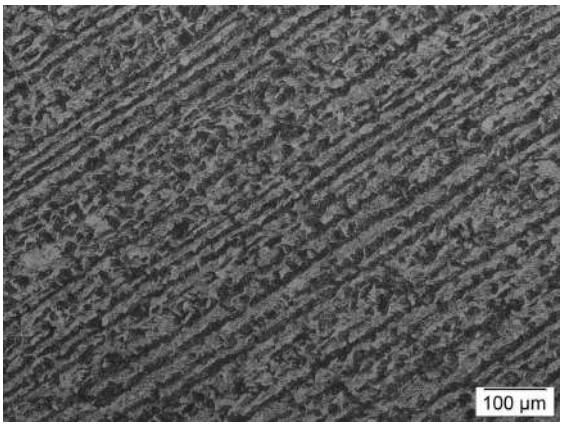
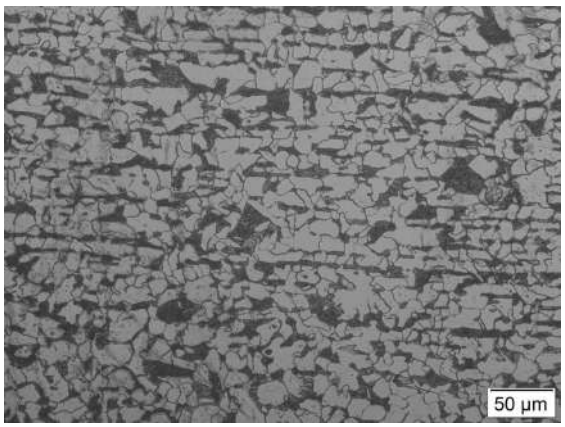
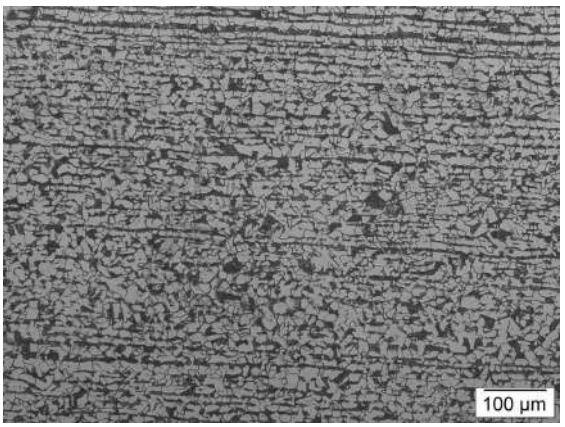
The base material microstructure is typical for that of plain carbon steels. In general the thinner (8mm) plate shows an equiaxed ferrite and pearlite microstructure and the thicker (16 mm) plate is that of a lamellar ferrite pearlite microstructure.

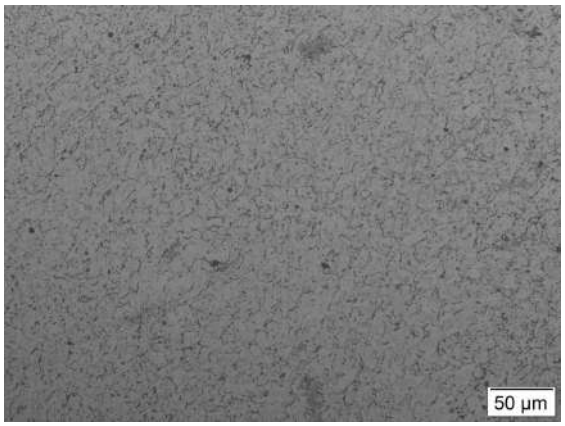
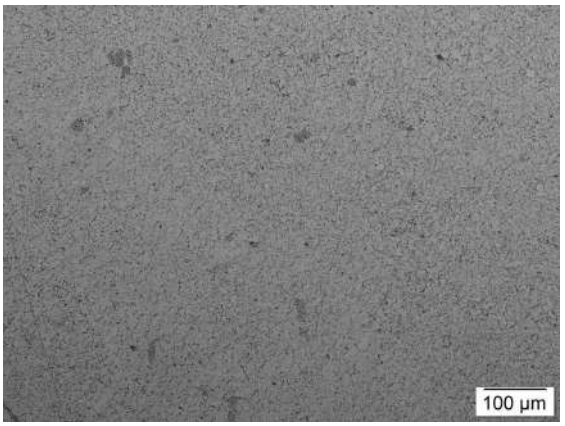
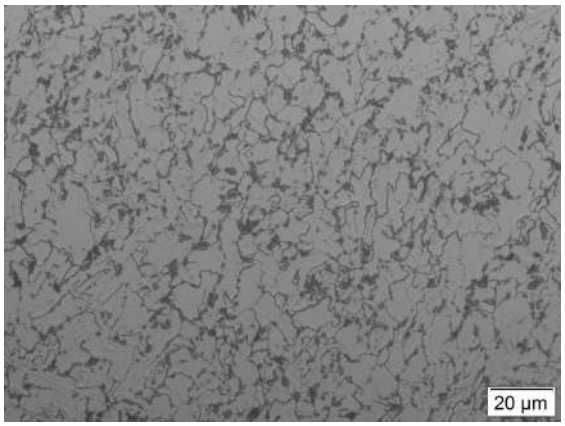
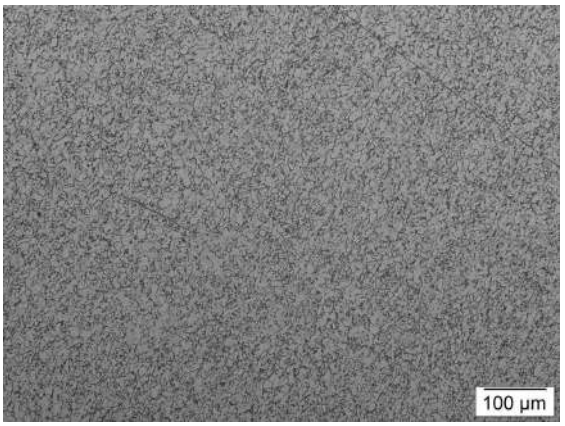
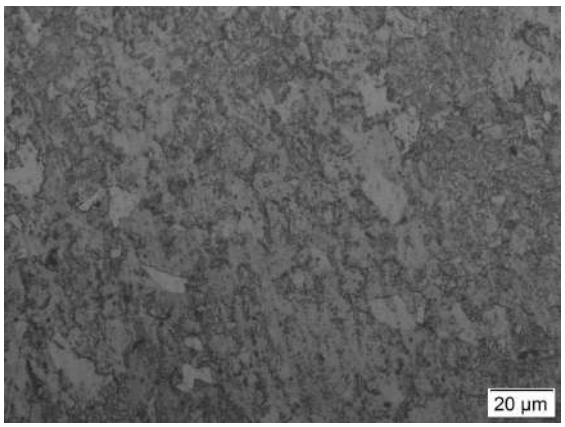
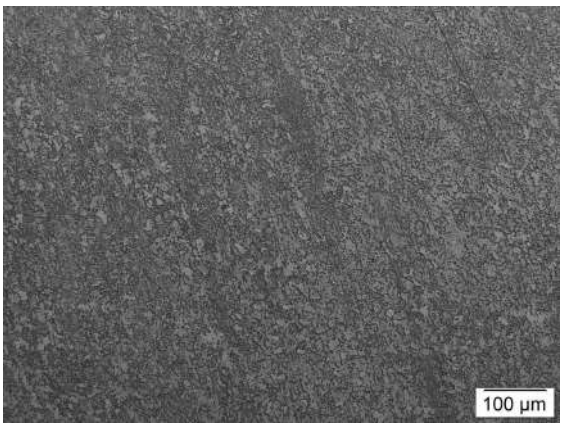
Table 18: Base Metal Microstructures

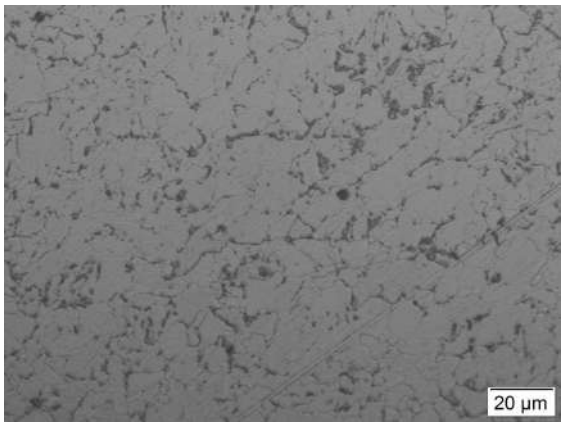
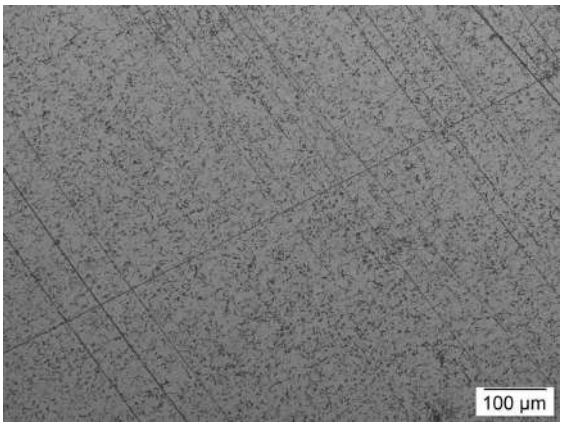
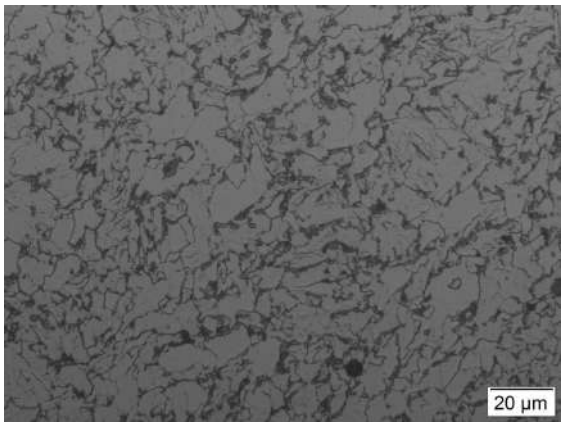
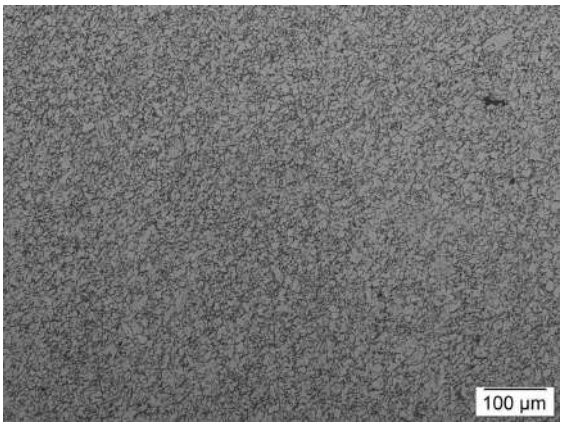
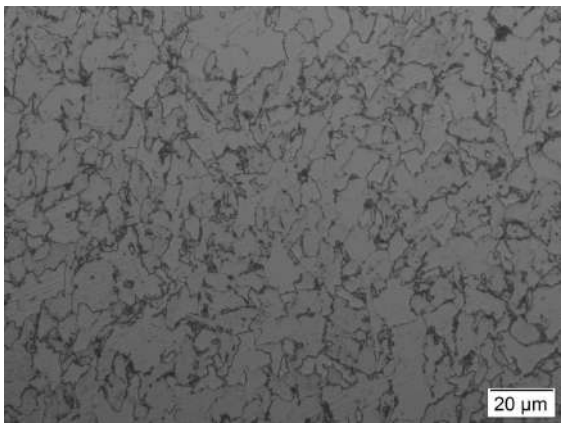
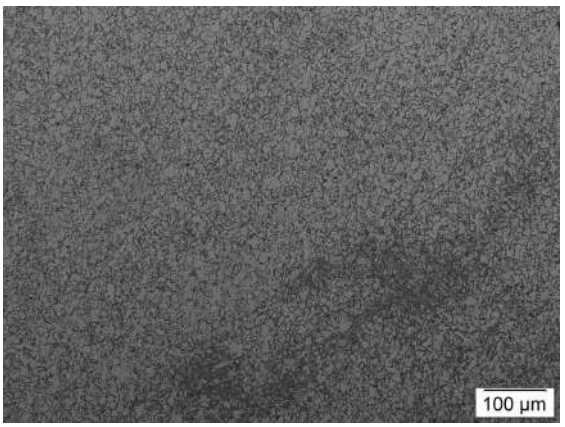
#	Image at 50X	Image at 10X
1		

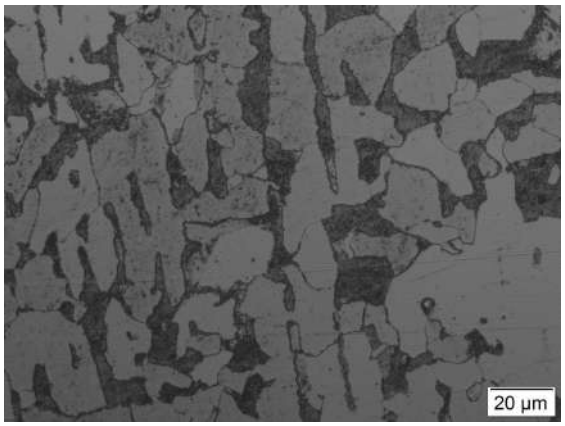
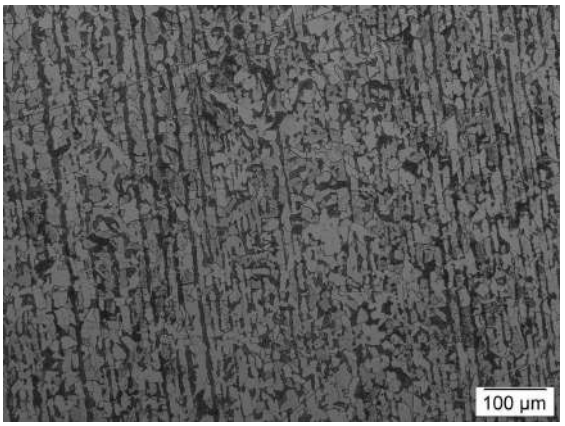
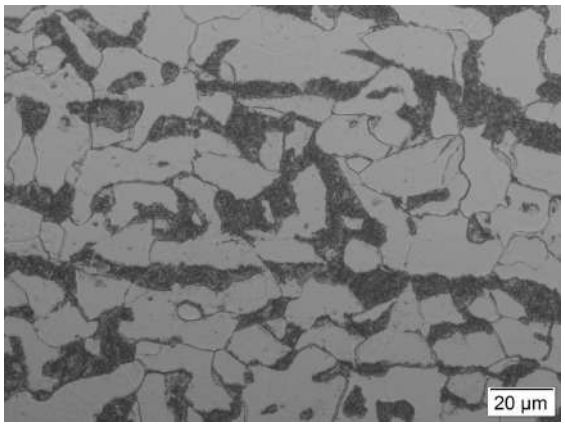
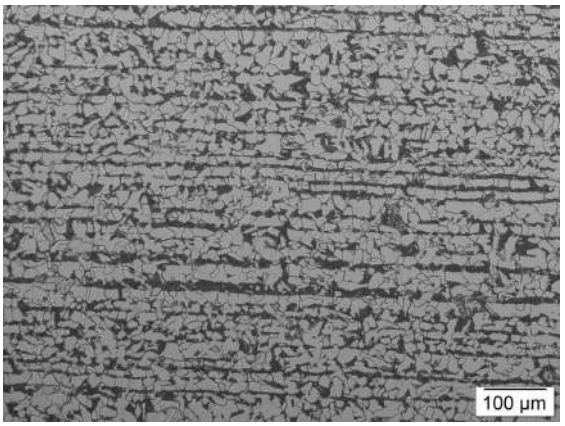
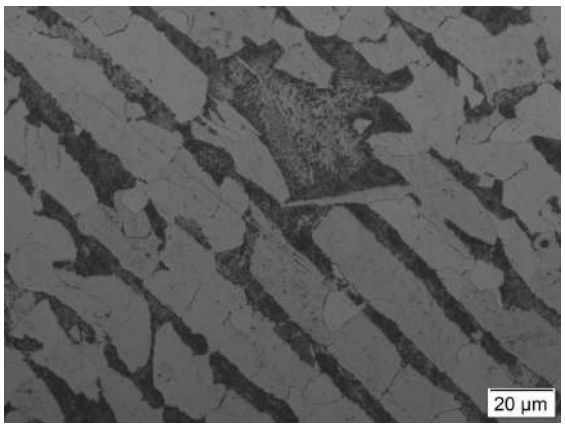
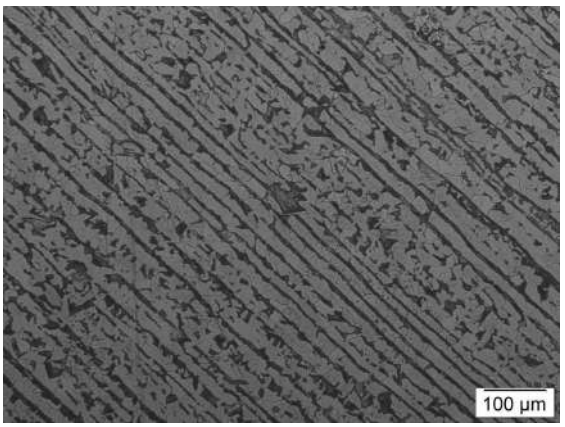
#	Image at 50X	Image at 10X
2		
3		
4		

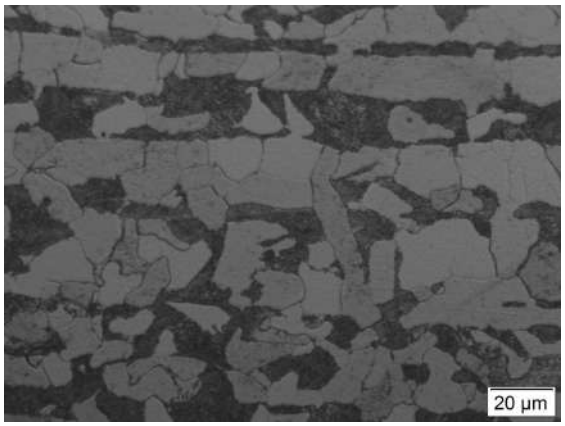
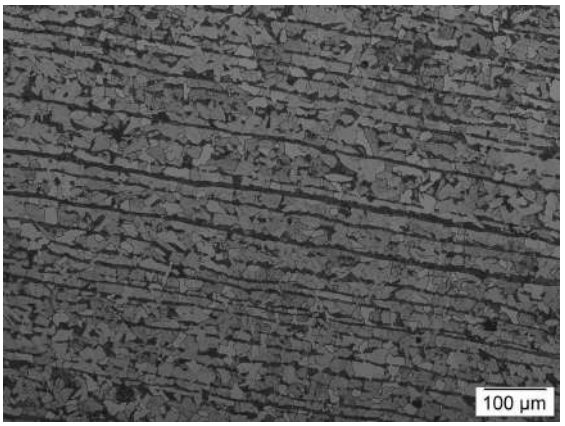
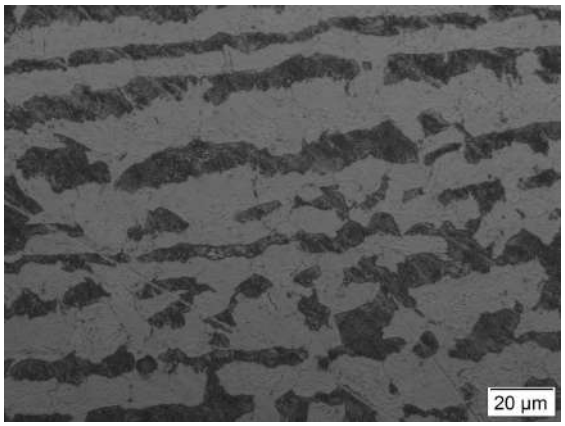
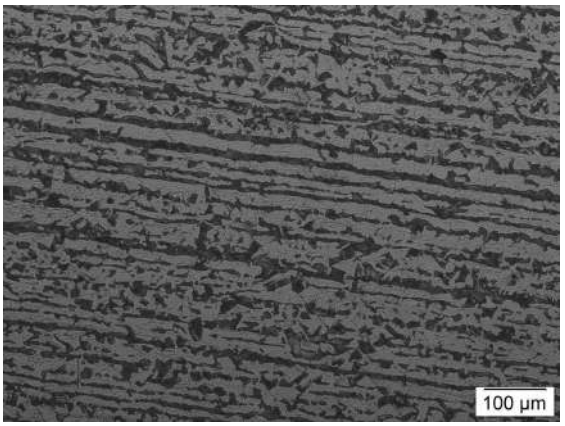
#	Image at 50X	Image at 10X
5		
6		
7		

#	Image at 50X	Image at 10X
8		
10		
11*		

#	Image at 50X	Image at 10X
13		
14		
15		

#	Image at 50X	Image at 10X
16		
17		
18		

#	Image at 50X	Image at 10X
19		
20		
21		

#	Image at 50X	Image at 10X
22		
23		

*Sample at 50 µm

Chapter 5 - Discussion

The study was carried out to characterise the cut face section of each sample and examine factors contributing to the slag adherence. The results of the experimental procedure on each cut sample include a visual examination of the cuts, a post-cutting macro examination, an evaluation of surface roughness, a transverse hardness, SEM and EDS analysis, and a microscopic evaluation.

5.1. Cutting Performance

During the sample cutting, the inclination of the cutting oxygen jet was observed at the bottom of the cut face to determine the direction of the flame for the progression of cutting. The cutting oxygen jet inclination varies with each of the samples and is observed as either forward, perpendicular, or backward. At times, the jet demonstrated either of these three progressions with an erratic behaviour that seemed to extinguish and ignite. The observed flame is a jet constituted by the cutting oxygen, slag, and molten steel as depicted in Figure 2. The flame is expelled at the bottom of the cut face with varying volume fractions of melt depending on the cutting parameters and conditions. An ideal cut quality has straight parallel edges from top to bottom, a smooth cut face with no gouges and back-run drag lines null or maximum 10 percent, a sharp top cut edge, and no adherent slag (Slotman & Edward, 1951).

Samples 1 - 6

Samples 1 - 6 are the 8 mm thick plates cut with acetylene. The cutting process of samples 1 - 3 was performed with a nozzle standoff of 6 mm at the incremental cutting speeds of 504, 632, and 755 mm/min, respectively. Samples 4 - 6 were cut with a nozzle standoff of 15 mm at the same incremental cutting speeds.

The inclination of the cutting oxygen jet for samples number 1 - 6 showed a variation of the three progressions, namely forward, perpendicular and backward. There was no observation of an erratic flame and all the samples seemingly have adherent slag. As shown in Figure 1, it is anticipated that the heat generated by the combustion of iron (H_{mc}) < the preheat flame (H_{phf}). Where H_{phf} ~ 60%, the volume percentage of unoxidised iron (free iron) is greater than the iron oxides (slag), thus the slag tends to be adherent. The post-cut quality of all these

samples showed the presence of slag at the bottom of the plate. The macro examination of samples 1 - 6 revealed no pattern of dragline inclination on the cut face and the cut faces are smooth with no gouges (Table 11).

The as-cut face of most samples exhibited minimal concavity with the exception of samples 3 and 6 as shown in Table 10. Samples 3 and 6 had a 6 mm and 15 mm standoff, respectively with a cutting speed of 755 mm/min. The cutting speed is 20% faster than the average nominal cutting speed of the selected nozzle used for the plate thickness.

The surface roughness results (Ra) of samples 1-6, in Table 12, varies from 27 - 83 µm whilst the Rz5 was measured to be in the range of 72 - 86 µm. The calculated values of Ra for samples 1,2, and 4 are below 30 µm whereas Ra for samples 5 and 6 are above 70 µm. The sample 3 has a Ra of 47 µm. This gives a range of 55 µm for the Ra and 14 µm for the Rz5 for samples 1 - 6. This suggests that increasing the cutting speed leads to an increase in surface roughness as the samples cut at nominal cutting speed minus 20% have the same Ra value of 28 µm and are smoother than the rest of the oxy-acetylene 8 mm samples, with the exception of the 6 mm standoff sample cut at the nominal cutting which has a Ra value of 27 µm.

Table 11 shows a degree of top-edge melting that is visible in all six samples. The top edge surfaces for samples 1, 2, 3, and 4 exhibit a sharp top edge whereas samples 5 and 6 show an overhang top edge. The selection of the cutting nozzle and the nozzle-to-plate distance influences the preheat gas flow, which affects the shape and degree of top-edge melting (Slotman & Edward, 1951). In this study, the preheat gas flow and nozzle type were kept fixed. It can be concluded that the nozzle standoff has the most effect on top-edge melting the nozzle standoff. In practice, it is not desirable to have an overhang top edge, as seen in samples 5 and 6 for a 15 mm standoff and cutting speeds of 632 mm/min and 755 mm/min, respectively. The slower cutting speed at 504 mm/min for sample 4 counters the influence of the nozzle standoff and results in a sharper top edge with a string of solidified droplets, as expected for a slower cutting speed.

Table 14 shows the transverse Vickers hardness results of samples 1 - 6. The surface cut of sample 5 has a maximum hardness (200 HV). A minimum of 122 HV corresponds to sample 1. The average hardness ranges from 171 HV (sample 1) to 187 HV (sample 5). It can be seen that the samples cut at the same cutting speed yield a similar hardness value, with the nominal cutting speed of 632 mm/min yielding 185-187 HV, the minus 20% of nominal cutting speed 504 mm/min measuring 171 - 172 HV and the plus 20% of the nominal cutting speed 755 mm/min measuring 178 HV, irrespective of the nozzle standoff.

Tables 15 and 16, SEM and EDS analysis of these samples reveals that all samples contained slag with samples 1, 3, and 6 showing no gap between the slag and base material whilst samples 2, 4, and 5 have a maximum gap measurement of 0. 85 µm, 2.42 µm and 1.57 µm respectively. The EDS slag composition of these samples contains 21 - 30 weight % oxygen and 63 - 76 weight % iron, combined these make up 84 - 96 % of the slag composition. The oxygen-to-iron ratio of samples 1-6 ranges from 1.1 - 1.6 and an average of 1.3 which indicates that the slag is mostly composed of magnetite (Fe_3O_4).

The chemical composition of the 8 mm plate is typical of plain carbon steels and has 0.15% carbon content with no other significant alloying elements (Table 9). Sample microstructures in Table 18 are comparable to plain carbon steels, revealing equiaxed ferrite with perlite islands for samples 1,2,3, 4, and 6. The microstructure of sample 5 shows predominantly pearlite at 20 X magnification. Sample 5 may have been mechanically cold-worked during metallographic sample preparation which has resulted in it having the highest average hardness, 187 HV of the six samples.

Samples 7 - 12

Similarly, acetylene was used to cut 16 mm thick plate samples 7 - 12. Samples 7 - 9 and samples 10 - 12 were cut with a nozzle standoff of 6 mm and 15 mm, respectively. The two batches of samples were cut at incremental cutting speeds of 467, 592, and 717 mm/min respectively (Table 4).

Samples 9 and 12 showed a seizure of the cutting process. This was due to the increase in the cutting speed and subsequently the preheat flame running over the surface of the plate. This

happened whilst incrementally increasing the cutting speed therefore sample 9 and 12 were classified as a “no cut” in Table 10.

For samples 7, 8,10, and 11, the inclination of the cutting oxygen jet reveals a variation of the two progressions (Table 10). The flame inclines in a forward direction for the nominal cutting speed minus 20% of 467 mm/min and becomes erratic at the nominal cutting speed of 592 mm/min for both the 6 mm and 15 mm nozzle standoffs. The slag is visually non-adherent on all samples except sample 11. Figure 1 shows that for a section thickness of 16 mm the heat generated by the combustion of iron (Hmc) > the preheat flame (Hphf) where Hphf (~ 40%). From this extrapolation, the volume percentage of unoxidised iron (free iron) is less than the iron oxides (slag) therefore the slag has a tendency to be non adherent.

Table 10 also shows no significant dross at the bottom of the cut face of all samples except sample 11, which has a relatively thick layer of adherent slag. Samples 7, 8, 10 and 11 have minimal concavity as shown in Table 10. The macro examination of sample 7 shows a shorter distance (n) and a smaller drag pitch (f) in contrast to sample 8, the draglines are throughout the thickness of both samples. Sample 10 has a short dragline distance (n) with a wide dragline pitch (f) and a predominantly smooth-cut face. Sample 11 has draglines that are prevalent on the top of the cut face with a greater distance (n) and smaller dragline pitch (f) than sample 10. The cut face of sample 11 becomes smooth below the draglines.

The surface roughness results (Ra) for samples 7 - 12 varies from 37 - 60 µm whilst the Rz5 values range from 115 - 161 µm (Table 12). The Ra values for samples 7 and 11 are 60 µm, and samples 8 and 10 have lower Ra of 48 and 37 µm respectively. The range in Ra is less spread for these 16 mm samples but the range in Rz5 is wider. The averaged Ra and Rz5 are 23 µm and 46 µm, respectively, for samples 7,8, 10, and 11. Samples 7 and 10 were cut at 467 mm/min, with sample 10 having the higher nozzle standoff and the smoothest surface roughness profile. Samples 8 and 11 were cut at the nominal cutting speed of 592 mm/min with samples 11 and 7 having the roughest surface profile.

Table 10 shows a degree of top edge melting for samples 7 and 8 with an overhang top edge and metal droplets whereas samples 10 and 11 show a rounded top edge. The nozzle standoff

for samples 11 and 12 is higher than that used for cutting samples 7 and 8. This suggests that the lower nozzle standoff of 6 mm leads to a non-desirable overhang top edge.
As shown in Tables 10 and 11, visual examination of the as-cut face of selected cut samples. All four samples exhibited no gouges, as found in the visual examination of samples 1 - 6. This suggests that the cutting oxygen was supplied at the correct pressure.

The measurement of Vickers hardness resulted in sample 7 having the maximum value of 365 HV while sample 8 had the minimum hardness of 139 HV, as shown in Table 14. The average hardness ranges from 145 HV (sample 8) to 295 HV (sample 7). Samples 7 and 10 were cut at the slowest cutting speed of 467 mm/min and had the highest averaged hardness values of 295 and 275 HV respectively. Sample 8 is the softest with an average hardness of 145 HV. This may be due to oxy-acetylene cutting conditions of the nominal cutting speed of 592 mm/min and 6 mm nozzle standoff whereby the slower cutting speed has a normalising heat treatment effect on the material and softening it .

In Tables 15 and 16, SEM and EDS analysis of tested samples shows the presence of slag at the bottom of the plate with a gap. The gap measured ranged from 1.32 - 3.38 μm, for samples 11 and 8 respectively. The EDS slag composition of these samples contains 20 - 28 wt% oxygen and 70 - 77 wt% iron, combined these make up 92 - 98 % of the slag composition with the balance consisting of carbon, manganese, and silicon. The oxygen-to-iron ratio for tested samples ranges from 0.9 - 1.4, with an average of 1.1. Based on the calculated atomic ratios between oxygen and iron, the composition of slag attached to samples 7 and 8 can be compared to a mixture of hematite (Fe_2O_3) and magnetite (Fe_3O_4) whilst the composition of slag from cutting samples 10 and 11 matches wüstite (FeO).

The chemical composition of the 16mm plate, in Table 9, falls within the typical group of plain carbon steels, with 0.16% carbon content and other minor alloying elements. The microstructures of different samples are shown in Table 18 and they reveal a typical microstructure of plain carbon steels with equiaxed ferrite and a pearlite band. Sample 10 seemingly has a relatively larger volume fraction of pearlite and the highest average hardness, 275 HV of the four samples.

Samples 13 - 18

Samples 13 - 18 were cut from 8 mm thick plates using propane. Samples 13 - 15 were obtained with a nozzle standoff of 6 mm at the incremental cutting speeds of 504, 632, and 755 mm/min respectively. Samples 16 -18 were cut with a nozzle standoff of 15 mm at the same incremental cutting speeds.

The visual observation for the inclination of the cutting oxygen jet shows a variation of the three progressions for samples number 13 -18. The flame inclines in a forward direction for the nominal cutting speed minus 20% of 504 mm/min for samples 13 and 16. Similar behaviour is observed during the cutting of sample 17 at the nominal speed of 632 mm/min. The increase in cutting speed tends to reverse the inclination of the cutting oxygen jet, which can become perpendicular for sample 14 at the nominal cutting speed of 632 mm/min and backward erratic for samples 15 and sample 18 at 755 mm/min, which is 20% more than the nominal cutting speed. The slag is visually non-adherent on all five samples except sample 14. The visual examination also shows significant dross at the bottom of the cut face of all six samples (Table 10). All tested samples have minimal concavity however samples 15 and 18 cut with 755 mm/min show slight concavity. The macro examination of samples 13, 16, and 17 shows perpendicular draglines on the top half of the cut face and a smooth texture on the remainder of the cut face. Samples 14, 15, and 18 have slightly slanted draglines on the bottom of the cut face, a smooth texture on the middle of the cut face, and a varying degree of top edge melting on the top section of the cut face. Sample 15 has a longer dragline distance (n) and samples (name them) have a narrow dragline pitch (f).

The surface roughness analysis shows that Ra varies from 30 - 98 µm whilst the Rz5 was measured to be in the range of 57 - 88 µm. Sample 14 has the highest Ra value of 98 µm and sample 17 has the lowest value of 30 µm (Table 12). The other samples (name them) have values below 55µm. The Rz5 for tested samples ranges from 57 - 88 µm with sample 13 having the minimum and sample 16 having the maximum value. The range of Rz5 is less spread for 8 mm thick samples but the range of Ra is wider. Sample 14, cut at the nominal cutting speed of 632 mm/min with a 6 mm nozzle standoff has the roughest surface profile whilst sample 17 cut at the same cutting speed with a 15 mm nozzle standoff has the smoothest surface profile.

Table 10 shows a degree of top edge melting for all 6 samples with predominately a molten edge irrespective of the nozzle standoff.

The visual examination of the as-cut face of 8 mm thick samples exhibited no gouges except the top of the cut face of sample 13 as shown in Tables 10 and 11.

Table 14 shows the transverse Vickers hardness results of tested samples, with sample 15 having a maximum of 188 HV and sample having a minimum of 130 HV. The average hardness ranges from 161 HV (sample 18) to 176 HV (sample 14). Samples 13 - 15 cut at the 6 mm nozzle standoff show a more consistent average hardness 3 HV range variation than samples 16 - 18 cut at a nozzle standoff of 15mm with a 12 HV range variation.

SEM and EDS analysis of these samples reveals that all six samples had slag at the bottom of the plate with a gap except sample 16 (Tables 15 and 16). The measured gap varies from 0.71 - 2.81 μm, for samples 14 and 17 respectively. The EDS slag composition of these samples contains 18 - 29 wt% oxygen and 70 - 74 w% iron and alloying elements such as manganese and silicon. The oxygen-to-iron ratio for tested samples ranges from 0.9 - 1.4, with an average of 1.2. The atomic ratio suggests that slags from samples 13 and 16 consist predominantly of hematite (Fe_2O_3), magnetite (Fe_3O_4) for samples 14, 15, and 17, and wüstite (FeO) for sample 18.

The chemical composition for 8 mm thick samples corresponds to typical plain carbon steels and has 0.15% carbon content with minor alloying elements (Table 9). The microstructures shown in Table 1 are of plain carbon steels showing equiaxed ferrite with perlite islands for samples 13, 14, 16, 17, and 18 whereas the microstructure of sample 15 shows predominantly pearlite. Sample 15 may have been mechanically cold-worked during metallographic sample preparation which has resulted in it having the highest maximum hardness, 188 HV of the six samples.

Samples 19 - 24

Samples 19 - 24 were prepared by cutting 16 mm thick plates with propane, whereby samples 19 - 21 were cut with a nozzle standoff of 6 mm at the incremental cutting speeds of 467, 592, and 717 mm/min respectively. Samples 22 -24 were cut with a nozzle standoff of 15 mm at the same incremental cutting speeds.

The cutting of sample 24 showed a seizure of the oxygen cutting with an increase in the cutting speed, and subsequently, the flame ran over the surface of the plate. This was due to the increase in the cutting speed and subsequently the preheat flame running over the surface of the plate. This happened whilst incrementally increasing the cutting speed therefore sample 24 was classified as a "no cut" in Table 10.

A variation of the two progressions was observed by the visual observation of the inclination of the cutting oxygen jet for samples 13 -18 (Table 10). The flame inclines in a forward direction for the nominal cutting speed minus 20% of 467 mm/min for samples 19 and 22. As the cutting speed increases the cutting oxygen jet's inclination tends to reverse and becomes perpendicular-erratic for samples 20 and 23 at the nominal cutting speed of 592 mm/min and nominal cutting speed plus 20% of 717 mm/min for sample 21. The slag is visually non-adherent on the samples cut with nominal cutting speed minus 20% and adherent for the remainder of the three samples 20, 21, and 23. Table 10 shows that all five samples have minimal concavity and the macro examination in Table 11 of the samples shows slightly slanted draglines throughout the cut face of the plate for sample 19 and mixed a smooth texture on the remainder of the samples.

The surface roughness results for tested samples show that Ra varies from 20 - 73 µm whilst the Rz5 ranges from 70 - 117 µm (Table 12). Sample 19 has the highest Ra value of 73 µm and sample 23 the lowest value of 20 µm followed by sample 22 with 34 µm whilst samples 20 and 21 measured 70 µm and 60 µm respectively. The Rz5 ranges from 70 - 117 µm with sample 23 having the minimum and sample 22 the maximum value. Sample 19, cut at the nominal cutting speed minus 20% of 467 mm/min with a 6 mm nozzle standoff has the roughest surface profile whilst sample 23 cut at the nominal cutting speed of 592 mm/min with a 15 mm nozzle standoff has the smoothest surface profile.

Table 10 shows a degree of top edge melting for all 5 samples with predominately a top edge overhang irrespective of the nozzle standoff.

From Tables 10 and 11, it is clear that visual examination of the as-cut face of all four 16 mm thick samples exhibited no gouges with the exception of the top of the cut face of sample 19.

Table 14 shows that the transverse vickers hardness results of these samples has a maximum 357 HV (sample 19) and a minimum of 130 HV (sample 22). The average hardness ranges from 145 HV (sample 22) to 291 HV (sample 19).

The examination by SEM and EDS of these samples reveals that all five samples had slag at the bottom of the plate (Tables 10 and 11). The gap between the slag and base material was found to vary from 1.14 - 1.31 μm for samples 20 and 21 respectively whilst samples 19, 22 and 23 had no gap. The EDS slag composition of these samples contains 17 - 28 wt% oxygen and 63 - 74 wt% iron, with varying proportions of manganese, silicon and aluminium. The oxygen-to-iron ratio of studied samples ranges from 0.8 - 1.3 and an average of 1.1. The atomic ratio for slag suggests that samples 19, 20, and 22 generated a slag of predominantly magnetite (Fe_3O_4), and samples 21 and 23, wustite (FeO).

The chemical composition of the 16 mm thick plate is typical of plain carbon steels and has 0.16% carbon content with no other significant alloying elements (Table 9). The microstructures of these samples are shown in Table 18 and are comparable to plain carbon steels showing equiaxed ferrite and a pearlite band.

5.2. Factors Affecting Slag Adherence

From the post-cutting visual examination, samples with apparent adherent slag were further analysed with the SEM. This approach aided in determining whether there was a gap between the base metal and the slag. A gap is associated with a non-adherent slag, while no gap between slag and steel indicates the slag adherence to the sample.

SEM results showed the formation of an apparent slag in 6 samples cut from an 8 mm thick plate using an oxy-dissolved flame. No gap between the slag and the base metal was detected in samples 1, 3, and 6, confirming the adherence of the slag to the base metal. Samples 2, 4

and 5 had a gap of less than 2 μm therefore non-adherent slag. For the four 16 mm thick samples cut with oxy-acetylene, a 1.32 - 3.38 μm gap between the slag and metal was measured in the samples, consequently the slag was non-adherent.

From SEM examination of 8 mm thick samples cut using oxy-propane flame, 6 samples (name them) had a gap of 1 - 3 μm between the slag and base metal, the slag is non-adherent. Sample 16 had no gap, confirming the adherence of slag to the base metal. The cutting of the 16 mm thick plate using an oxy-propane flame produced 3 samples (19, 22, and 23) with adherent slag. No gap was observed. 2 samples 20 and 21 had a gap of 1 μm between the slag and base metal, the slag is non-adherent.

The factors affecting slag adherence include the proportion of iron oxides, free iron, preheat, plate thickness, fuel gas type, cutting equipment, and cutting parameters (Slotman & Edward, 1951). Investigating each of these factors for the samples with adherent slag, namely samples 1, 3 and 6 from 8 mm oxy-acetylene cut plates, samples 16 from 8 mm oxy-propane cuts, and samples 19, 22, and 23 from the 16 mm oxy-propane cut plates. The atomic oxygen: iron ratios for the selected samples with adherent slag are shown in Figure 45. Samples 1, 3, and 23 have an oxygen-iron ratio of approximately 1.0. FeO phase is the prevalent oxide and it is anticipated that there may be more free iron in this slag, resulting in beading (Slotman & Edward, 1951). Samples 6, 16, 19, and 22 have an atomic oxygen-iron of ~ 1.3, confirming the prevalence of Fe_3O_4 compared to other iron oxide phases.

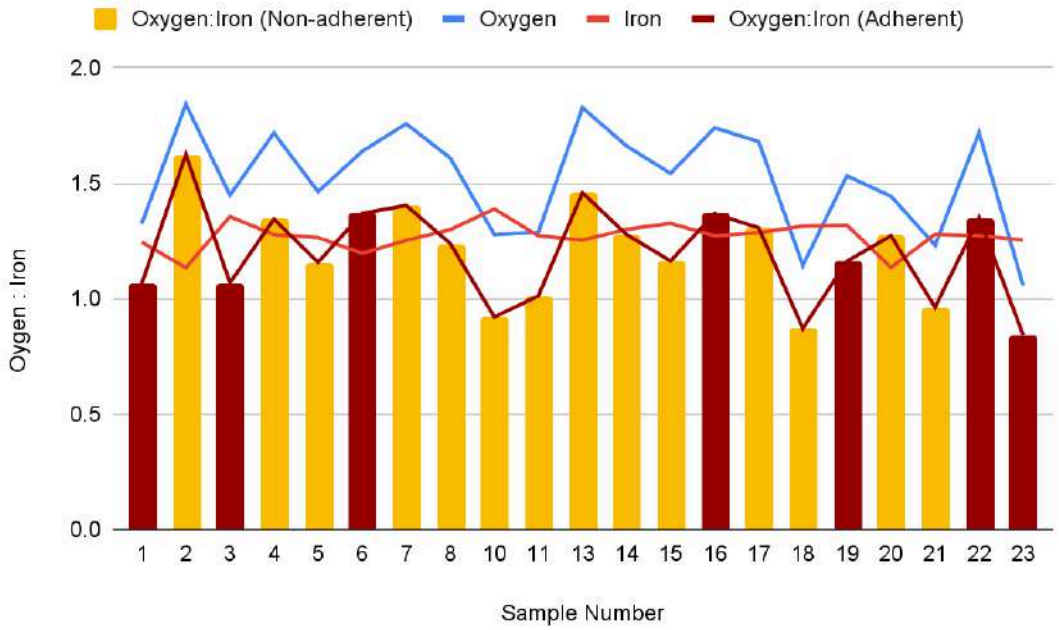


Figure 45. Slag oxygen to iron atomic ratio

The preheat temperature was not measured; however it was observed that the preheat time for samples 16, 19, 22, and 23 cut with oxy-propane was longer than that for samples 1, 3, and 6 obtained by oxy-acetylene cutting. This is expected as the inner cone maximum flame temperature for Oxy-acetylene is hotter than oxy-propane with orders of magnitude of 3160 ℃ and 2810 ℃ respectively (Abdulateef, Mustafa & Salman, 2010). In addition, one-third of the heat distribution is concentrated in the inner cone of the oxy-acetylene whilst oxy-propane has one-tenth of the heat distributed in the inner cone (Munoz-Escalona et al., 2006).

The theoretical preheat fuel gas flow rate for the oxy-acetylene was estimated to be 0.54 m^3/hr for the 8 mm plate and 1.08 m^3/hr for the 16 mm plate whereas the 6290-2 VAX nozzle used approximates the fuel gas flow rates to be 0.45 m^3/hr. For the oxy-propane, the theoretical fuel gas flow rate for the 8 mm plate is 0.33 m^3/hr, which is similar to that of the 6290-3/0VVC nozzle (0.30 m^3/hr). The same approach can be applied to the oxy-acetylene cutting of the 16 mm plate, which has an theoretical fuel gas flow rate of 0.67 m^3/hr, and where the 6290-0VVC nozzle with 0.70 m^3/hr can be used. The required heating power for the respective 8 mm and 16 mm plates is 7 kW and 8 kW and the 6290-2 VAX oxy-acetylene

nozzle approximates a heating power of 7 kW. The oxy-propane 6290-0VVC nozzle has a heating power of 8 kW however the 6290-3/0VVC gives a heating power of 18 kW.

In principle, thinner sections are expected to have more adherent slag than thicker sections. This observation was confirmed for the thicker 16 mm samples cut with oxy-acetylene. Samples 7, 8, 10, and 11 from an 16 mm thick plate cut had no adherent slag, however, the thicker 16 mm oxy-propane cut samples 19, 22, and 23 had adherent slag.

In addition, a tip with light preheat, for example, those that have one preheat hole advancing in front of the cutting oxygen hole and those that have a design that seeks to separate the preheat flame from the workpiece are better suited at reducing slag adherence. The selected cutting tips Harris 6290*VVC and the 6290-2VAX for the oxy-propane and oxy-acetylene respectively had several preheat holes surrounding the central cutting oxygen. Machine cutting has a consistent tip-to-workpiece distance and travel speeds compared to manual cutting, thus the slag tends to be less adherent with machine cutting (Slotman & Edward, 1951).

Slower cutting speeds decrease the likelihood of having free iron in the slag which reduces the slag adherence as observed for samples 4 and 5 cut at 15 mm standoff with oxy-acetylene. This is not observed for the oxy-propane samples which have adherent slag for samples cut at lower cutting speeds for both 8 mm and 16 mm thick plate samples 19 and 22. The excessive preheat used for samples 19 and 16 is suspected to be the cause as it results in more than required heating power.

Due to the low heat intensity and characteristic heat distribution of the oxy-propane flame, it is anticipated that the oxy-propane samples will have less slag adherence in comparison to the oxy-acetylene samples (Munoz-Escalona et al., 2006). The oxy-acetylene cutting of thinner plate (8 mm thickness) produced more samples with adherent slag, samples 1, 3, and 6 in comparison to the oxy-propane with one sample 16. For thicker (16 mm thickness) plate cuts, the oxy-acetylene cutting had no samples with adherent slag whilst oxy-propane had three samples 19, 22, and 23 with adherent slag. The heating power required for the 16 mm plate is 8 kW whereas the nozzle used on the 16 mm oxy-propane samples 19, 22, and 23 gives a heating power of 18 kW which is excessively higher than required and higher than

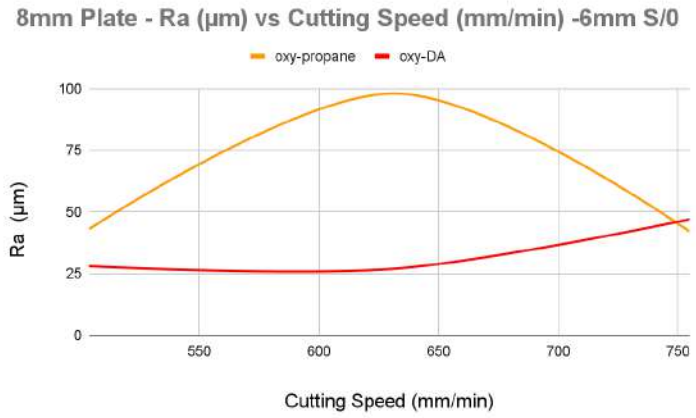
that of the oxy-acetylene which generates 7 kW. At a slower cutting speed, the slag adherence tendency increases with an increase in the heating power of the flame and free iron concentration in the slag.

5.3. Comparison with Previous Studies

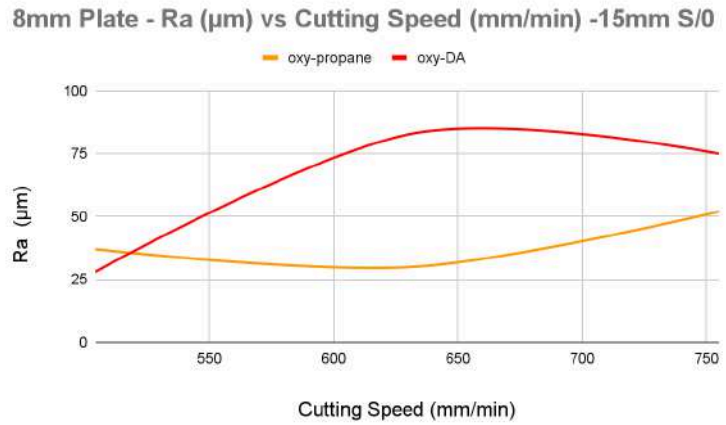
Munoz-Escalona et al. (2006) observed that the top surface of oxy-acetylene cuts had flakes on the top edge of the cut face, as shown in Figure 32. In the current study, different equipment and parameters were used when compared to the work by Munoz-Escalona et al. (2006). Similar flakes were observed for samples 1 - 3 cut from the 8 mm plate using oxy-acetylene flame and a 6 mm nozzle standoff. Table 11 shows that the coverage of flakes in samples 1 - 3 tends to decrease with increasing cutting speed (Figure 32 - Cutting speed of 250-300 mm/min), which agrees with observations by Munoz-Escalona et al. (2006).

In addition, Munoz-Escalona et al. (2006) reported that the oxy-acetylene and oxy-propane cutting of 20 mm thick samples showed cut faces with a heat tint as shown in Figure 36 (a), 36 (b) for the oxy-acetylene and Figure 36 (c), 36 (d) for the oxy-propane. This heat tint was a result of the heat of slag, giving localised heating on parts of the cut face. For the 16 mm plates cut in this research, the oxy-acetylene sample showing heat tint is sample 11 (Table 10) wherein the cutting speed was the nominal cutting speed of 592 mm/min at 15 mm standoff. Sample 23 also showed a heat tint for oxy-propane cutting at the same cutting speed and nozzle standoff.

Munoz-Escalona et al. (2006) also reported that the oxy-acetylene cut face from a 25 mm thick plate had a higher surface roughness than the oxy-propane cuts across all cutting speeds. As shown in Figure 33, the surface roughness decreases with increasing cutting speed up to a minimum, then it increases with a further increase in cutting speed. Additionally, this investigation found that the 8 mm oxy-propane cut face with 6 mm standoff had a higher surface roughness than the oxy-acetylene cut. Whilst with the 15 mm standoff, the surface roughness of oxy-propane is lower than oxy-acetylene as shown in Figure 46. The higher standoff inputs less power than required by the 8 mm plate (7 kW).



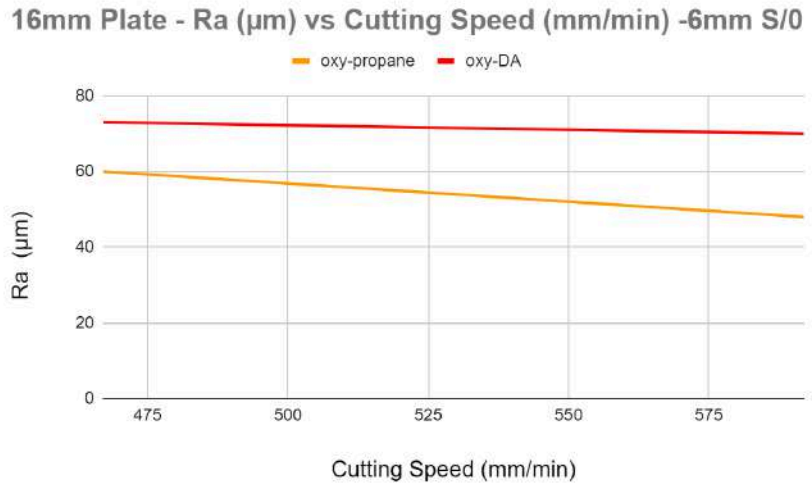
(a)



(b)

Figure 46. Variation of roughness with cutting speed for 8 mm mild steel plate at 6mm nozzle standoff (a) and 15mm nozzle standoff (b)

For the 16 mm plate as shown in Figure 47, the oxy-acetylene cut face with 6 mm standoff had a higher surface roughness than the oxy-propane cut. The oxy-propane and oxy-acetylene have surface roughness decreasing with increasing cutting speed. The 15 mm standoff cut face shows an opposite behaviour, wherein the oxy-propane has surface roughness increasing with increasing cutting speed and the oxy-acetylene surface roughness decreases with increasing cutting speed. Figure 47 (b) shows a behaviour similar to that described by Munoz-Escalona et al. (2006), wherein the oxy-propane has a surface roughness increasing with increasing cutting speed for the oxy-propane whilst the surface roughness decreases with increasing cutting speed for the oxy-acetylene.



(a)



(b)

Figure 47. Variation of roughness with cutting speed for 16 mm mild steel plate at 6mm nozzle standoff (a) and 15mm nozzle standoff (b)

Abdulateef et al. (2010) used preheat times of 15, 20, and 25 seconds to investigate the surface roughness of a 20 mm plate cut with oxy-acetylene. The study found that the surface roughness decreases when increasing the cutting speed from 350 to 500 mm/min as shown in Figure 38. Similar trends were observed for 16 mm thick plate cuts with oxy-acetylene and 6 mm nozzle standoff with oxy-propane flame. The surface roughness decreases with increasing cutting speed, however, the oxy-propane cut plate at 15 mm nozzle standoff shows an increase in surface roughness with increasing cutting speed.

Abdulateef et al. (2010) also observed that increasing the cutting speed of a 20 mm oxy-acetylene cut plate, at preheat times of 15 and 20 s, from 250 mm/min, 350 mm/min, and

500 mm/min results in an increase in hardness for an increase in cutting speed from 250 mm/min to 350 mm/min then a decrease in hardness for further increases, as shown in Figure 37.

Though the parameters are not the same, the hardness related to the 8 mm thick plate in Figures 48 (a) and 48 (b) of oxy-acetylene cut samples shows similar patterns described by Abdulateef et al. (2010), whereby the average hardness increases in value with increasing cutting speed from 504 mm/min to 632 mm/min then decreases in value with increasing cutting speed from 632 mm/min to 755 mm/min. The oxy-propane 8 mm cut samples are softer than the oxy-acetylene cut samples whereby the 6 mm nozzle standoff shows a consistent hardness across all cutting speeds and the 15 mm nozzle standoff has a sharp decrease from the cutting speed of 632 mm/min to 755 mm/min.



(a)

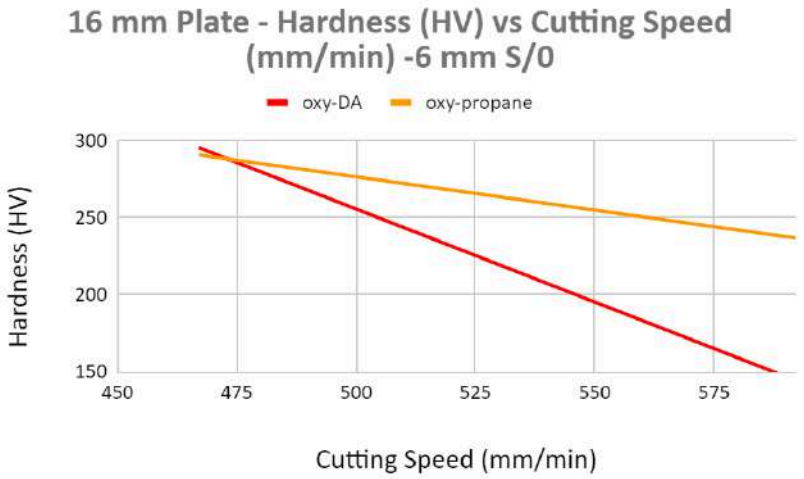


(b)

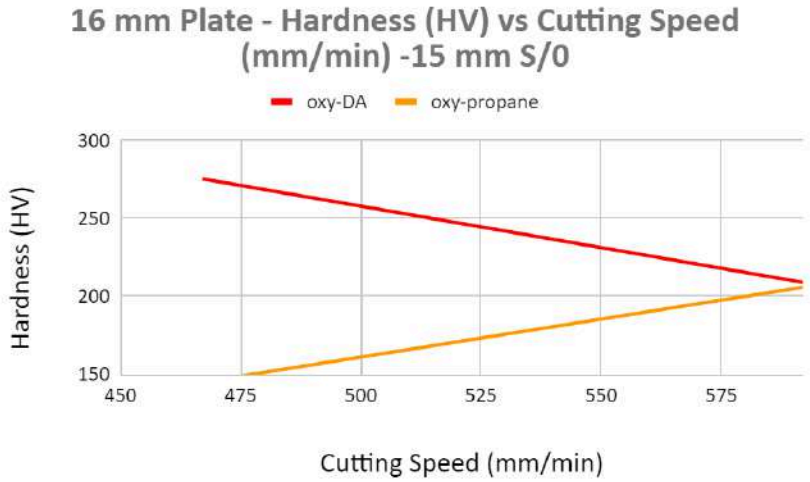
Figure 48. Variation of hardness with cutting speed for 8 mm mild steel plate at 6mm nozzle standoff (a) and 15mm nozzle standoff (b)

The 16 mm plate in Figure 49 shows a decrease in hardness with increasing cutting speed from 467 mm/min to 592 mm/min for the oxy-acetylene cut samples and the oxy-propane cut at 6 mm nozzle standoff. There is an increase in hardness with increasing cutting speed from 467 mm/min to 592 mm/min for the oxy-propane cut at 15 mm nozzle standoff. This could be attributed to a lengthy preheat time as the oxy-propane preheat time took longer than that

of the oxy-acetylene, particularly for the 16 mm plates, and the nozzle used for cutting produced a flame with higher energy than required heating power of 18 kW.



(a)



(b)

Figure 49. Variation of hardness with cutting speed for 8 mm mild steel plate at 6mm nozzle standoff (a) and 15mm nozzle standoff (b)

Munoz-Escalona et al. (2006) concluded that using oxy-propane resulted in less adherent slag in comparison to oxy-acetylene. This research shows that three out of the ten oxy-acetylene cut samples, from the 8 mm thick plate had adherent slag whilst the 16 mm thick plate oxy-acetylene had no adherent slag. In contrast, four of the eleven oxy-propane cut samples had adherent slag, one 8 mm thick (sample 16) and three 16 mm thick (samples 19, 22 and 23). It can also be seen that the 8 mm oxy-acetylene cuts had more adherent slag samples, whilst 16 mm oxy-propane cuts had more adherent slag samples.

5.4. Slag Adherence Mechanisms and Explanations

For thinner thicknesses less than approximately 10 mm, the heat generated by the combustion of iron (Hmc) is less than preheat flame (Hphf) as shown in Figure 1. The heat required to sustain the cut is mostly from the preheat flame. If the combustion of iron taking place in the kerf is insufficient, free iron (Fe) will be more significant than iron oxides (Fe_xO_y) in the slag. It is anticipated that the slag will adhere to the base metal for thinner thicknesses. However, only three samples out of the six 8 mm oxy-acetylene samples have adherent slag. For the 8 mm oxy-acetylene cut, the fastest cutting speed of nominal plus 20% (755 mm/min) at both the 6 mm and 15 mm nozzle standoff produced samples with adherent slag. This can be due to the insufficient time for the combustion of iron at fast cutting speeds with the two samples showing a backward cutting oxygen jet inclination during cutting and concavity of the cut face after cutting.

The oxy-propane cutting of an 8 mm thick plate produced one sample with adherent slag. Sample 16 was cut at the nominal cutting speed minus 20%, 504 mm/min at 15 mm standoff. This sample had no gap measured between the slag and base metal. Three samples cut at 15 mm standoff had the highest oxygen-iron ratio of 1.4 of the three corresponding samples cut with oxy-propane flame at 6 mm standoff. It was anticipated that this sample would have non-adherent slag however the excessive preheat time, approximately 42 seconds resulted in the base material having high heat input and the heat from metal combustion is greater than the heat from the preheat flame. For the 8 mm plate, the heat from metal combustion is lesser than the heat from the preheat flame.

For thicker thicknesses greater than approximately 10 mm, the heat generated by the combustion of iron (Hmc) is higher than the preheat flame (Hphf) (Figure 1). Cutting is mostly energy-driven by the combustion of iron which is also the rapid oxidation of the metal. The combustion of iron is significant than the preheat energy thus, resulting in lower free iron content compared to iron oxides Fe_xO_y in the slag. Commonly, the slag will not adhere to the base metal for thicker plate cuts. In this study, four 16 mm oxy-acetylene samples had non-adherent slag.

Three samples from oxy-propane cutting of a 16 mm thick plate had an adherent slag. One was cut at the nominal cutting speed minus 20%, 467 mm/min at 6 mm standoff, the other at the same cutting speed at 15 mm standoff, and the third at the nominal cutting speed of 592

mm/min at 15 mm nozzle standoff. Oxy-propane cutting of thicker plates seems to have predominantly adherent slag as three of the five 16 mm samples have adherent slag. The preheat time for these three samples was approximately 30 seconds for the 6 mm standoff and 80 seconds for the 15 mm standoff.

The surface roughness Ra values of the 8 mm oxy-acetylene cut samples have a relatively wide range in comparison to the maximum profile height Rz5 values. The samples with adherent slag have a maximum profile height (Rz5) of 72 - 77 μm which is the lowest of all the oxy-acetylene cut samples, including the 16 mm samples. For the oxy-acetylene cuts, the slag tends to be adherent when the Rz5 is below 80 μm. This suggests that 8 mm samples with a smoother profile height can have adherent slag at the bottom of the plate due to the slag thickness remaining stable in the kerf and in contact with the molten steel and not periodically moving behind the cutting oxygen to create draglines that make the surface rough. Should the slag move behind the cutting oxygen, it becomes enriched with iron combustion products before settling on the sidewall at the bottom of the cut. In this instance, the slag becomes enriched with free iron from the molten steel while remaining in contact with the molten steel in the kerf and settles on the sidewalls at the bottom of the cut, favouring its tendency to be adherent to the sidewall at the bottom of the cut.

5.5. Practical Implications

A traditional metal fabrication workshop adopts and applies a variety of methods to manufacture products that can be used in various industries including automotive, oil and gas, railway, marine, aerospace, and power generation. The methods used to fabricate the parts are preceded by cutting the raw materials which are predominantly metal plates into lengths that are then further processed by forming, welding, heat treatment, and corrosion protection as required.

The oxy-fuel gas cutting (OFC) process is the oldest and underdeveloped of the mainstream cutting methods, however, it is still widely used and requires controlling the inputs and process parameters to produce a quality part that can be used effectively in the subsequent fabrication processes. The adherence of the slag to the parent metal is a factor in processing efficiency and may result in additional work to remove the slag which may lead to additional labour and material cost and downtime.

During this research, it was demonstrated that for thinner 8 mm thick samples, oxy-propane had less adherent slag than oxy-acetylene cut samples. The slag was non-adherent on five of the six oxy-propane cut samples. Varying the cutting speed and nozzle standoff seeked to simulate the effect of manual hand cutting as hand cutting is prone to fluctuations in the cutting speed and nozzle standoff. To minimise slag adherence, propane is recommended as better-suited fuel gas for cutting thinner thicknesses below 10 mm. The 8 mm oxy-acetylene samples have non-adherent slag at the nominal cutting speed for both nozzle standoffs. The acetylene gas is most effective when using machine cutting on thinner thicknesses below 10 mm..

For the thicker 16 mm samples, it was established that oxy-propane cuts had more adherent slag than the oxy-acetylene. The slag was adherent on the oxy-propane samples at the nominal minus 20% cutting speed and all the 15 mm nozzle standoff samples. The longer preheat time of the oxy-propane, slower cutting speeds, and higher nozzle standoff promote the slag to be adherent. Cutting at the nominal cutting speed at 6 mm nozzle standoff is most effective for the thicker thickness. To minimise slag adherence, acetylene is recommended as better-suited fuel gas for cutting thicker thicknesses above 10 mm.

5.6. Limitations

To further validate and refine the findings of this research there are some factors and variables that could have been optimised and or approached differently.

The oxygen-fuel cutting process is still relevant in the fields of fabrication but the investigations on OFC are limited in open literature. The works by Muñoz-Escalona et al. (2006), Abdulateef et al. (2010), Harish and Babu (2017), and most recently Jokiaho et al (2019) focused on other aspects of the OFC technique and not on the slag adherence. The slag adherence in general in OFC is depicted in the book of Slotman et al. (1951) wherein the variables and factors affecting the slag adherence of OFC are explained.

For the oxy-acetylene samples, the 6290-2 VAX nozzle used is prescribed for 8 - 15 mm plate thicknesses. Though the 16 mm samples cut with oxy-acetylene had no adherent slag, two of the samples with the nominal plus 20 percent of the cutting speed samples 9 and 12

had no cut initiated subsequent to preheat as a result of the 6290-2 VAX nozzle not being optimal for this thickness. Due to the narrower range of nozzle selection, the propane fuel gas is better optimised than the acetylene (acetylene).

The calculated nominal average cutting speed for the 8 mm and 16 mm plates were 623 and 607 mm/min respectively as shown in Table 4. The potentiometer dial of the machine increases at 0.5 increments as shown in Table 5 and potentiometer dials corresponding to this were not achievable. Thus potentiometer dial number 8 of 632 mm/min was the closest to 623 mm/min and potentiometer dial number 7.5 of 592 mm/min was closest to 607 mm/min. This is a deviation of - 1.4 % for the 8 mm and -2.4% for the 16 mm nominal average cutting speeds.

The Harris equipment used described in section 3.1 of this report does not allow for separate quantifying of the preheat oxygen and cutting oxygen pressure as the oxygen is supplied through a common cylinder and pressure regulator. The supply of both the preheat and cutting oxygen is combined through a common cutting torch through the nozzle and adjusted with separate valves for activation as shown in Figure 39. The Harris cutting charts and theoretical calculations were used to determine the respective fuel gas flow rates, preheat oxygen, and cutting oxygen.

The EDS analysis used is prone to limitations concerning the detection of carbon and oxygen. The atomic ratios of iron and oxygen, and the oxygen to iron used to determine the composition of the slag were thus subject to a margin of error.

Chapter 6 - Conclusion and Recommendations

6.1. Conclusion

The present dissertation aimed to study the slag adherence variation of oxy-fuel cutting gases by experimental measurements. The study also reviewed the concepts of oxy-fuel flame cutting to better understand slag adherence to the base metal. The contributions of this study concerning the proposed scope of work are as follows.

The oxy-fuel cutting is often carried out based on process parameters prescribed in the cutting chart of the various OEMs . These parameters generally yield a good-quality cut with no adherent slag. Though not the most optimised cutting nozzle concerning plate thickness, the cutting parameters (nozzle selection, cutting pressures, cutting speed and nozzle stand) used for the oxy-acetylene and oxy-propane were selected to achieve a face cut of acceptable quality for 8 mm and 16 mm thick plain steel plates.

During analysis it was deduced that the thinner 8 mm thick oxy-acetylene plate samples were more prone to adherent slag than the oxy-propane and the thicker 16 mm oxy-propane samples were more prone to adherent slag than the oxy-acetylene. For the 8 mm plate the slag was adherent due to the heat generated by the combustion of iron smaller than the preheat flame and there is insufficient combustion of iron taking place in the kerf at the faster cutting speeds thus the amount of free iron is greater than the content of oxidised iron in the slag (Fe_xO_y). For the 16 mm plate, the tendency of the slag to be adherent was due to the excessive heating power and preheat time of the oxy-propane nozzle at the slower cutting speed which increases the likelihood of free iron content.

Utilising the Harris nozzles, the oxy-propane is most suited in minimising adherent slag when manual cutting thinner thicknesses whereas oxy-acetylene is best suited for machine cutting of similar thickness. The Oxy-acetylene nozzle is optimised for manual cutting of the thicker 16 mm thickness.

6.2. Recommendations

The relationship between surface roughness and adherent slag on the fatigue life utilising oxy-propane, oxy-acetylene and additional fuel gas mixtures used in industry for OFC, namely LPG and Chemtane are topics that may be further investigated.

The free iron content of the slag was not quantified and it is a major factor contributing to the adherence of the slag. Further work that measures the free iron content is recommended.

Two nozzles were used to cover the section thickness for the oxy-propane cuts however the heating power in Appendix B ranges from 6700 (8) - 15600 (18) Kcal/h (kW) for 6 - 50 mm whereas theoretically it is 6 - 10 kW (eq 2.3.6). Further research with an optimised nozzle from a different OEM may be a consideration for further investigation.

References

/1/ American Welding Society. 2001. Standard Welding Terms and Definitions (AWS A3.0:2001). American Welding Society

/2/ Suzan, S. (2014). RIC Training - Flame Processes [Presentation]. Retrieved from https://drive.google.com/file/d/123zQOSFNlfPvYBr-L2_UuJm8Uza0FNHW/view?usp=sharing

/3/ Slotman, G.V and Edward, H.R. 1951. *Oxygen Cutting. 1st ed.* New York, Toronto, London: McGraw-Hill Book Company

/4/ Garcia, T. Cicero, S. Alvarez, J. Carrascal, I. and Martin-Meizoso, A. 2015. Effects of Thermal Cutting Methods on the Fatigue Life of High Strength Structural Steel S690Q in American Society of Mechanical Engineers, Pressure Vessels and Piping Division (Publication) PVP, DOI: 10.1115/PVP2015-45174

/5/ Glizmanenko, D. and Yeveseyev, G. 1961. Gas Welding and Cutting. Moscow: Peace Publishers

/6/ Cariston, C.L. 2002. Laser Cutting: Guide for Manufacturing. Dearborn, Michigan: Society of Manufacturing Engineers

/7/ Cox, I. and Arthur, N. 2002, Allen's Astrophysical Quantities. 4th ed. New York: Springer Science + Business media

/8/ Harish, M. and Babu, P.K. Analysis of Oxy-fuel Process Cutting Parameters Using Grey Taguchi Technique for Mild Steel HRE350. *International Journal of Innovative Technology and Research*, vol. 5, issue. 2, pp. 5777 - 5783

/9/ Jokiaho, T. Santa-Aho, S. Peura, P. and Vippola, M. 2019. Role of Steel Plate Thickness on the Residual Stress Formation and Cracking Behavior During Flame Cutting. *Metallurgical and Materials Transactions A.* Vol 50, pp 4178–4192

/10/ Ramakrishna, C. Raghuram, K. and Avinash ben, B. 2018. Process Modeling and Simulation Analysis of CNC Oxy-fuel Cutting Process on A516 Grade 70 Carbon Steel. *Materials Today*. Proceedings 5, pp 7818 - 7827

/11/ Charles, J.A. and Chater, W.J. 1978. Oxygen Cutting, Metals Technology, 5:1. 163-175, DOI: 10.1179/mt.1978.5.1.163

/12/ Pond, T.L. and Martin, C.R. 2020. Electrical characteristics of the oxy-fuel flame while cutting steel. *Experimental Thermal and Fluid Science.* 112. 109985

/13/ Munoz-Escalona P. Payares, M.C. Dorta, M. and Diaz, R. 2006. Analysis and Influence of Acetylene and Propane Gas During Oxy-fuel Gas Cutting of 1045 Carbon Steel. *ASM International.* Journal of Materials Engineering and Performance. Vol 15, pp 684-692

/14/ Abdulateef, O.F. Mustafa, F.F. and Salman, S.A. 2010. Prediction The Effect Of Flame Cutting Parameters On The Quality Of Metal Surface In CNC Flame Cutting Machine Using Artificial Neural Network. *The Iraqi Journal For Mechanical And Material Engineering*, Vol 10, No. 3

/15/ Cicero S. García T. Álvarez J.A.Bannister A. Klimpel A. Martín-Meizoso A. and Aldazabal J.2016. Fatigue behaviour of structural steels with oxy-fuel, plasma and laser cut straight edges. Definition of Eurocode 3 FAT classes. *Engineering Structures,* Vol 111 pp 152–161

/16/ Genna S. Menna E. Rubino G. and Tagliaferri V. 2020. Experimental Investigation of Industrial Laser Cutting: The Effect of the Material Selection and the Process Parameters on the Kerf Quality. *Applied Sciences.* 10. 4956. DOI:10.3390/app10144956

/17/ Wandera C. 2006. Laser Cutting of Austenitic Stainless Steel with a High Quality Laser Beam. LUT University. DOI:

https://lutpub.lut.fi/bitstream/handle/10024/30302/TMP.objres.256.pdf?sequence=1&isAllowed=y

/18/ Orishich, A.M. Shulyatyev, V.B. and Golyshev, A.A. (2016). The Utmost Thickness of the Cut Sheet for the Qualitative Oxygen-Assisted laser cutting of low-carbon steel. *Physics Procedia.* 83. pp 296 - 301

/19/ O'Neill, W. and Gabzdyl, J.T. 2000. New Developments in Laser-Assisted Oxygen Cutting. *Optics and Lasers in Engineering.* 34. pp 355 - 367

/20/ Golnabi, H. and Bahar, M. 2008. Investigation of optimum condition on oxygen gas-assisted laser cutting. *Optics & Laser Technology.* Vol. 4. pp 454–460

/21/ Lai, S. Jia, Y. Han,B. Wang, J. Liu, Z. Ni, X. Shen, Z. and Lu, J. 2017. Lumped Parameter experiments for Single Mode Fiber Laser Cutting of Thin Stainless Steel Plate. *IOP Conf. Series: Journal of Physics: Conf.* Series 844. 012062 DOI:10.1088/1742-6596/844/1/012062

/22/ The Harris Products Group. *Equipment Catalogue - International.* *https://www.harrisproductsgroup.com/en/*

/23/ ISO. 2006. ISO9013: Thermal Cutting - Classifications of Thermal Cuts - Geometrical Product Specification and Quality Tolerances. *SABS.*

/24/ G·WEIKE Laser. 2024. Fibre Laser. Shandong. Available from: https://www.gwklaser.com/fiberlaser/LF4020GH.html [Accessed 14 July 2024]

/25/ Davis, D. 2024. An Overview of Oxy-fuel Cutting. The Fabricator. Available from: https://www.thefabricator.com/thefabricator/article/oxy-fuelcutting/an-overview-of-oxy-fuel-cutting [Accessd 30 June 2024]

/26/ Benscoter, A. and Bramfitt, B.. Metallography and Microstructures of Lo-Carbon and Coated Steels. *ASM Handbook : Metallography and Microstructures*. Vol 9 pp 588 - 607

Appendices

Appendix A - Cutting Machine

HARRIS PLUS

MODEL

HARRIS PORTABLE CUTTING SYSTEM

Harris Plus is a more portable version of the Harris Super, designed with the same precision and capabilities.

FEATURES

- Straight line and circle oxy fuel cutting
- Stepless Drive System, maintaining constant travel speed even with high temperatures and ensuring stable, trouble-free cutting
- Light weight - 9,5 kg - easy to carry and use
- Modular straight 1800 mm rail sections (to be ordered separately)

PACKAGE INCLUDES

- Cutting machine with connecting lead and rubber connection hose from machine to cutting torch
- Harris cutting torch Model 198 with 3 tips
- Tool set
- Operation manual



Model shown with additional accessories to be ordered separately

MODEL NO.	DESCRIPTION	NOTE
PCS-PLUS-110F	Harris Plus 110 V	Propane
PCS-PLUS-220F	Harris Plus 220 V	
PCS-PLUS-110	Harris Plus 110 V	Acetylene
PCS-PLUS-220	Harris Plus 220 V	

SPECIFICATIONS	
Cutting Thickness	3-150 mm
Cutting Speed	150-800 mm/min
Speed control	Single cone speed system, mechanical regulation
Power Source	110 V, 220 V AC
Weight	9,5 kg
Overall Measurement	360 mm (L) x 140 mm (W) x 175 mm (H)
Cutting Torch	Propane: 198-4F Acetylene: 198-4
Cutting Tips*	Propane: 6290-VVC (size 5/0 to 2½) Acetylene: 6290-VAX (size 1 to 5)

Appendix B - Cutting Tips

VVC NH

6290 MODEL

MACHINE CUTTING TIPS

FEATURES:

- High-speed oxy-alternative fuel gas cutting tips
- Minimalize kerf
- Increased cutting speeds, reduced heat input
- High quality machine cuts, reduces afterwork
- Use with low cost fuel gases
- 6290-VVC plated shell, 6290-NH unplated



6290-VVC 6290-NH

OXY-PROPANE CUTTING

PART NO.	PLATE THICKNESS (mm)	CUTTING SPEED (mm/min)	CUTTING OXY PRESSURE (bar)	PREHEAT OXY PRESSURE (HIGH¹ - LOW) (bar)	CUTTING OXY FLOW (l/h)	PREHEAT OXY FLOW (HIGH - LOW) (l/h)	PREHEAT FUEL FLOW (HIGH - LOW) (l/h)	HEATING POWER (HIGH - LOW) (Kcal/h)	KERF WIDTH (mm)
6290-5/0VVC	1 - 4	750 - 550	4,0	0,7 - 0,4	650	1410 - 900	350 - 230	7800 - 5100	1,3
6290-4/0VVC	4 - 6	700 - 520	2,5	1,0 - 0,5	1130	1410 - 900	350 - 230	7800 - 5100	1,5
6290-3/0VVC	6 - 9	650 - 480	5,0	2,5 - 0,7	2260	2800 - 1200	700 - 300	15600 - 6700	1,8
6290-00VVC	9 - 12,5	630 - 450	5,0	2,5 - 0,7	2540	2800 - 1200	700 - 300	15600 - 6700	1,8
6290-0VVC	12,5 - 20	600 - 400	6,0	2,5 - 0,7	3530	2800 - 1200	700 - 300	15600 - 6700	2,0
6290-0½VVC	20 - 35	550 - 360	7,0	2,5 - 0,7	4000	2800 - 1200	700 - 300	15600 - 6700	2,0
6290-1VVC	35 - 60	480 - 220	7,0	2,5 - 0,7	5560	2800 - 1200	700 - 300	15600 - 6700	2,3
6290-1½VVC	60 - 75	310 - 200	6,5	2,5 - 0,7	7070	2800 - 1200	700 - 300	15600 - 6700	2,8
6290-2VVC	75 - 100	280 - 190	6,5	2,5 - 0,7	8000	2800 - 1300	700 - 330	15600 - 7400	3,0

VAX VPM NHM

6290 MODEL

MACHINE CUTTING TIPS

FEATURES:

- High-speed oxy-fuel gas cutting tips
- Minimalize kerf
- Increased cutting speeds, reduced heat input
- High quality machine cuts, reduces afterwork
- 6290-VAX & 6290-VPM plated shell, 6290-NHM unplated



6290-VAX 6290-VPM 6290-NHM

OXY-ACETYLENE CUTTING

PART NO.	PLATE THICKNESS (mm)	CUTTING SPEED (mm/min)	CUTTING OXY PRESSURE (bar)	CUTTING OXY FLOW (l/h)	PREHEAT OXY FLOW (l/h)	ACETYLENE FLOW (l/h)	HEATING POWER (Kcal/h)
6290-1VAX	0 - 8	650	2,5 - 4,0	850 - 1250	400	350	4740
6290-2VAX	8 - 15	600	5,0	2400	450	420	5690
6290-3VAX	15 - 35	550	7,0	4000	500	440	5960
6290-4VAX	35 - 75	450	7,0	5000	580	500	6780
6290-5VAX	75 - 150	300	5,0	9000	660	600	8130
6290-6VAX	150 - 200	150	6,5	13500	600	800	10840

Appendix C - Cut Quality Chart

MACHINE CUTTING GUIDE

CORRECT CUTS



PERFECT CUT - Regular surface with slightly sloping drag lines indicates a perfect cut. A slight amount of scale at the top of the cut is caused by preheat flames and is easily removed. This surface can be used for many purposes without machining.

PRODUCTION CUT - Moderately sloping drag lines and a reasonably smooth surface characterize a production cut. For production operations a cut of this type represents the best combination of quality and economy.

DIRTY TIP



DIRTY TIP - Dirt or scale in the tip will deflect the oxygen stream and cause one or more of the following problems: excess slag on the steel, an irregular cut surface, pitting and undercutting.

CUTTING SPEED



EXTREMELY FAST - Rake angle of drag lines shows extremely fast cutting speed. Top edge is good and cut face is smooth. However, slag adheres to the bottom side and there is danger of losing the cut. Not enough time is allowed for slag to blow out of the kerf. Cut face often slightly concave.

EXTREMELY SLOW - Pressure marks indicate too much oxygen for cutting conditions. Either the tip is too big, cutting oxygen pressure too high, or speed is too slow as shown by a rounded or beaded top edge as in this case. As oxygen volume nears correct proportions, pressure marks appear closer to the bottom edge until they finally disappear.

SLIGHTLY TOO FAST - Drag lines incline backwards, but a "drop cut" is still attained. Top edge is good. Cut face is smooth and slag free. Quality is satisfactory for most production work.

SLIGHTLY TOO SLOW - Cut is high quality although there is some surface roughness caused by vertical drag lines. Top edge is usually slightly beaded. Quality is generally acceptable, faster speeds are more desirable.

TIP DISTANCE



TOO CLOSE - Grooves and deep drag lines caused by unstable cutting action. Part of preheat cone burns inside kerf where normal gas expansion deflects oxygen cutting stream.

TOO HIGH - Top edge is beaded or rounded, cut face is not smooth and often is slightly beveled when preheat effectiveness is partially lost due to the tip being held too high. Cutting speed is reduced because of the danger of losing the cut.

GAS ADJUSTMENT



TOO MUCH CUTTING OXYGEN - Pressure marks are caused by too much cutting oxygen. When more oxygen is supplied than can be consumed in oxidation, the remainder goes around the slag creating gouges, or pressure marks. Correct this fault by lowering cutting oxygen pressure, increasing speed, or using a smaller tip. As oxygen volume nears correct proportion, pressure marks appear closer to the bottom edge until they finally disappear.

TOO HOT PREHEAT - Rounded top edge caused by too much preheat. Excess preheat does not increase cutting speed, it only wastes gases.

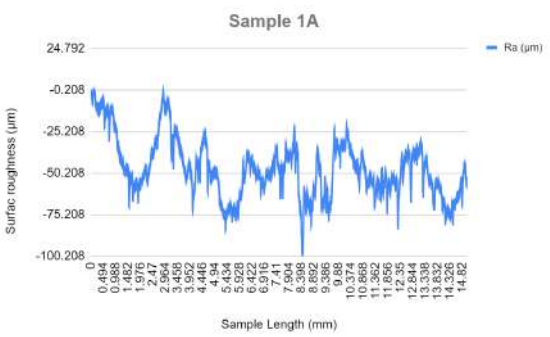
WHAT TO LOOK FOR IN BEVEL CUTTING

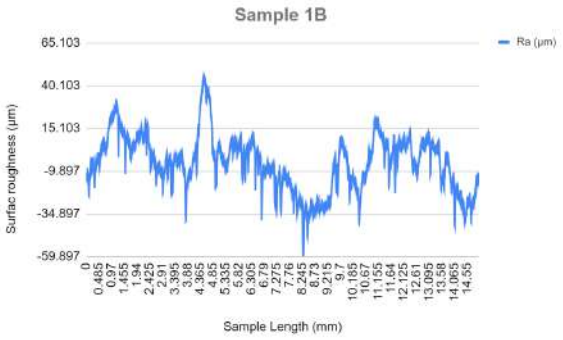


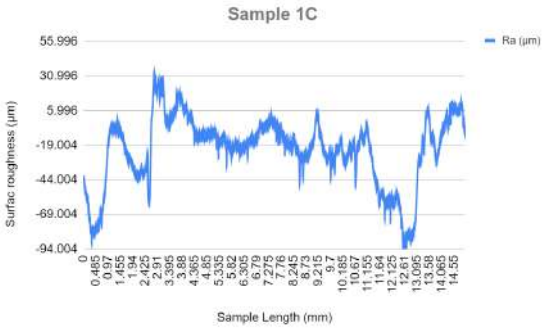
GOOD QUALITY - Top edge is excellent and cut face extremely smooth. Slag should be easy to remove and the cut part dimensionally accurate. Cutting speed is slower than vertical cutting because preheat effect is partially deflected from plate.

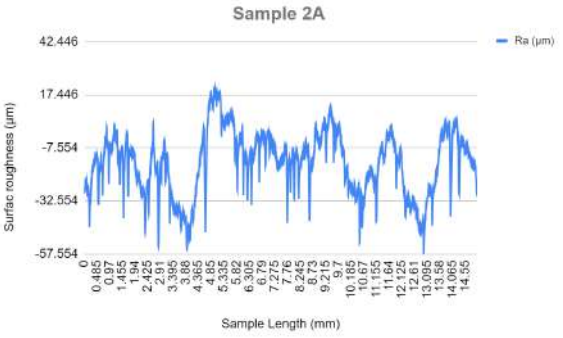
POOR QUALITY - Gouging is the most common fault. It is caused by either a speed that is too fast or preheat flames that are too mild. Another fault is a rounded top edge, caused by too much preheat, indicating excessive gas consumption.

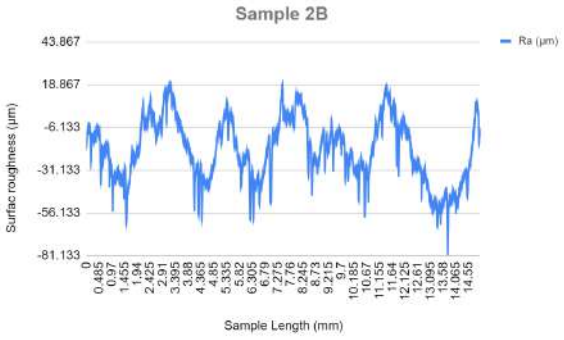
Appendix D - Roughness Test Results

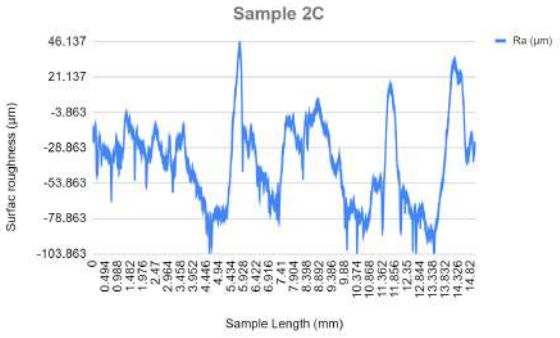


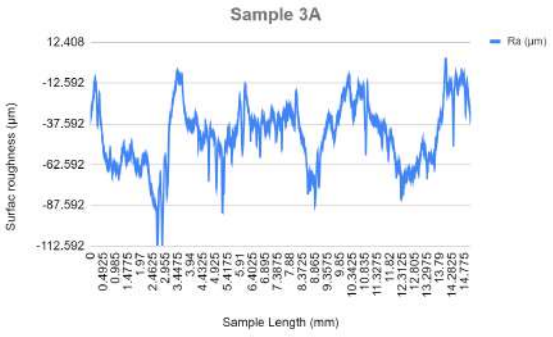


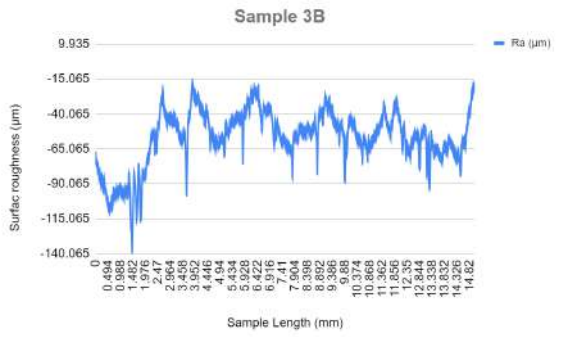


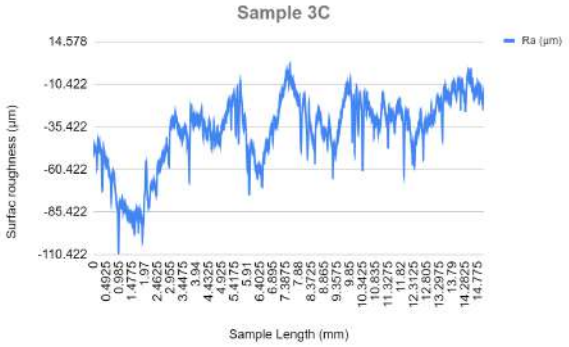


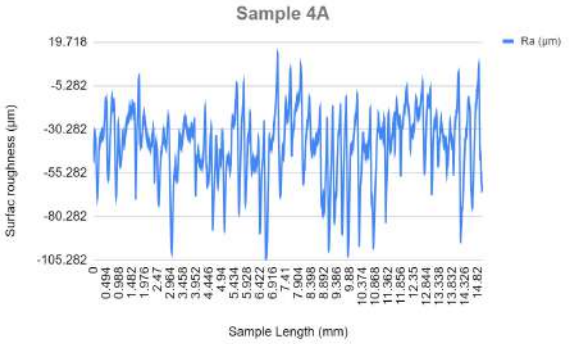


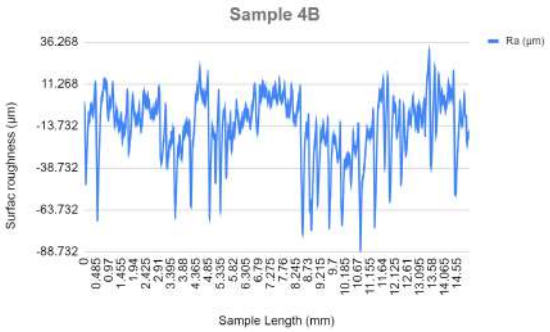


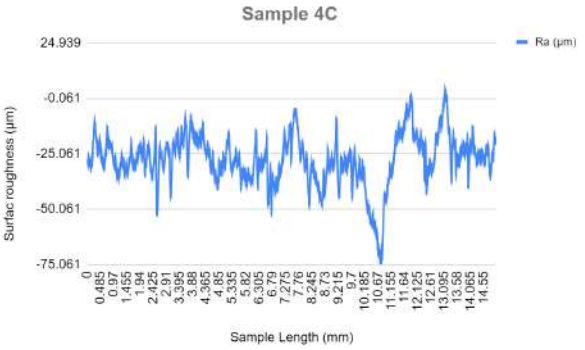


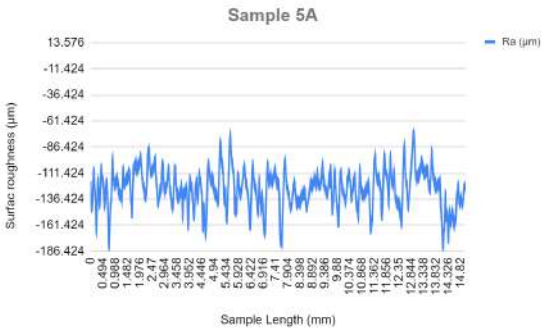


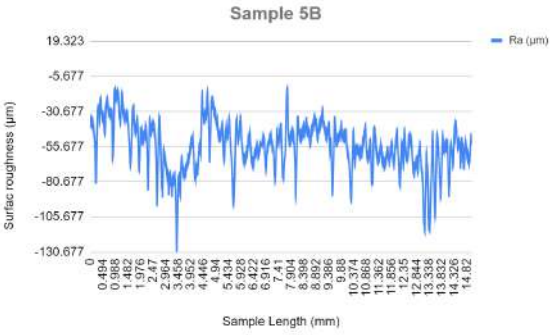

Sample 3C
Ra (µm)
Surfac roughness (µm)
Sample Length (mm)

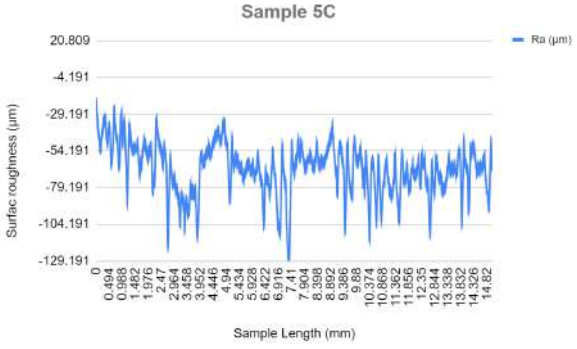

Sample 4A
Ra (µm)
Surfac roughness (µm)
Sample Length (mm)

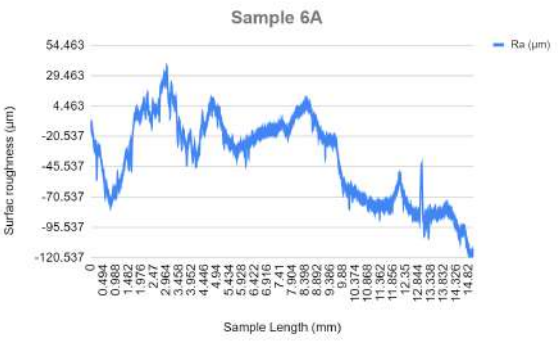

Sample 4B
Ra (µm)
Surfac roughness (µm)
Sample Length (mm)

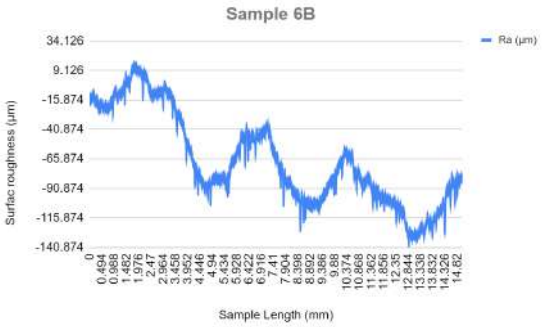

Sample 4C
Ra (µm)
Surfac roughness (µm)
Sample Length (mm)

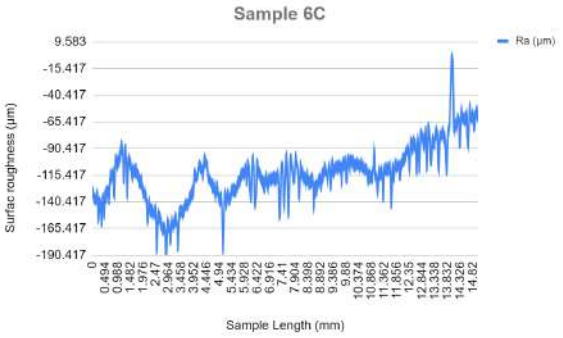

Sample 5A
Ra (µm)
Surfac roughness (µm)
Sample Length (mm)

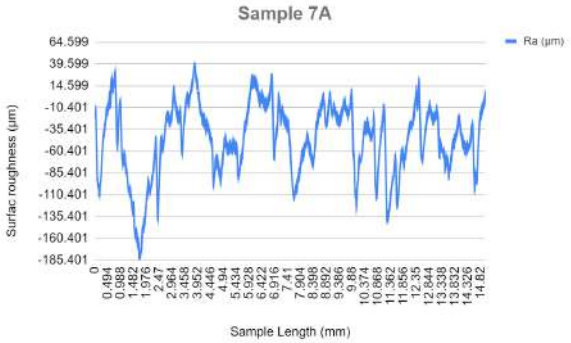

Sample 5B
Ra (µm)
Surfac roughness (µm)
Sample Length (mm)

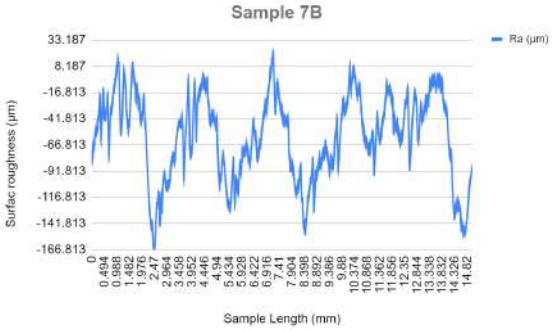

Sample 5C
Ra (µm)
Surfac roughness (µm)
Sample Length (mm)

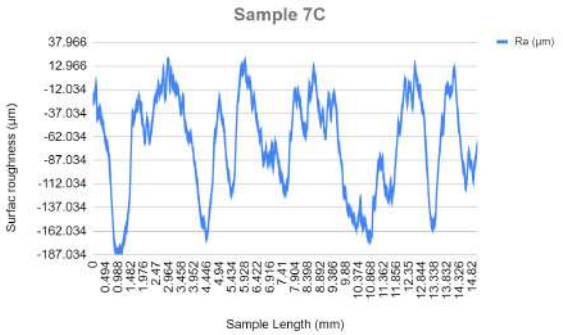

Sample 6A
Ra (µm)
Surfac roughness (µm)
Sample Length (mm)

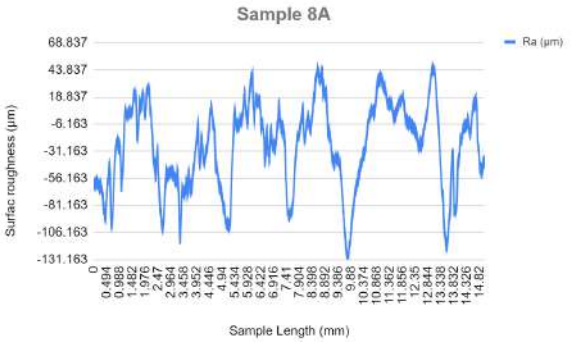

Sample 6B
Ra (µm)
Surfac roughness (µm)
Sample Length (mm)

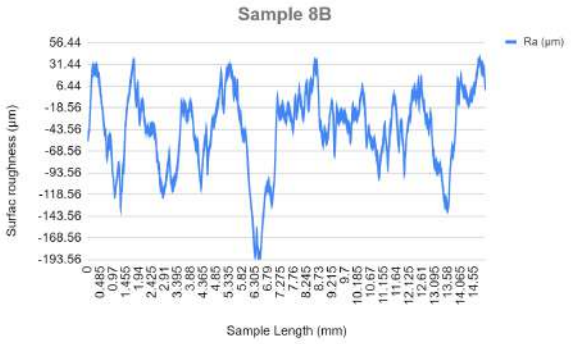

Sample 6C
Ra (µm)
Surfac roughness (µm)
Sample Length (mm)

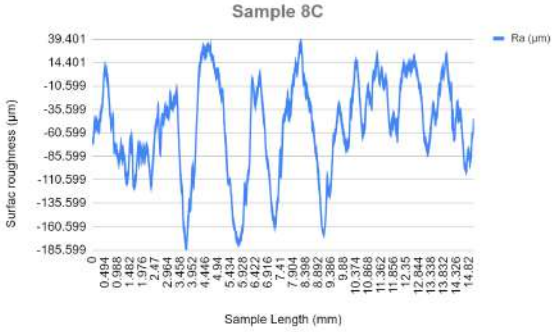

Sample 7A
Ra (µm)
Surfac roughness (µm)
Sample Length (mm)

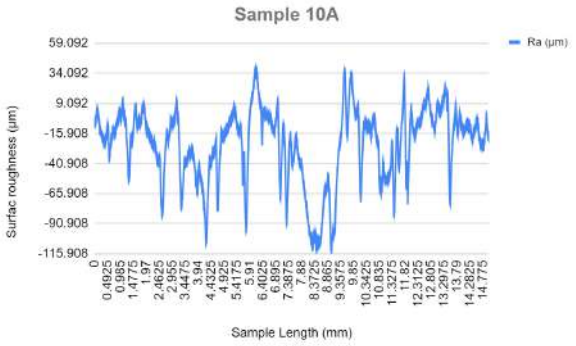

Sample 7B
Ra (µm)
Surfac roughness (µm)
Sample Length (mm)

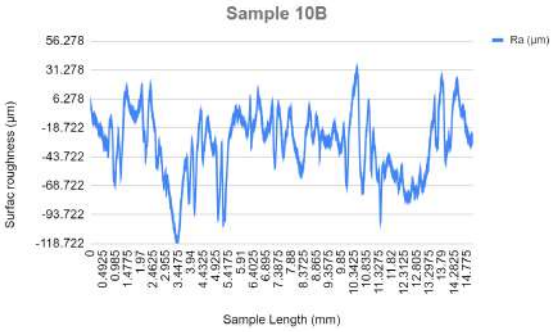

Sample 7C
Ra (µm)
Surfac roughness (µm)
Sample Length (mm)

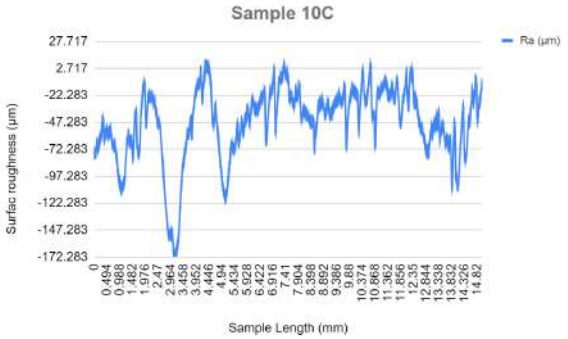

Sample 8A
Ra (µm)
Surfac roughness (µm)
Sample Length (mm)

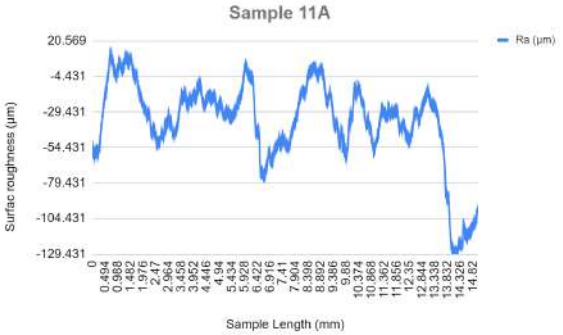

Sample 8B
Ra (µm)
Surfac roughness (µm)
Sample Length (mm)

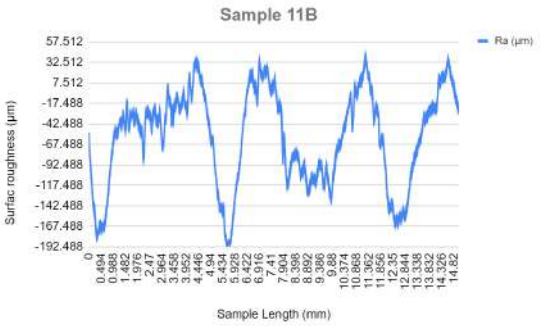

Sample 8C
Ra (µm)
Surfac roughness (µm)
Sample Length (mm)

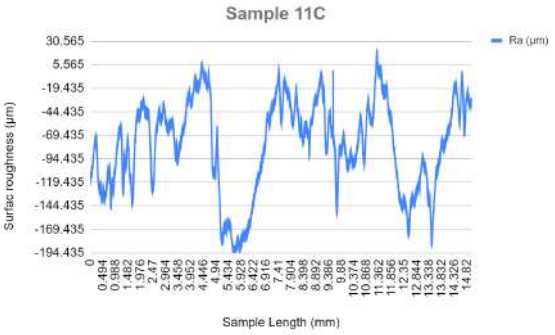

Sample 10A
Ra (µm)
Surfac roughness (µm)
Sample Length (mm)

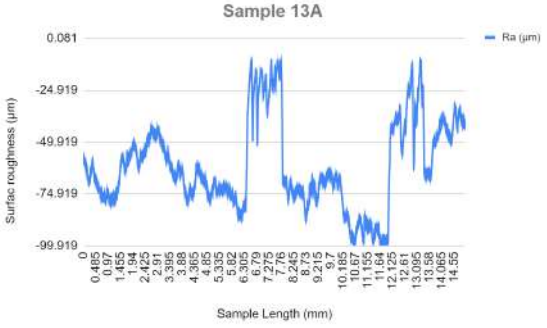

Sample 10B
Ra (µm)
Surfac roughness (µm)
Sample Length (mm)

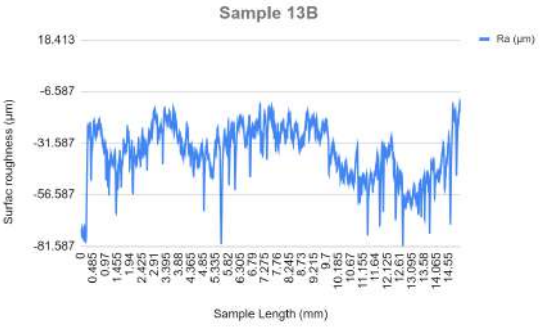

Sample 10C
Ra (µm)
Surfac roughness (µm)
Sample Length (mm)

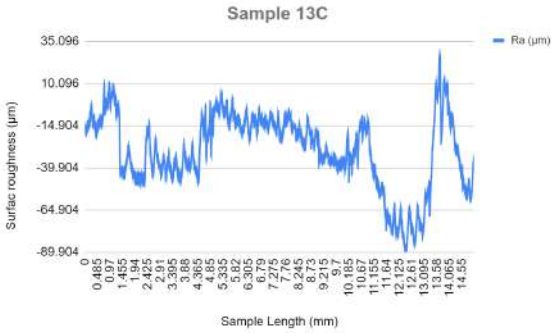

Sample 11A
Ra (µm)
Surfac roughness (µm)
Sample Length (mm)

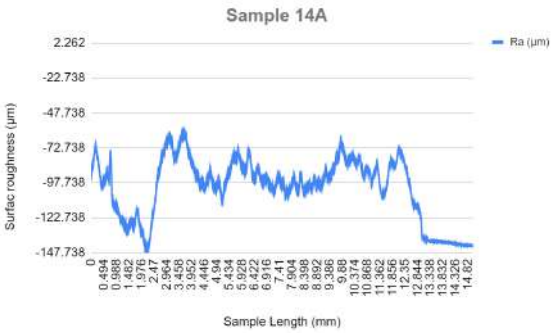

Sample 11B
Ra (µm)
Surfac roughness (µm)
Sample Length (mm)

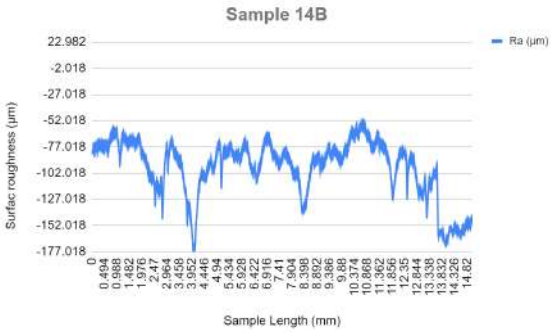

Sample 11C
Ra (µm)
Surfac roughness (µm)
Sample Length (mm)

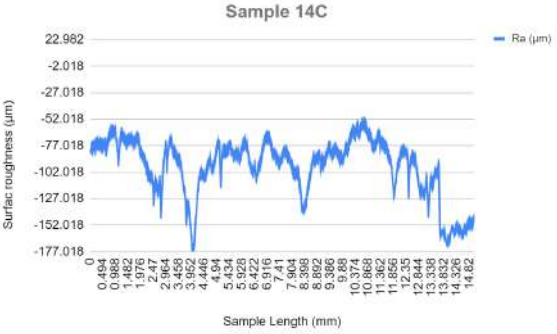

Sample 13A
Ra (µm)
Surfac roughness (µm)
Sample Length (mm)

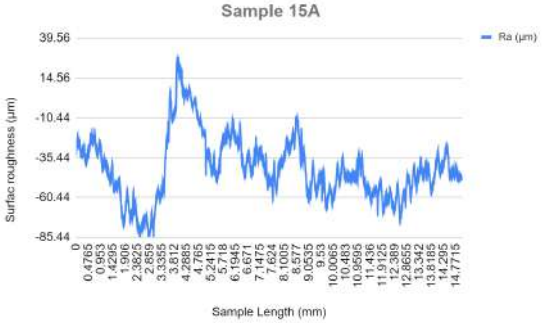

Sample 13B
Ra (µm)
Surfac roughness (µm)
Sample Length (mm)

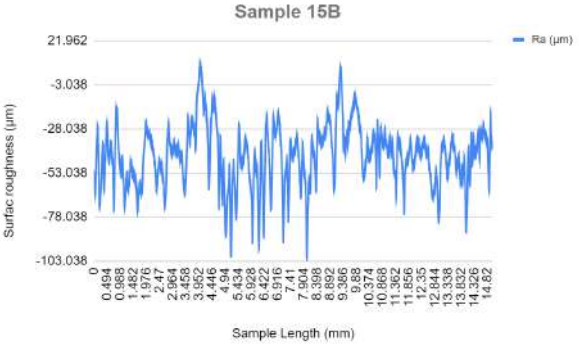

Sample 13C
Ra (µm)
Surfac roughness (µm)
Sample Length (mm)

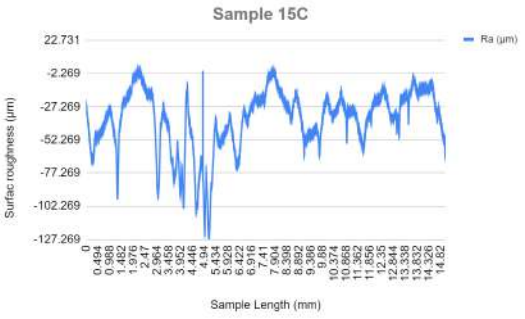

Sample 14A
Ra (µm)
Surfac roughness (µm)
Sample Length (mm)

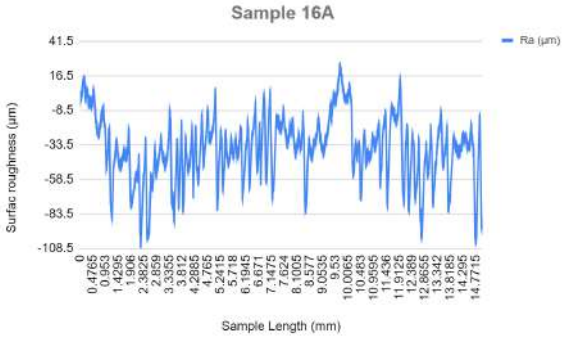

Sample 14B
Ra (µm)
Surfac roughness (µm)
Sample Length (mm)

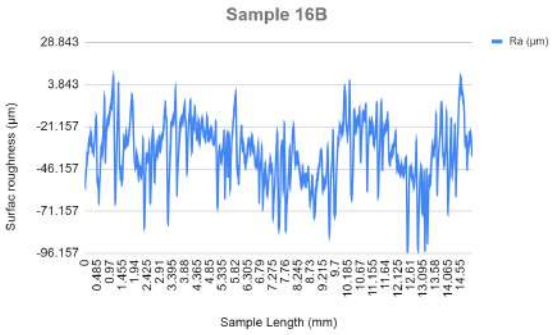

Sample 14C
Ra (µm)
Surfac roughness (µm)
Sample Length (mm)

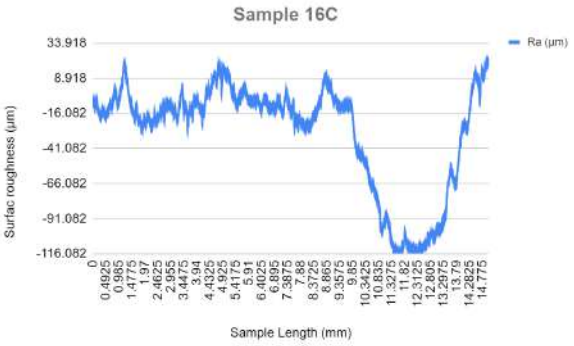

Sample 15A
Ra (µm)
Surfac roughness (µm)
Sample Length (mm)

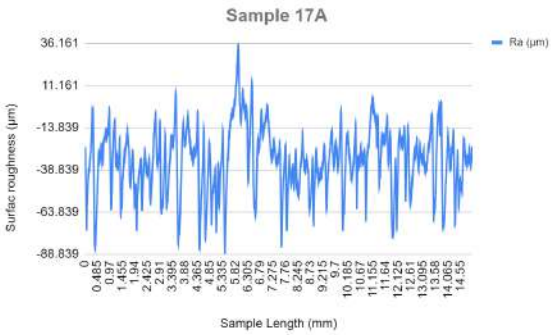

Sample 15B
Ra (µm)
Surfac roughness (µm)
Sample Length (mm)

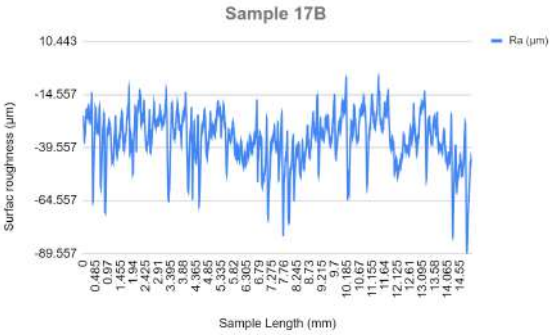

Sample 15C
Ra (µm)
Surfac roughness (µm)
Sample Length (mm)

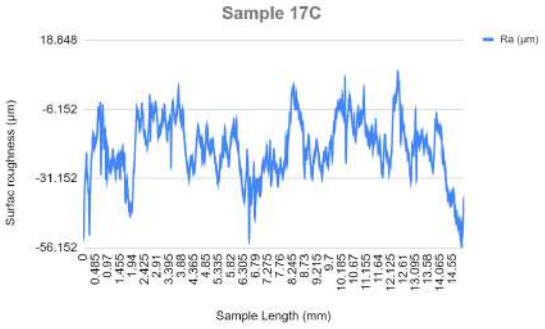

Sample 16A
Ra (µm)
Surfac roughness (µm)
Sample Length (mm)

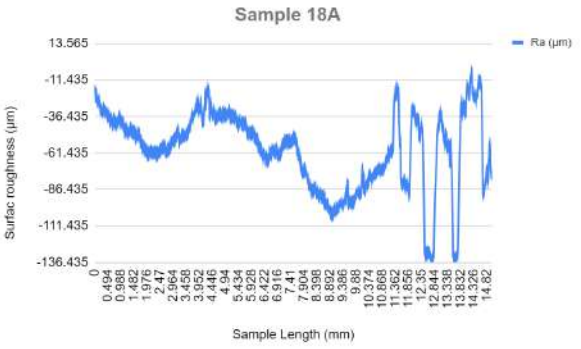

Sample 16B
Ra (µm)
Surfac roughness (µm)
Sample Length (mm)

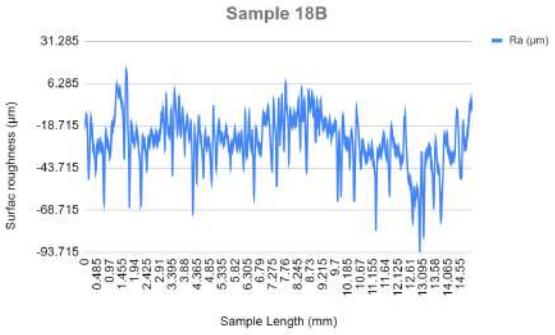

Sample 16C
Ra (µm)
Surfac roughness (µm)
Sample Length (mm)

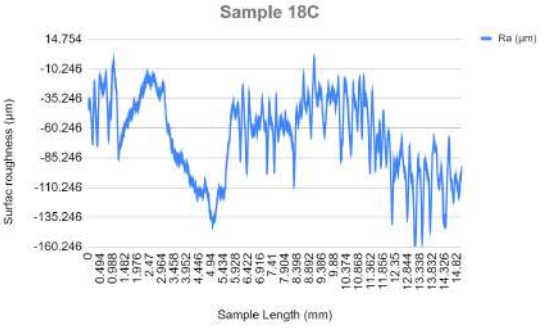

Sample 17A
Ra (µm)
Surfac roughness (µm)
Sample Length (mm)

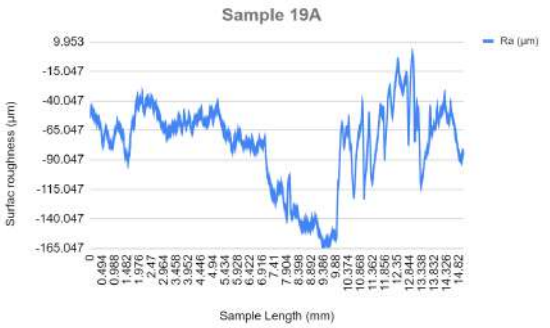

Sample 17B
Ra (µm)
Surfac roughness (µm)
Sample Length (mm)

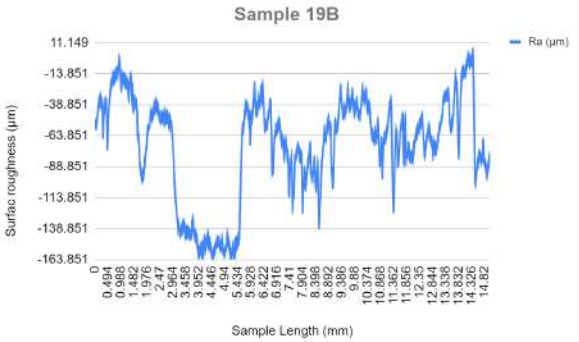

Sample 17C
Ra (µm)
Surfac roughness (µm)
Sample Length (mm)

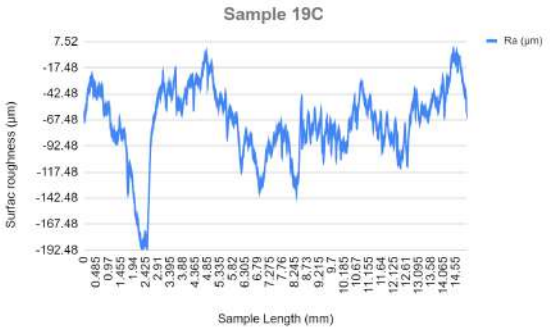

Sample 18A
Ra (µm)
Surfac roughness (µm)
Sample Length (mm)

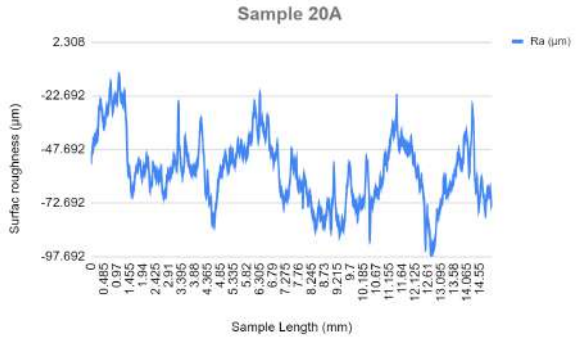

Sample 18B
Ra (µm)
Surfac roughness (µm)
Sample Length (mm)

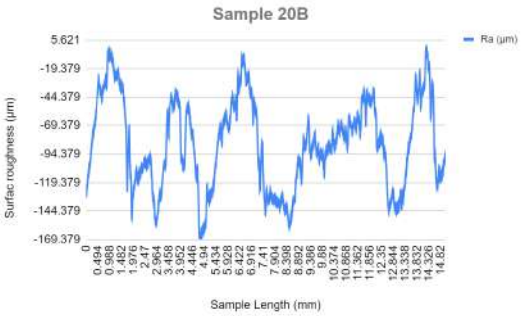

Sample 18C
Ra (µm)
Surfac roughness (µm)
Sample Length (mm)

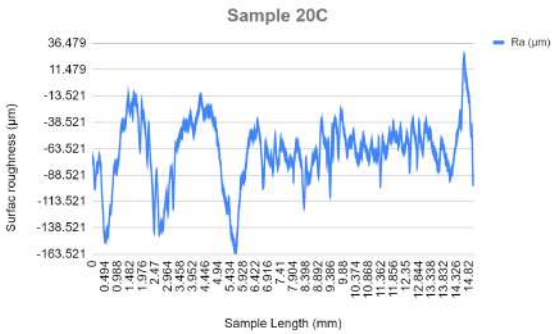

Sample 19A
Ra (µm)
Surfac roughness (µm)
Sample Length (mm)

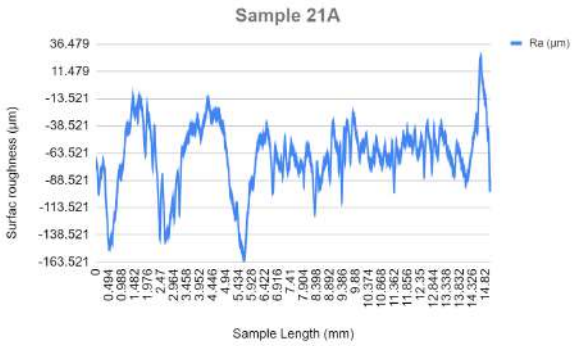

Sample 19B
Ra (µm)
Surfac roughness (µm)
Sample Length (mm)

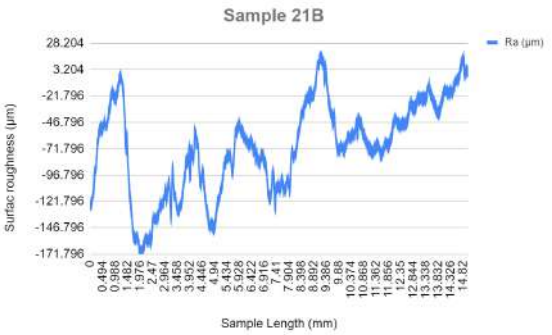

Sample 19C
Ra (µm)
Surfac roughness (µm)
Sample Length (mm)

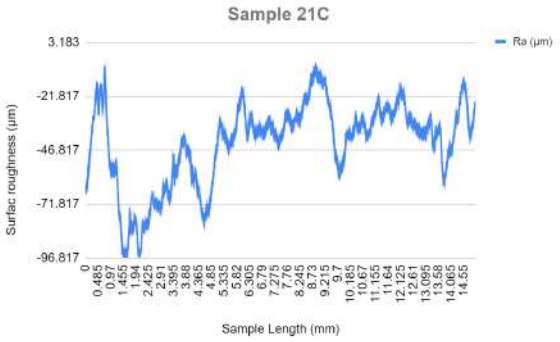

Sample 20A
Ra (µm)
Surfac roughness (µm)
Sample Length (mm)

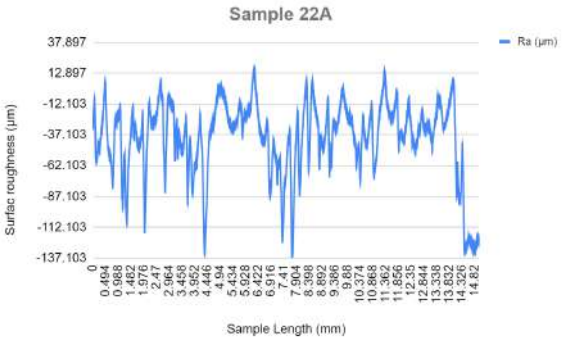

Sample 20B
Ra (µm)
Surfac roughness (µm)
Sample Length (mm)

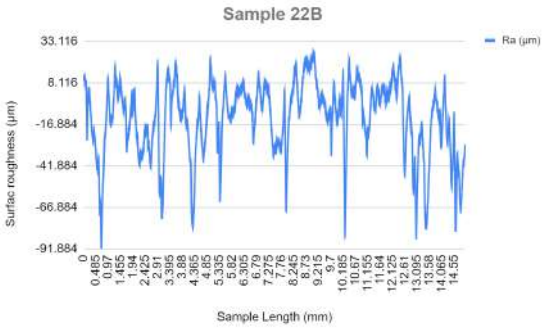

Sample 20C
Ra (µm)
Surfac roughness (µm)
Sample Length (mm)

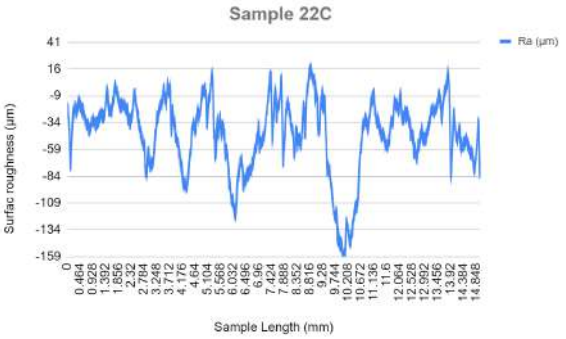

Sample 21A
Ra (µm)
Surfac roughness (µm)
Sample Length (mm)

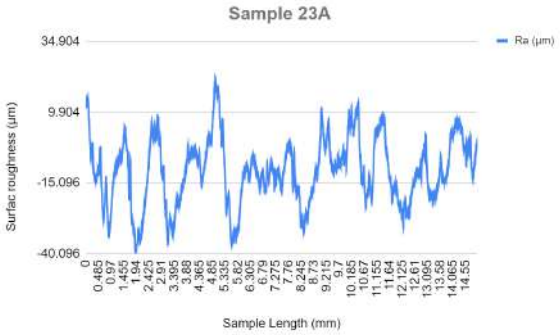

Sample 21B
Ra (µm)
Surfac roughness (µm)
Sample Length (mm)

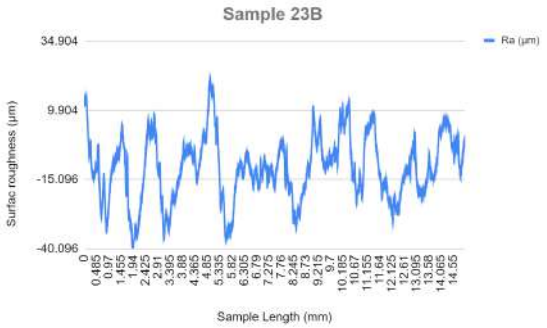

Sample 21C
Ra (µm)
3.183
-21.817
-46.817
-71.817
-96.817
Surfac roughness (µm)
Sample Length (mm)

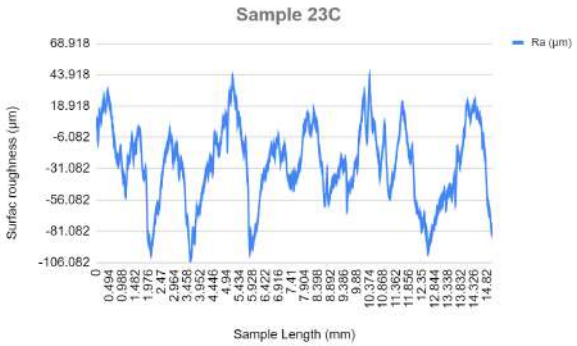

Sample 22A
Ra (µm)
37.897
12.897
-12.103
-37.103
-62.103
-87.103
-112.103
-137.103
Surfac roughness (µm)
Sample Length (mm)


Sample 22B
Ra (µm)
33.116
8.116
-16.884
-41.884
-66.884
-91.884
Surfac roughness (µm)
Sample Length (mm)


Sample 22C
Ra (µm)
41
16
-9
-34
-59
-84
-109
-134
-159
Surfac roughness (µm)
Sample Length (mm)


Sample 23A
Ra (µm)
34.904
9.904
-15.096
-40.096
Surfac roughness (µm)
Sample Length (mm)


Sample 23B
Ra (µm)
34.904
9.904
-15.096
-40.096
Surfac roughness (µm)
Sample Length (mm)


Sample 23C
Ra (µm)
68.918
43.918
18.918
-6.082
-31.082
-56.082
-81.082
-106.082
Surfac roughness (µm)
Sample Length (mm)

Appendix E - Hardness Test Results

Sample 1		Sample 2		Sample 3		Sample 4	
HV	Distance (µm)	HV	Distance (µm)	HV	Distance (µm)	HV	Distance (µm)
177.3	154.96	173.5	150.84	161	151.62	173	150.33
181.5	149.3	191	150.84	175.4	150.46	180.2	150.33
177.7	149.3	187.6	150.84	180	150.46	192.1	150.33
178.5	150.83	189.2	155.97	168.6	150.46	171.2	158.45
188.7	150.83	185.5	146.61	184.2	150	125.4	148.45
180.3	148.14	192.8	148.61	190.8	150	174	149.07
184.4	151.31	190.6	149.75	173.3	150	163.1	150.23
183.2	149.43	187.2	150.56	174.8	150.74	165.2	150.23
186	149.43	179.8	150.56	174.1	147.5	164.3	150.23
171.8	149.43	163.6	150.56	188.9	150.04	177.3	150.85
172.6	150.98	183.4	148.76	180.5	150.04	174.1	150.85
148.7	150.86	187.6	148.76	176.3	150.04	180.5	152.31
186.7	150.86	188.6	149.84	179.4	150.04	182.8	147.92
128.7	150.86	186	149.86	182.1	148.95	182.5	147.92

Sample 5		Sample 6		Sample 7		Sample 8	
HV	Distance (µm)	HV	Distance (µm)	HV	Distance (µm)	HV	Distance (µm)
192.6	151.68	172.7	154.93	236.1	149.64	149.7	154.51
188	150.67	181.9	148.57	319.9	149.72	141.2	152.24
187.3	150.64	185.9	151.59	365	151.02	143.8	152.24
189.1	150.64	187.6	151.59	322.2	151.02	139.2	153.45
189.2	150.64	179.8	151.59	356.1	151.02	150.6	150.32
170.9	150.64	182.5	148.35	360.6	150.03	141.6	150.32
165.2	150.64	187	152.23	357.3	151.44	141.1	151.34
183.1	150.64	176.7	152.23	322.3	147.52	153.1	151.34
196.1	148.05	180.7	150.44	308.5	150.26	140	149.45

190.3	151.21		155	152.16		291.4	150.26		146.4	151.14
200	151.21		168	150.01		269.5	149.65		139	152.03
191.8	147.8		181.3	147.62		220.06	149.65		145	152.03
186.4	155.2		177.8	152.98		239.6	149.65		147.6	152.03
183	145.12		169.9	151.21		230.1	150.13		146.4	152.03
191.4			177.6			233.8			145.5	

Sample 10			**Sample 11**			**Sample 13**			**Sample 14**	
HV	**Distance**		**HV**	**Distance (µm)**		**HV**	**Distance (µm)**		**HV**	**Distance (µm)**
336.3	155.28		262.5	153.92		169.5	150.89		185.9	146.6
357.5	147.88		276.4	150.09		176.6	150.89		179.3	148.97
374.7	151.02		271.6	150.09		175.6	150.89		171.3	148.97
331.3	152.51		221	154.17		175.7	152.46		176.5	153.58
340.7	148.8		196.7	150.42		180	151.21		165.1	148.76
322.2	151.92		198.8	150.42		174	151.46		181.5	150.53
312.6	151.92		202	150.42		172.1	151.46		181.1	150.53
252.2	151.92		187	152.59		150.4	151.46		174.2	150.53
258.8	149.64		189.5	151.59		173.2	151.46		173.4	151.86
229.9	150.76		184.1	151.1		175.4	149.59		174.6	147.88
224.3	150.76		182.4	151.1		170.3	152.2		174.8	151.94
211.8	150.37		193.6	151.1		175.7	147.46		174.1	153.23
200.4	150.37		194.7	151.1		181.3	151.86		173.2	174.42
188.6	153.88		188.7	151.25		181.5	151.86		176	150.06
190.1			186.7			163.6			174.6	

Sample 16			**Sample 17**			**Sample 15**			**Sample 18**	
HV	**Distance (µm)**		**HV**	**Distance (µm)**		**HV**	**Distance (µm)**		**HV**	**Distance (µm)**
175.9	155.34		161.8	155.55		182.8	152.59		162.7	149.11
180.7	150.58		174.3	151.02		174.6	148.03		166.3	149.9

179.2	152.49		166.5	151.02		173	148.03		168	150.08
180	152.49		167.2	151.02		165.9	151.46		161.9	150.08
185.9	152.49		168.3	151.02		163.4	151.46		161.8	150.11
160.5	150.9		163.4	151.79		172.4	148.94		158.5	150.11
177.7	154.69		169.1	151.79		175.3	152.04		145.9	154.99
187.6	150.51		153.9	154.38		174	152.04		130.4	150.7
181.5	151.93		161.2	147.9		174.5	150.87		151	150.7
176.7	151.93		178.7	153.16		172.2	150.87		171	150.7
137.2	153.05		175.5	154.42		170.9	151.59		162.9	150.7
169.7	150.14		171.7	148.64		168.1	151.59		171.8	150.7
173	154.38		170.2	151.11		172.4	151.59		177.7	150.7
170.7	151.78		168.4	157.93		184.1	151.78		163.3	150.7
168.3			168.1			173			162.7	

Sample 19			**Sample 20**			**Sample 21**			**Sample 22**			**Sample 23**	
HV	**Distance**		**HV**	**Distance (µm)**		**HV**	**Distance (µm)**		**HV**	**Distance (µm)**		**HV**	**Distance (µm)**
356.6	154.43		245.8	153.3		261.5	153.38		188.9	154.65		269.7	153
349.2	151.9		252.5	153.3		321.2	150.34		162.8	153.74		304.9	150.83
344.8	151.9		291.6	152.12		276.6	151.22		154.7	150.47		289.3	150.83
312.8	154.08		337.4	159.81		225.3	151.22		147.2	150.47		262.1	150.29
276.7	147.7		149.7	154.04		200.9	151.22		142.8	150.47		225.8	150.29
289.9	152.68		210.7	148.99		177.5	151.22		144.4	150.47		212.4	152.52
311.1	152.68		250.3	157.5		174.3	151.65		134.1	150.47		196.6	152.52
308.9	150.47		271.2	156.32		158.4	154.46		130.3	152.05		185.8	148.38
286.2	150.47		235.4	151.08		167.3	148.47		133.4	149.15		175.4	152.71
298.1	150.47		227.7	155.49		171.4	152.75		144.1	153.29		164.4	151.32
258.2	150.47		257	157.38		171	151.87		133.5	153.29		160.5	151.32
255.7	150.47		238.5	153.52		159.7	151.87		134.6	148.01		167.7	151.32
262.7	152.95		218.9	153.52		163.2	151.87		142.3	152.36		166.5	151.32
237.3	152.95		184.7	153.52		165.5	151.87		140.3	152.26		155.3	151.78
213.1			181.4			162.2			143.2			153.32	

Appendix F - Base Metal Test Certificates

产品质量证明书
INSPECTION CERTIFICATE

订货单位 PURCHASER			钢种 STEEL GRADE	低合金高强度结构钢 High strength low alloy structural steel	
收货单位 CONSIGNEE			合同号 CONTRACT NO.	YGRIZANN230201003-02	
技术标准/牌号 SPEC./STEEL GRADE	EN 10025-2:2019 / S355J0+A+R	交货状态 DELIVERY CONDITION	热轧/AR	签发日期 DATE OF ISSUE	20230313
车 号 TRAIN NO.			炉批号 HEAT NO.	2303032000268	

炉号 HEAT NO.	批号 LOT NO.	钢板号 PLATE NO.	规格 SIZE mm	数量 QTY	重量 WEIGHT kg	分析方法 ANALYSIS METHOD	化学成分 CHEMICAL ANALYSIS % C	Si	Mn	P	S	Cr	Mo	Ni	Al	Cu	V	Nb	Ti	N	CEV	CET	Pcm
							≤1.0	≤1.0	≤1.0	≤1.0	≤0.3	≤1.0	≤1.0	≤1.0	≤1.0	≤1.0	≤1.0	≤1.0	≤1.0	≤1.0	≤1.0	≤1.0	≤1.0
							80% 实测	80% 实测	实测														
2303032000268	2303032000268	2303032000268	8×1500×12000	1	1.885	1	0.14	0.20	1.41	0.010	0.002	0.04	0.01	0.02	0.041	0.02	0.001	0.001	0.002	0.0040	0.37	0.24	0.13
2303032000269	2303032000269	2303032000269	8×1500×12000	1	1.885	1	0.14	0.20	1.41	0.010	0.002	0.04	0.01	0.02	0.041	0.02	0.001	0.001	0.002	0.0040	0.37	0.24	0.13
2303032000270	2303032000270	2303032000270	8×1500×12000	1	1.885	1	0.14	0.20	1.41	0.010	0.002	0.04	0.01	0.02	0.041	0.02	0.001	0.001	0.002	0.0040	0.37	0.24	0.13
2303032000271	2303032000271	2303032000271	8×1500×12000	1	1.885	1	0.14	0.20	1.41	0.010	0.002	0.04	0.01	0.02	0.041	0.02	0.001	0.001	0.002	0.0040	0.37	0.24	0.13
2303032000272	2303032000272	2303032000272	8×1500×12000	1	1.885	1	0.14	0.20	1.41	0.010	0.002	0.04	0.01	0.02	0.041	0.02	0.001	0.001	0.002	0.0040	0.37	0.24	0.13
2303032000273	2303032000273	2303032000273	8×1500×12000	1	1.885	1	0.14	0.20	1.41	0.010	0.002	0.04	0.01	0.02	0.041	0.02	0.001	0.001	0.002	0.0040	0.37	0.24	0.13
2303032000274	2303032000274	2303032000274	8×1500×12000	1	1.885	1	0.14	0.20	1.41	0.010	0.002	0.04	0.01	0.02	0.041	0.02	0.001	0.001	0.002	0.0040	0.37	0.24	0.13
2303032000275	2303032000275	2303032000275	8×1500×12000	1	1.885	1	0.14	0.20	1.41	0.010	0.002	0.04	0.01	0.02	0.041	0.02	0.001	0.001	0.002	0.0040	0.37	0.24	0.13
2303032000276	2303032000276	2303032000276	8×1500×12000	1	1.885	1	0.14	0.20	1.41	0.010	0.002	0.04	0.01	0.02	0.041	0.02	0.001	0.001	0.002	0.0040	0.37	0.24	0.13
			共计 Total	10	18.850																		

注释 NOTES

1. 成份成分 CHEMICAL COMPOSITION
2. 拉伸试验 MECHANICAL PROPERTIES TEST
3. 冲击试验 IMPACT TEST, 20°C, 纵向 LONGITUDINAL
4. 弯曲 CLOSE TO 90 BEND, 无裂纹 NO CRACK
5. 180° - FREE BEND TEST
6. 180° - TENSILE STRENGTH
7. ISO 377 - SPECIMEN LOCATION AND PREPARATION

ASTM E 29

A370-18 IMPACT TEST A
A370-18 IMPACT TEST B
A370-18 IMPACT TEST C
A370-18 IMPACT AVERAGE

本产品已按照标准要求进行制造和检验，其技术符合要求，特此证明。
WE HEREBY CERTIFY THAT MATERIAL DESCRIBED HAS BEEN MANUFACTURED AND TESTED WITH SATISFACTORY RESULTS IN ACCORDANCE WITH THE REQUIREMENTS OF THE ABOVE MATERIAL SPECIFICATION

野牛

冶金技术处处长
DIRECTOR OF METALLURGICAL DEPARTMENT

5169

新余钢铁股份有限公司
XINYU IRON & STEEL CO., LTD.

产品质量证明书
INSPECTION CERTIFICATE

地址：江西省新余市钢铁路1号 邮编:338001
No.1 STEEL ROAD, XINYU CITY, JIANGXI PROVINCE, CHINA
POST CODE: 338001
TEL: +86 0790-6291172/6294257

CUSTOMER	CHEUNGFULI HONG KONG) COMPANY LIMITED	PRODUCT	Hot Rolled Plate Products of Normalloy Structural Steels	DELTAIL NO.	FN22-12090	CERTIFICATE NO.	ZB12220346830
PURCHASER	新钢公司九江分公司XGEO-12212024 6Y	SPECIFICATION	EN10025-2:2019	STATE OF DELIVERY (2)	AR	DATE OF ISSUE	2022-12-22
CONTRACT NO.	XGEO-1221202467	LICENSE NO.	2814/CPR/0038/CPR/SHA/0071129/1	TRAIN NO.	赣KB7936	DATE OF DELIVERY	2022-12-21

NO	PLATE ID.	HEAT NO.	STEEL GRADE	MATERIAL DESCRIPTION THICK	WIDTH	LENGTH		WEIGHT MT	分析区分 (1)	CHEMICAL COMPOSITION % C	Si	Mn	P	S	Cr	Ni	Cu	Nb	V	Ti	Als	Mo
				mm						N	B	CEV										
1	Z2-6826A.2.2	J21-106299	S355J0+AR	16	3480	18000	1	3.014	L	0.15	0.240	1.40	0.023	0.003	0.08	0.01	0.03	0.001	0.053	0.016	0.034	0.01
										0.006	0	0.39										
2	Z2-6953A.4.4	J27-145414	S355J0+AR	16	3000	8000	1	2.01	L	0.16	0.300	1.38	0.016	0.002	0.07	0.01	0.02	0.004	0.003	0.011	0.021	0.003
										0.003	0.0003	0.41										
3	Z2-6953A.5.1	J27-145414	S355J0+AR	16	3000	8000	1	2.01	L	0.16	0.300	1.38	0.016	0.002	0.07	0.01	0.02	0.004	0.003	0.011	0.021	0.003
										0.003	0.0003	0.41										
4	Z2-6953A.5.2	J27-145414	S355J0+AR	16	3000	8000	1	2.01	L	0.16	0.300	1.38	0.016	0.002	0.07	0.01	0.02	0.004	0.003	0.011	0.021	0.003
										0.003	0.0003	0.41										
5	Z2-6953A.5.3	J27-145414	S355J0+AR	16	3000	8000	1	2.01	L	0.16	0.300	1.38	0.016	0.002	0.07	0.01	0.02	0.004	0.003	0.011	0.021	0.003
										0.003	0.0003	0.41										

NO	PLATE ID.	试验区分 (6)	拉伸试验 TENSILE TEST 位置方向 (4)	温度 T	屈服 Y.S ReH	抗拉 T.S Rm	断长率 E.L A	弯曲 BEND	冲击试验 IMPACT TEST 位置方向 (4)	试样尺寸 (5)	温度 T	KV1	KV2	KV3	AVE	产品来源
				℃	MPa	MPa	%				℃	J	J	J	J	
1	Z2-6826A.2.2	H	T	室温	403	546	34.9	合格	L	A	20	173.9	180.8	119.4	177.7	
2	Z2-6953A.4.4	H	T	室温	397	538	36.0	合格	L	A	20	219.9	221.0	202.7	213.4	
3	Z2-6953A.5.1	H	T	室温	360	526	36.9	合格	L	A	20	216.8	223.9	201.7	213.4	
4	Z2-6953A.5.2	H	T	室温	397	535	36.6	合格	L	A	20	216.8	222.8	200.7	213.4	
5	Z2-6953A.5.3	H	T	室温	349	535	36.5	合格	L	A	20	216.8	222.8	202.7	213.4	

TOTAL PIECES	5	TOTAL WT	11.054	ACCEPTABLE VISUAL AND DIMENSIONS
REMARKS				

NOTES: (1)分析区分 ANALYSIS: L=熔炼分析 LADLE ANALYSIS P=成品分析 PRODUCT ANALYSIS. (2)交货状态 STATE OF DELIVERY: AR=热轧 AS HOT ROLLED (3)试验分区 SAMPLING POSITION: B=底部 BOTTOM. H=头部 TOP. A=任意 Any. (4)位置方向 LOCATION AND ORIENTATION: S=表面 SURFACE. T=横向 TRANS. D=45°. L=纵向 LONG. (5)试样方向 THICKNESS DIRECTION. (6)弯曲 BEND. 按产品标准进行试验. TESTED ACCORDING TO PRODUCT CRITERION 无要求时, 弯曲试验结果不作交货条件. BENDING TEST IS NOT A DELIVERY CONDITION OF SUPPLY WHERE NOT REQUIRED. (5)试样尺寸 SPECIMEN SIZE: A=10*10mm;B=10*7.5mm;C=10*5mm;D=10*4mm;E=10*2.5mm;F=10*1.5mm;G=10*0.5mm;H=12*6*55;I=10*6.7*55;J=10*5*55 (7)CEV=C+Mn/6+(Cr+V+Mo)/5+(Cu+Ni)/15

本产品已按上述要求进行检查和检验，其结果符合要求。特此证明。(符合 EN 10204 3.1证书)
WE HEREBY CERTIFY THAT THE MATERIALS DESCRIBED HEREIN HAVE BEEN MANUFACTURED AND TESTED WITH SATISFACTORY RESULTS.
THIS CERTIFICATE IS IN CONFORMITY WITH EN 10204 3.1

CE 2814/CPR

质量检验专用章
QUALITY INSPECTOR